Investigation on the Mechanisms of Elastomechanical Behavior of Resilin

Md Shahriar K. Khandaker

Dissertation submitted to the faculty of the Virginia Polytechnic Institute and State University in partial fulfillment of the requirements for the degree of

Doctor of Philosophy

In

Engineering Mechanics

David A. Dillard, Co-chair

Eric P. Beers, Co-chair

Daniel M. Dudek

David R. Bevan

Robert B. Moore

Tijana Z. Grove

November 12, 2015

Blacksburg, VA

Keywords: Resilin; Elastomeric proteins; Molecular modeling; Molecular cloning; Time temperature concentration superposition principle; Doubly-shifted modulus master curves; Glass transition temperature; Recombinant resilin; Hydrogen bonds; Adhesive properties; Hydrogel.

Investigation on the Mechanisms of Elastomechanical Behavior of Resilin

Md Shahriar K. Khandaker

ABSTRACT

Resilin is a disordered elastomeric protein and can be found in specialized regions of insect cuticles. Its protein sequence, functions and dynamic mechanical properties vary substantially across the species. Resilin can operate across the frequency range from 5 Hz for locomotion to 13 kHz for sound production. To understand the functions of different exons of resilin, we synthesize recombinant resilin-like hydrogels from different exons, and investigate the water content and dynamic mechanical properties, along with estimating surface energies relevant for adhesion. The recombinant resilin-like hydrogel has 80wt% water and does not show any sign of tack even though it satisfies the Dahlquist criterion. Finally, doubly shifted dynamic moduli master curves are developed by applying the time-temperature concentration superposition principle (TTCSP), and compared to results obtained with natural resilin from locusts, dragonflies and cockroaches. The resulting master curves show that the synthetic resilin undergoes a prominent transition, though the responsible mechanism is unclear. Possible explanations for the significant increase in modulus include the formation of intramolecular hydrogen bonds, altered structural organization, or passing through a glass transition, all of which have been reported in the literature for polymeric materials. Results show that in nature, resilin operates at a much lower frequency than this glass transition frequency at room

temperature. Moreover, recombinant resilins from different clones have comparable resilience with natural resilin, though the modulus is around 1.5 decades lower. Results from the clones with and without chitin binding domains (ChBD) indicate that the transition for the clone without ChBD occurs at lower frequencies than for those with the ChBD, perhaps due to the disordered nature of the clone without ChBD.

Atomistic molecular modeling is applied on the repetitive motifs of resilin and different elastomeric proteins to better understand the relationship between elastomeric behavior and amino acid sequences. Results show that the motifs form a favorable bent conformation, likely enabled by glycine's lack of steric hindrance and held in place through intramolecular hydrogen bonds. During Steered Molecular Dynamic (SMD) pulling of these motifs, the hydrogen bonds break and they reform again when the peptides are released to move freely, returning to similar bent conformations. The transition seen in the master curves of recombinant resilins might be due to either these intramolecular hydrogen bonds or to glass transition behavior, though evidence indicates that the transition probably due to the glass transition. What we learned from the synthesized recombinant resilin and simulating the repetitive motifs of resilin may be applicable to the biology and mechanics of other elastomeric biomaterials, and may provide deeper understanding of their unique properties.

Dedication

I dedicate this dissertation to my family. My family has always provided me with emotional and financial support and inspired me to complete the work. Without their support, I would not have been able to complete even a small portion of this work.

Acknowledgments

It would have been impossible to complete this work without the input of my previous advisor, Dr. Daniel Dudek and my current co-advisors, Dr. David Dillard and Dr Eric Beers. I always felt so lucky to be a student of Dr. Dudek and to pursue my Ph.D. degree under his supervision. Throughout the past five years, I have learned a lot from him not only for doing scientific research, but also for being a better person. Special thanks to Dr. Beers for allowing me to use his lab facility and guiding me for my molecular biology experiments all these years. I also want thank Dr. Dillard for accepting me as his student after Dr. Dudek and guiding me towards the completion of my degree. Over the last one and a half years, there have been many times when I have overlooked key details that he quickly spotted and brought to my attention. I would also like to thank Dr. David Bevan for mentoring me on my molecular modeling works.

I want to thank Dr. Chengsong Zhao and Earl Petzold in Dr. Beers' lab for helping me with knowledge and instructions on my molecular biology work. Without their help, I could not learn the molecular biology techniques so quickly.

I thank Dr. Philips for providing me the fruit flies for my experiments. Also, thanks to Dr. Richard Helm for allowing me to use his freeze dryer and mass spectroscopy and also his lab specialists Jody Jervis and Keith Ray for helping me to use these instruments. Former Dr Dudek's student Achu Byju taught me the operating procedures of the custom made DMA and without that none of the DMA testing would be possible. Thanks to Dr Bruce Orler for his contribution on the hydrogen bonding discussions and also for helping me to use TGA owned by

ICTAS. Also, thanks to Dr. Boreyko in ESM for helping and allowing me to use his instrument to measure surface energy.

I thank to Dr. David Bevan's graduate students Anne M. Brown and former ESM graduate student Albert L. Kwansa, for their help with the use of GROMACS and NAMD. We also thank the Biomedical Engineering and Mechanics (BEAM) Department for use of the Linux Computer Cluster and Virginia Tech for providing us with computational resources on the ARC Blueridge computer.

I gratefully acknowledge funding from an ICTAS junior faculty award to Dr Dan Dudek which allowed him to support me for 1st two years of my PhD and also ESM department for supporting me as teaching assistant.

I also thank to my committee members Dr. Robert Moore and Dr. Tijana Grove for taking time out of their busy schedules to give valuable feedback and suggestions on my research. I also thank the entire ESM staff, especially Anne-Marie, Linda, Lisa, and Melissa for always going out of their way to provide me with all of the support.

Last, but certainly not least, I thank my family and friends for all of their support. They provided motivation whenever I was feeling down, and provided guidance whenever I was lost and confused. It is impossible to overstate how much they have influenced in making me who I am today.

Attributions

I would like to thank my collaborators for their input in my dissertation. Specifically, I would like to thank Drs. Dillard, Dudek and Beers for their help and advice in my experimental works on the biomaterials for expression, crosslinking and developing modulus master curves of recombinant resilin (Chapter 2 of this document) and investigation on the functions of exons and chitin binding domain (ChBD) on the mechanical properties of resilin (Chapter 3 of this document). I wish to further thank Drs. Bevan, Dillard and Beers for their insight and advice for my molecular modeling work in determining the elastomeric properties of repeating units and building blocks of resilin (Chapter 4 of this document) and the molecular modeling work on the repeating motifs of disordered elastomeric proteins (Chapter 5 of this document).

Contents

List of Figures

List of Tables

Chapter 1: Introduction

Elastomeric proteins are present in a wide range of living organisms, and their critical features include structural disorder and associated hydration[1]. Moreover, about 40% of highly structured proteins contain disordered domains[2]. The secondary structures of these proteins typically are in dynamic equilibrium between extended poly-proline II (PPII) and β-strands) and folded (mainly β-turn) conformations[3]. Functional and structural properties of proteins are determined by chemical properties and sequential arrangement of their constituent amino acid residues. However, despite the ubiquity of unstructured proteins, we have little understanding of how variations in their amino acid sequences affect their macroscopic material properties. Therefore, in depth comparisons between the amino acid sequences of ordered and disordered proteins are needed to improve the understanding of structural and functional properties of disordered proteins[4].

Resilin is a disordered elastic protein in a family of functionally similar proteins that includes, among others, elastin, gluten, gliadin, abductin, and spider silks. Resilin can be stretched to 300% of its resting length and reportedly suffers neither from creep nor stress relaxation even after weeks of sustained straining, though experimental details are unclear[5-6]. In 1962, Jensen and Weis-Fogh[7] explored the dynamic mechanical properties of resilin from locust and found energy loss less than 5% even at 200 Hz at constant temperature (25˚C). Furthermore, resilin has been reported to have long fatigue life sustaining millions of cycles in nature without failure[8]. For example, in fruit flies (*Drosophila* species), resilin survives during the entire lifetime of the insects at 720,000 cycles per hour, with resilience higher than that of synthetic polybutadiene, a high resilience rubber[9-10]. Whether this long fatigue life is an inherent property of resilin or results from a natural *in-vivo* repair mechanism is not yet known.

First discovered in 1960 by Weis-Fogh[5], resilin has remarkably diverse functions. In addition to its multiple locomotor functions described[7], resilin plays a role in feeding (salivary pump of assassin bugs[11]), sound production (cicada tymbal mechanism[12]), and structural support at leg joints (cockroach[13]). Resilin works across a broad frequency range from as high as 13 kHz in cicada[14] and moth[15] sound production to as low as 6 Hz in cockroach locomotion[16-17]. Hence, resilin can be used as a spring over a wide range of speeds, and for enabling other rapid motions in insects, such as in jumping fleas[18-19,]. Resilin can also be used to simplify the complex mechanism of wing-folding in insects.[20]

In addition to this functional diversity, resilin is also structurally diverse at both the macro- and microscopic levels of organization. It can be either a pure polymer, as in dragonfly tendons, or a composite of chitin and resilin, as in locust pre-alar arms, cockroach tarsal pads, and fruit fly wing hinges[21]. At the molecular level, resilin is believed to be highly unstructured with little or no secondary structures such as α-helices or β-sheets [21-22]. The level of disorder in resilin is so high that when stretched to nearly the breaking point and slowly dried, it does not show any trace of crystallization[23]. Like other elastomeric proteins (gliadin, elastin, spider silks), resilin contains distinct repetitive domains in its polymeric sequence to confer elastic properties. These flexible polymer chains form a rubber network due to crosslinking of tyrosine residues forming di- and tri-tyrosine[24]. Unlike the other elastomeric proteins, however, the genes of resilin have both conserved and non-conserved domains across insect lineages, and the conserved domains usually participate in crosslinking. Thus, each species has its own form of resilin, likely matched to its function within that species[25].

Most insect resilin genes are comprised of three protein coding regions, or exons (Fig. 1-1). Both exon 1 and exon 3 contain repeating elastomeric units while exon 2 is known as chitin

binding domain (ChBD)[26]. The ChBD allows strong interaction and binding between chitin and resilin during the process of resilin deposition and construction of cuticle composite. Resilin contains distinct repetitive units that appear to confer elastomeric properties to proteins in ways similar to other elastomeric proteins like elastin, spider silk and gliadin[27]. Some insects, such as dragonfly, have a resilin gene with only a single exon homologous to exon 1, i.e. they produce pure resilin without ChBD[25].

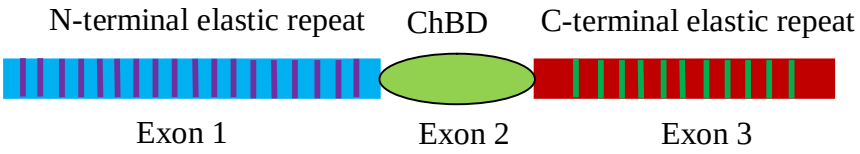

Fig. 1-1. Exons in resilin where exon-1 is known as N-terminal elastic repeat and exon-3 known as C-terminal elastic repeat. Exon 2 is known as ChBD, which binds the chitin and helps the process of construction of the cuticle composite.

To exploit the unique properties of resilin for biomedical applications, it may be necessary to synthesize full-length recombinant resilin. However, a thorough understanding of protein structure and functions of different fragments of resilin may also lead to specific engineering applications based on partial resilin sequences, and alter or potentially improve certain properties beyond those of natural resilin. Elvin et al.[9] were the first to successfully insert the gene of pro-resilin (protein-like resilin) into *Escherichia Coli (E. Coli)* and also crosslinked this product to cast large structures with adequate flexibility.

A hallmark of resilin is the repeatability of certain amino acid motifs. These repeating motifs vary among insect species; however most insects have a repeating motif that includes the tetrapeptide YGAP. Examples of repeating motifs are shown in Fig. 1-2. Functional resilin is

generated by the crosslinking among tyrosines within YGAP repeats to form dityrosine and trityrosine[24]..

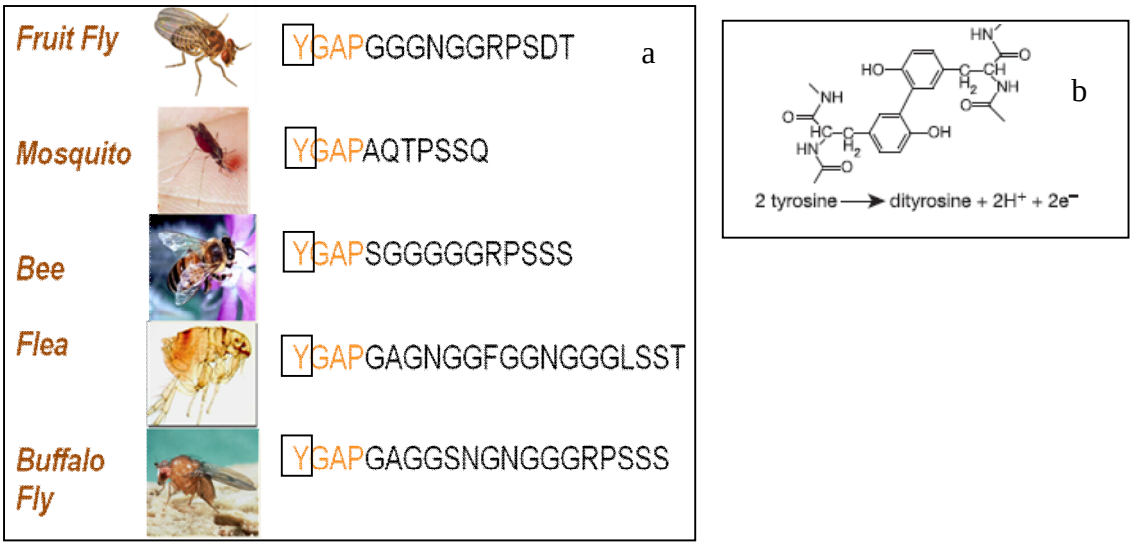

Fig. 1-2. Repetitions in the protein sequence for different insects. They have different number of amino acid repeats but "YGAP" is conserved as tyrosines (Y) for crosslinking site (boxes) (www.google.com/images, 2015) (b) Chemical formulae of dityrosine after crosslinking.

The presence of resilin can easily be identified by exposing the insect to UV light under which insect body parts containing resilin fluoresce blue. For molecular cloning and synthesis of recombinant protein, the stage of insect's life during which the protein is expressed has to be identified. Elvin et al.[9] worked on the Drosophila CG15920 gene encoding resilin and showed that during the pupal stage, resilin was expressed several thousand times faster than at any other stages. In locusts, resilin is expressed during the first three weeks of adult life[28-29].

One of the goals of this work is to synthesize and characterize resilin-like recombinant proteins from *Drosophila melanogaster* (Canton S strain). Ardell and Andersen[30] first identified the *Drosophila melanogaster* resilin gene having two significant elastic repeat motifs; 18 pentadecapeptide repeats (GGRPSDSYGAPGGGN) found in the N-terminal domain and 11

tridecapeptide repeats (GYSGGRPGGQDLG) found in the C-terminal domain. The N- and C-terminal repeats are restricted to exons 1 and 3, respectively. Exon 2 of the gene is known as chitin binding domain (ChBD) of the type R&R-2 (PAKYEFNYQVEDAPSGLS FGHSEMRDGDFTTGQYNVLLPDGRKQIVEYEADQQGYRPQIRYEGDANDGSGPSGP)[27]. During the process of resilin deposition and cuticle composite construction, ChBD allows direct binding and strong interaction between the resilin and chitin. A schematic of the full-length protein is shown in Fig. 1-1.

Elvin et al.[9] and Qin et al.[27] successfully synthesized recombinant protein based on the 1st exon, though the mechanical properties were much weaker than of native protein. For protein expression, they have utilized *E. Coli* as the expression system for its cost effectiveness, scalability and simple culture conditions. After getting the soluble recombinant, resilin-like protein was obtained by crosslinking at some tyrosine sites similar to native protein. There are two main methods of crosslinking: chemical and photo crosslinking. Elvin et al.[9] applied chemical crosslinking process by peroxidases (Horseradish peroxidase (HRP), lactoperoxidase and *Arthromyces ramosus* peroxidase) and photo crosslinking, while for Qin et al.[27], they only utilized the horseradish peroxidase method for crosslinking. Both of them followed the chemical crosslinking process of dityrosine developed by Malencik and Anderson[31]. For photo crosslinking, the method described by Fancy and Kodadek was utilized with slight modification[32]. To analyze the resilience of the recombinant protein, Elvin et al.[9] used scanning probe microscopy (SPM), where crosslinked resilin displayed negligible hysteresis upon compression and sample were about 90% resilient, though the modulus was far below than that of natural resilin. The properties of native resilin from insects are still far better in terms of the

stiffness and resilience, when compared with the recombinant resilin synthesized during later work.

Jensen and Weis-Fogh[33] analyzed viscoelastic properties of locust resilin within the biological range (10-200 Hz) using dynamic mechanical analysis (DMA). Andersen and Weis-Fogh[13] found that resilin starts to lose resilience at 100 Hz. According to Ferry[34], viscoelastic materials show a reduction in resilience during transitions, including the prominent shift from the rubbery state to glassy state when subjected to high frequencies. The percent of elastic energy stored by resilin can be calculated by the ratio of the area under the unloading curve and the area under the loading curve of force verses displacement plot, and that is equal to:

$$R = 100e^{(-\frac{\pi}{2}\tan\delta)}$$

where tan δ is the ratio of imaginary and real components of the complex modulus at a corresponding frequency and R is the percent of resilience[34]. Even though the resilience of locust resilin starts to decrease at 100Hz[13], cicadas reportedly use resilin at 13 kHz with a resilience of about 80%[35]. To better understand this discrepancy, King[25] conducted DMA on the dragonfly resilin, while Choudhury[36] conducted similar tests on cockroach resilin to determine the glass transition frequency. According to them, dragonfly resilin has higher resilience (97%) compared to cockroach resilin (79%) at 25 Hz. However, the resilience of dragonfly resilin is about 30% at the estimated glass transition frequency (2 MHz) while for cockroach resilin, resilience is about 47% (200 kHz)[36].

The time-temperature superposition principle (TTSP) can be used to investigate dynamic mechanical properties of viscoelastic materials[34]. Typically, storage modulus, loss modulus and tan δ are measured over several decades of frequencies at different temperatures, and then these

results are shifted to develop a single master curve at a selected reference temperature that spans multiple decades of time/frequency[25, 34, 36]. The shift factor that allows the curves to form the master curve depends on the temperature, solvent concentration and mechanical dilatation[37]. If TTSP is not sufficient to develop a master curve and determine the glass transition frequency, varying hydration level and using time concentration superposition can be used to form the complete master curve[38]. King[25] and Choudhury[36] used both TTSP and time-concentration superposition to develop the master curves for dragonfly and cockroach resilin. One of the goals of this dissertation is to synthesize recombinant resilin from the fruit fly and study the dynamic mechanical properties using both TTSP and time-concentration superposition.

There is little definitive information on the molecular basis for elastomeric properties of disordered proteins like resilin and elastin[1]. While both natural and recombinant forms of resilin and other elastomeric proteins have been studied, their conformational heterogeneity and insolubility have precluded the use of conventional structural determination methods, including solution NMR and X-ray crystallography[39]. Moreover, such proteins do not allow for investigation of the contributions of small repeating units to the properties of full length resilin[40]. Molecular dynamics (MD) simulations have therefore been useful in developing an atomic-level description of the structure because simulations are not hindered by conformational disorder, although the scope of these studies has been limited to small oligopeptides[41] and short time scales[42].

Petrenko et al.[23] used the NAMD2.6 package[43] for their simulations to assess the flexibility of simulated peptides. They reported a high level of disorder due to a lack of stable secondary structure and lack of stable intra-protein hydrogen bonds. In another study, Kappiyoor

et al.[22] used the GROMACS package[44-45] for simulating the effect of polarity on the elastic properties, and found that increased polarity led to higher extensibility and lower stiffness.

The purpose of this project is to take advantage of resilin's natural diversity in order to develop a fundamental understanding of the elastomeric properties of resilin. Master curves of recombinant resilin synthesized from the different fragments and species are generated to determine macroscopic mechanical properties, while molecular dynamics simulations on the repetitive motifs and building blocks are performed to elucidate the molecular mechanisms responsible for generating such remarkable behavior.

In chapter 2, resilin-like hydrogels are synthesized from clone-1 (exon 1 + exon 2). Then, we investigate the adhesive properties, water content and dynamic mechanical properties of the hydrogel. Finally, doubly shift master curves are developed by applying time-temperature concentration superposition principle (TTCSP) for storage modulus (E'), loss modulus (E") and tan δ over a wide range of frequencies and temperatures, and also compared with the native resilin from locust, cockroach and dragonfly.

In chapter 3, recombinant resilins are synthesized from different clones as well as full length gene from fruit fly to understand the properties of different exons. The dynamic mechanical properties of each clone is investigated in water (fully hydrated) and doubly shifted master curves are developed of each clone using TTCSP for E', E" and tan δ. Finally, master curves are compared with the reported master curve of natural resilin of cockroach.

In chapter 4, molecular modeling (MD) simulations is used on repetitive motif of resilin from exon 1 to develop a fundamental understanding of the mechanism responsible for the remarkable behavior exhibited by insect resilin at molecular level.

In chapter 5, MD simulations are applied on the elastomeric repetitive motifs from different elastomeric proteins from different species. We investigate whether they follow the similar mechanism as discovered in chapter 4 for repetitive motifs from exon 1 of insect resilin.

References

1. S. Rauscher, S. Baud, M. Miao, F. W. Keeley and R. Pomes, Proline and Glycine Control Protein Self-Organization into Elastomeric or Amyloid Fibrils. *Structure*, 2006, **4**, 1667–1676.
2. P. Tompa, Intrinsically unstructured proteins. *Trends in Biochemical Sciences*, 2002, **269**, 2-12.
3. B. Bochicchio, A. Pepe and T. A. M., Investigating by CD the molecular mechanism of elasticity of elastomeric proteins. *Chirality*, 2008, **20**, 985-994.
4. F. X. Theillet, L. Kalmar, P. Tompa, K. H. Han, P. Selenko, A. Keith Dunker, G. W. Daughdrill and V. N. Uversky, The alphabet of intrinsic disorder: I. Act like a Pro: On the abundance and roles of proline residues in intrinsically disordered proteins. *Intrinsically Disordered Proteins*, 2013, **1**, 1-13.
5. T. Weis-Fogh, A rubber-like protein in insect cuticle. *Journal of Molecular Biology*, 1960, **37**, 889-907.
6. T. Weis-Fogh, Molecular interpretation of the elasticity of resilin, a rubber-like protein. *Journal of Molecular Biology*, 1961, **3**, 648-667.
7. M. Jensen and T. Weis-Fogh, Biology and Physics of Locust Flight V. Strength and Elasticity of Locust Cuticle. *Phil. Trans. R. Soc. Lond.*, 1962, **B 245**, 137-169.
8. R. E. Lyons, Lesieur, E., Kim, M.,Wong, D.C.C., Huson, M.G., Nairn, K. M., Brownlee, A. G., Pearson, R. D., Elvin, C. M., Design and facile production of recombinant resilin-like polypeptides: gene construction and a rapid protein purification method. *Protein Engineering, Design & Selection*, 2007, **20**, 25-32.

9. C. M. Elvin, A. G. Carr, M. G. Huson, J. M. Maxwell, R. D. Pearson, T. Vuocolo, N. E. Liyou, D. C. C. Wong, D. J. Merritt and N. E. Dixon, Synthesis and properties of crosslinked recombinant pro-resilin. *Nature*, 2005, **437**, 999-1002.
10. S. Lv, Dudek, D., Cao, Y., Balamurali, M. M., Gosline, J. and Li, H., Designed biomaterials to mimic the mechanical properties of muscles. *Nature*, 2010, **465**, 69-73.
11. S. J. Edwards, Predation and digestion in assassin bugs (Heteroptera, Reduviidae. University of Cambridge, UK, 1960.
12. D. Young and H. C. Bennet-Clark, The role of tymbal in cicada sound production. *Journal of Experimental Biology*, 1995, **198**, 1001-1019.
13. S. O. Andersen and T. Weis-Fogh, Resilin. A rubber-like protein in arthropod cuticle. *Advances in Insect Physiolology*, 1964, **2**, 1-65.
14. H. C. Bennet-Clark, Daws, A. G., Transduction of mechanical energy into sound energy in the cicada Cyclochila australasiae. *The Journal of Experimental Biology*, 1999, **202**, 1803-1817.
15. N. Skals, Surlykke, A., Sound production by abdominal tymbal organs in two moth species: the green silver-line and the scarce silver-line (Noctuoidea: Nolidae: Chloephorinae). *Journal of Experimental Biology*, 1999, **202**, 2937-2949.
16. D. Neff, S. F. Frazier, Identification of resilin in the leg of cockroach, Periplaneta americana: confirmation by a simple method using pH dependence of UV fluorescence. *Arthropod Structure and Development*, 2000, **29**, 75-83.
17. R. Kram, B. Wong, Three-dimensional kinematics and limb kinetic energy of running cockroaches. *Journal of Experimental Biology*, 1997, **200**, 1919-1929.

18. H. C. Bennet-Clark and E. C. A. Lucey, The Jump of the Flea: A Study of the Energetics and a Model of the Mechanism. *The Journal of Experimental Biology*, 1967, **47**, 59-76.
19. S. N. Patek, D. M. Dudek and M. V. Rosario, From bouncy legs to poisoned arrows: elastic movements in invertebrates. *The Journal of Experimental Biology*, 2011, **214**, 1973-1980.
20. F. Haas, S. Gorb and R. J. Wootton, Elastic joints in dermapteran hind wings: materials and wing folding. *Arthropod Structure and Development*, 2000, **29**, 137-146.
21. G. F. Elliott, A. F. Huxley and T. Weis-Fogh, On the structure of resilin. *Journal of Molecular Biology*, 1965, **13**, 791-795.
22. R. Kappiyoor, Balasubramanian, G. , Dudek, D. M. and Puri, I. K., Elastomechanical properties of resilin. *Soft Matter*, 2011, **7**, 11006-11009.
23. R. Petrenko, Computer simulations of resilin-like peptides. Doctoral Dissertation, University of Cincinnati, 2010.
24. S. O. Andersen, The cross links in resilin identified as dityrosine and trityrosine. *Biochimica et Biophysica Acta*, 1964, **93**, 213-215.
25. R. King, Dynamic Mechanical Properties of Resilin. Master's, Virginia Polytechnic Institute and State University, 2010.
26. G. Qin, Hu, X., Cebe, P. and Kaplan, D. L., Mechanism of Resilin Elasticity. *Nature Communication*, 2012, **3**, 1-18.
27. G. Qin, S. Lapidot, K. Numata, X. Hu, S. Meirovitch, M. Dekel, I. Podoler, O. Shoseyov and D. L. Kaplan, Expression, Cross-Linking, and Characterization of Recombinant Chitin Binding Resilin. *Biomacromolecules*, 2009, **10**, 3227–3234.
28. A. C. Neville, Growth and deposition of resilin and chitin in locust rubber-like cuticle. *Journal of insect Physiology*, 1963, **9**, 265-272.

29. A. C. Neville, Daily growth growth layers in locust rubber-like cuticle influenced by an external rhythm. *Journal of Insect Physiology*, 1963a, **9**, 177-186.
30. D. H. Ardell and S. O. Andersen, Tentative identification of a resilin gene in Drosophila melanogaster. *Insect Biochemistry and Molecular Biology*, 2001, **10**, 965-970.
31. D. A. Malencik and S. O. Anderdon, Dityrosine Formation in Calmodulin: Cross-Linking and Polymerization Catalyzed by *Arthromyces* Peroxidase. *Biochemistry*, 1996, **35**, 4375-4386.
32. D. A. Fancy and T. Kodadek, Chemistry for the analysis of protein- protein interations : rapid and efficient cross-linking triggered by long wavelength light. *PNAS*, 1999, **96**, 6020-6024.
33. M. Jensen and T. Weis-Fogh, Biology and Physics of locust flight. V. Strength and elasticity of locust cuticle. *Philosophical Transactions of the Royal Society B*, 1962, **245**, 137-169.
34. J. D. Ferry, Viscoelastic Properties of Polymers. Wiley, New York, 1980.
35. H. C. Bennet-Clark, Tymbal mehcanics and the control of songs frequency in the cicada *Cyclochila australasiae*. *Journal of Experimental Biology*, 1997, **200**, 1681-1694.
36. U. Choudhury, Dynamic Mechanical Properties of Cockroach (Periplaneta americana) Resilin. Master's Thesis, Virginia Polytechnic Institure and State University, 2012.
37. W. G. Knauss and I. J. Emri, Non-linear viscoelasticity based on free volume consideration. *Computers & Structures*, 1981, **13**, 123-128.
38. M. A. Lillie and J. M. Gosline, The effects of hydration on the dynamic mechanical properties of elastin. *Biopolymers*, 1990, **29**, 1147-1160.
39. M. S. Pometun, E. Y. Chekmenev and R. J. Wittebort, Quantitative observation of backbone disorder in native elastin. *Journal of Biological Chemistry*, 2004, **279**, 7982–7987.

40. M. S. Khandaker, D. M. Dudek, E. P. Beers and D. A. Dillard, Expression, Crosslinking and Developing a Modulus Master Curve of Recombinant Resilin. in prep.
41. M. Baer, E. Schreiner, A. Kohlmeyer, R. Rousseau and D. Marx, Inverse temperature transition of a biomimetic elastin model: reactive flux analysis of folding/unfolding and its coupling to solvent dielectric relaxation. *Journal of Physical Chemistry*, 2006, **B 110**, 3576–3587.
42. B. Li, D. O. V. Alonso and V. Daggett, The molecular basis for the inverse temperature transition of elastin. *Journal of Molecular Biology*, 2001, **305**, 581–592.
43. L. Kal´e, R. Skeel, M. Bhandarkar, R. Brunner, A. Gursoy, N. Krawetz, J. Phillips, A. Shinozaki and K. Varadarajan, NAMD2: Greater scalability for parallel molecular dynamics. *Journal of Computational Physics*, 1999, **151**, 283–312.
44. B. Hess, C. Kutzner, D. Van Der Spoel and E. Lindahl, GROMACS 4: Algorithms for Highly Efficient, Load-Balanced, and Scalable Molecular Simulation. *Journal of Chemical Theory and Computation*, 2008, **4**, 435-447.
45. D. Van Der Spoel, E. Lindahl, B. Hess, G. Groenhof, A. E. Mark and H. J. Berendsen, GROMACS: fast, flexible, and free. *Journal of Computational Chemistry* 2005, **26**, 1701-1718.

Chapter 2: Expression, Crosslinking and Developing Modulus Master Curves of Recombinant Resilin

2.1 Abstract

Resilin is a disordered elastomeric protein found in specialized regions of insect cuticles, where low stiffness and high resilience are required. It has a wide range of functions and varies with the insect species – operating across a wide frequency range from 5 Hz for locomotion to 13 kHz for sound production. We synthesize a recombinant resilin from clone-1 (exon-1 + exon-2) of the gene, and determine the water content and dynamic mechanical properties, along with estimating surface energies relevant for adhesion. The recombinant resilin-like hydrogel has 80wt% water and does not show any sign of tack even though it satisfies the Dahlquist criterion. Finally, dynamic moduli master curves have been developed by applying the time-temperature superposition principle (TTSP) and time-temperature concentration superposition principle (TTCSP), and compared with the reported master curves for natural resilin from locusts, dragonflies and cockroaches. The resulting master curves show that the synthetic resilin undergoes a pronounced transition with increasing ethanol concentrations, with the storage modulus increasing by approximately three orders of magnitude. Although possibly a glass transition, alternate explanations include the formation of intramolecular hydrogen bonds or that the chitin binding domain (ChBD) and the exon in the clone might change the secondary structure into more ordered conformations that limit deformation. All these possibilities have been reported in the literature for polymeric materials.

Keywords: Resilin; Doubly-shifted modulus master curve; Glass transition temperature; Recombinant resilin; Hydrogen bonds; Adhesive properties, Temperature dependence, Concentration dependence, Hydrogel

2.2 Introduction

Resilin is an elastomeric protein similar to elastin, gluten, gliadin, abductin, and spider silks. It reportedly suffers neither from creep nor stress relaxation even after weeks of straining and can be stretch to 300% of its resting length, though experimental details are unclear[1-2]. Furthermore, Lyon et al.[3] reported that resilin have long fatigue life sustaining millions of cycles in nature without failure. Resilin was first discovered by Weis-Fogh in 1960[1]. It has multiple locomotor functions described[7] including role in sound production (cicada tymbal mechanism[4]), feeding (salivary pump of assassin bugs[5]), and structural support at leg joints (cockroach[6]). Resilin has natural functions within a broad range of frequency from 6 Hz in cockroach locomotion[7-8] to 13 kHz in cicada[9] and moth[10].

Most insect resilin genes have three protein coding regions, or exons. Among the exons, both exon 1 and exon 3 contain elastomeric repeating units while exon 2 is designated the chitin binding domain (ChBD)[11]. However, some insects resilin do not contain ChBD, as in dragonfly tendons[12] and they only have exon-1.

The resilin can be identified by exposing it under the UV light where resilin glows and emits blue fluorescence light. However, it's important to identify the stage of insect's life when the protein is expressed for molecular cloning and to synthesize recombinant protein. Elvin et al.[13] discovered that Drosophila CG15920 gene has few thousand higher expression level compared to any other stages.

The amino acid sequences, composition and dynamic mechanical properties differ with the functions of the insects, though there are some conserved regions in the protein sequences. The variations suggest that the sequence and properties may be tuned through natural evolution over the years. These variations in sequence and composition need to be understood and also synthetic resilins need to be synthesized with comparable properties, if anyone wants to apply these variation and materials in biomedical applications. Elvin et al.[13] were the first and later Qin et al.[14] and some others synthesized synthetic resilin from recombinant protein. The mechanical properties of these synthesized resilin were much weaker compared to the natural resilin, and also, to our knowledge, none of these previous works tried to determine the dynamic mechanical properties of the recombinant resilin and compare with the natural resilin to understand the properties at different frequencies, temperatures, and diluent concentrations. King[15] and Choudhury[16] conducted dynamics mechanical analysis (DMA) on natural resilin from dragonfly and cockroach to determine the glass transition frequency and explore their dynamical mechanical properties using both time-temperature and time-concentration superposition.

During this work, recombinant resilin was synthesized from the exon-1 and exon-2 (clone-1) of the gene, and determined the water content, adhesive properties and dynamic mechanical properties in water and at different ethanol concentrations used to shift the master curve to the left so that the glass transition frequency moves into the measurable range. Finally, we developed a master curve by applying the time-temperature concentration superposition principle (TTCSP) to determine the storage modulus (E'), loss modulus (E") and tan δ over a wide range of frequencies, and compared the results with natural resilin results reported for locust, dragonfly and cockroach.

2.3 Materials and Methods

2.3.1 Plasmid Construction. *Cloning of resilin genes.* Total RNA was extracted from light colored *Drosophila melanogaster* pupae of the Canton S fruit fly strain (obtained from Dr. Philip's lab, Biological Sciences, Virginia Tech) using TRIZOL Reagent (Life Technologies^{TM}, USA). A reverse transcription of the resilin gene mRNA was conducted to obtain complementary DNA (cDNA) using an AccuScript High Fidelity 1st Stand cDNA synthesis kit (Agilent Technologies, USA) with oligo (dT) primer according to the manufacturer's instructions. Gene specific primers were used to amplify the target segment using the cDNA as a template. The genes were amplified using the following Polymerase Chain Reaction (PCR) program: 94°C for 5 min, 32 cycles of 94°C for 30 sec, 55°C for 30 sec, 72°C for 1:30 min, 72°C for 5 min. The PCR product was ligated to the pGEM T-Easy vector (Promega, Madison, WI, USA). Following transformation of *E. coli* with the resulting vectors (as described below) a clone was selected for resistance to carbenicillin (100 µg/ml).

For sub-cloning to the expression vector, the following gene-specific primers were used to amplify clone-1 (exon-1 + exon-2): Forward primer 5′-CTCGAGCCGGAGCCACCAGTT AACTCGTA-3′, Reverse primer 5'-CTGCAGCTAAGGACCGCTGGGACCACTGC-3′. The resulting cloned DNA fragment was prepared for insertion into the bacterial expression vector PColdI (TaKaRa Bio Inc., NJ, USA) by partial digestion with restriction enzymes *XhoI* and *PstI*. The expression vector PColdI was also digested with *XhoI* and *PstI* for insertion. A 10 µl ligation mixture was prepared combining T4 DNA ligase with the insert and digested PColdI vector.

Transformation. An aliquot of α-Select silver competent cell (Bioline Inc., USA) was thawed on ice. The ligation mix was transferred into a micro-centrifuge tube containing competent cells and mixed carefully. The tube was kept on ice for 20 min followed by 37°C for

40 sec, and again on ice for 2 min. After addition of the SOC broth (300 µl), cells were incubated at 37°C for 20 min. Finally, the transformed cells were plated on a LB-agar plate containing 100µl carbenicillin and incubated at 37°C overnight. The recombinant expression plasmid was isolated from α-Select silver competent cell (Bioline Inc., USA) with selection for carbenicillin resistance (100μg/mL). The correct construct was verified by DNA sequence analysis of the plasmid that isolated from a single transformant using mini-prep kit (Qiagen, USA).

2.3.2 Protein Expression. PColdI contains an N-terminal poly-histidine tag and a Factor Xa protease cleavage site. The former enables affinity purification of the protein on a nickel-nitrilotriacetic acid (Ni-NTA) column, while the latter allows removal of the poly-histidine tag if desired. The expression vector was transformed into *E. Coli* strain BL21 (Bioline Inc., USA). The strain was grown overnight at 37°C in 2xTY with 100 μg/mL carbenicillin in a shaker. The cultures were used for inoculation of 100mL 2xTY culture volume with 100 μg/mL carbenicillin to a 0.10 OD and allowed to grow to mid-log phase, 0.45-0.50 OD at 37°C in a shaker (3 hr). PColdI is a cold shock expression vector, and it works at 15˚C, while expressions of all the other proteins are halted. Thus, the cultures were incubated at 15°C for 30 min and then induced by IPTG (Isopropyl β-D-1-thiogalactopyranoside) to final concentration 1mM. The induced cultures were allowed to grow with vigorous aeration for 24hr at 15°C in a shaker, and bacteria were harvested by centrifugation (12000 g for 20 min at 4°C), and pellets were stored at -80°C.

2.3.3 Protein Purification. The cell pellets were thawed and re-suspended in 35mL extraction buffer (20mM Tris-HCl, pH 8.0, 5mM imidazole). Cells were lysed with a sonicator (15 sec continuous followed by 15 sec pause from sonication for 6 cycles) in an ice water bath to keep the temperature low. The lysed cells were centrifuged at 15000 g at 4°C for 20 min to harvest the cell debris. The soluble protein fraction was collected from the resulting clarified supernatant,

and filtered with a 0.45 μM syringe membrane (Millex-HV Syringe Filter Unit, item # SLHV033RS). The polyhistidine-tagged recombinant resilin was purified by affinity chromatography on 5ml HisTrap High Performance (HP) Ni-NTA pre-packed column, AKTAprime plus Fast Protein Liquid Chromatography (FPLC) (GE, Sweden), which is pre-equilibrated following the protocol provided by the manufacturer. The recombinant proteins were purified as follows: extraction buffer, 20mM Tris-HCl of pH 8.0 and 5mM imidazol; elution buffer , 20mM Tris-HCl of pH 8.0 and 200mM imidazol; (1) 5-10 column volumes (CV) of extraction buffer at 5 mL/min, (2) 35 mL injection of the lysate at 5 mL/min, (3) 5-10 CV wash with the extraction buffer, (4) elute the protein from the column using elution buffer at FPLC (at 1 mL/ min. The column can be regenerated by following the regeneration protocol for Ni-NTA 5mL pre-packed column, where the column was washed with 5-10 vol. of stripping buffer (20mM Tris-HCl, 100mM EDTA and 500mM NaCl) and recharged with Ni2+ salt before regeneration. Purity and recovery rates of the protein were assessed by Sodium Dodecyl Sulfate-Polyacrylamide Gel Electrophoresis (SDS-PAGE). Protein identity was verified by sequencing the protein using Mass Spectrometry.

2.3.4 Scale-Up. The auto induction method was applied to protein expression scale-up using Studier protocol[17] with some modification. Briefly, a total of 5μL of glycerol stock was added to 10mL 2xTY culture volume and grown overnight with 100μg carbenicillin at 37°C in a shaker, and this culture was used for inoculation of 500 ml ZYP 5052 to a 0.015 OD. This culture was grown with vigorous aeration in a 2L baffled flask at 300 rpm for 6 hr at 37°C, long enough to obtain a high cell density (A_{600} = 4-5), before transferring to 15°C at 300 rpm for 24 hr for protein expression.

2.3.5 Freeze Drying of Protein. The recombinant resilin was dialyzed (dialysis tubing pore size 12 kDa) against H_2O overnight at 4°C. Water was replaced every 2-3 hrs. The dialyzed protein was lyophilized using 4.5 Liter Freeze Dry System (Labconco model #7751020).

2.3.6 Crosslinking of Recombinant Resilin. Photo or chemical crosslinking methods were used to produce a solid resilin hydrogel if the protein concentration is less than 100 mg/ml[13]. Consequently, a resilin concentration at 200mg/ml was used for chemical crosslinking following the procedure described by Malencik and Anderson[18] and photo crosslinking, following the method described by Fancy and Kodadek[19] with slight modification. For chemical crosslinking, horseradish peroxidase (HRP) (50 µg/mg of resilin) and superoxide dismutase (50 µg/ml of resilin solution) were added followed by dropwise addition with stirring of 35% hydrogen peroxide to a final concentration of 5 mM to initiate the crosslinking. For photo crosslinking, 2 150 W tungsten-halide lamps were used. Lyophilized resilin was dissolved in phosphate buffered saline (PBS) to a final concentration of 200 mg/ml. Ammonium persulfate (APS) (20 mM final concentration) and $[Ru(bpy)_3]^{2+}$ (2mM final concentration) were added to the resilin solution. The resulting photo crosslinking solution was poured into an 8mm x1.5mm x 1mm polytetrafluoroethylene (PTFE) mold and positioned approximately 15 cm away from the light source for 4-5 min at room temperature.

2.3.7 Characterization. The resilin-like hydrogel sample was characterized to measure the composition, physical and mechanical properties.

2.3.7.1 Thermogravimetric Analysis (TGA). Thermogravimetric analysis is a thermal analysis method and one of features is to measure the water content of a sample through evaporation as a function of increasing temperature[20]. Thermogravimetric analysis was conducted using a TA Instruments TGA SA Q5000 to measure the water content in the

crosslinked solid resilin-like hydrogel sample. During the process, temperature was increased to around 500˚C, allowing any water to evaporate as well as initiate other degradation processes.

2.3.7.2 Adhesive Properties. According to the Dahlquist criterion, if a material's elastic modulus is below about 100 kPa, then that material should be tacky[21], and resilin's elastic modulus was within that range. Equilibrium contact angle measurements are another widely used method to characterize surface properties, including the work of adhesion (W_{adh}), which ultimately drives the wetting behavior and bond stability. This important property, W_{adh}, also plays a role in whether a material is tacky or not. A goniometer (Rame-Hart model 560) was used for contact angle measurements, along with the Young-Dupre equation to calculate the work of adhesion[22]. During the process, droplets of liquid were placed on the resilin surface, and the left contact angle (θ_L) and right contact angle (θ_R) were measured. Work of adhesion was calculated using the following Young-Dupre equation:

$$W_{adh} = \gamma_L (1 + \cos\theta)$$

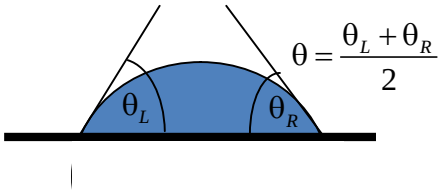

Here, γ_L is the surface energy of liquid and θ is the average of the right and left contact angles.

2.3.7.3 Dynamic Mechanical Analysis (DMA). Dynamic mechanical analysis is a technique to characterize the viscoelastic properties of polymers, where the complex modulus is calculated from measured displacement and load data, along with geometric properties of the specimen. During DMA tests, frequency and temperature can both be incremented to measure the resulting response, and a master curve can be generated from these results by applying TTSP to identify dynamic mechanical properties the polymers. Some cases, a complete temperature sweep cannot be carried out due to temperature and frequency limitations, such as some

hydrogels always need to be immersed in water so experiments cannot be conducted at sub-zero temperatures. In those cases, varying ethanol concentration can be applied to effectively reduce the hydration level within the specimen and shift the curve to the left along the frequency axis to bring the glass transition temperature into the measurable range[23]. Reduced water concentration due to ethanol in the environmental chamber draws water from the hydrogel. According to Gosline and French[24], an elastomeric material (elastin) stiffened only 10% of water loss. Lillie and Gasoline[25] showed that varying solvent content in elastin shift the curves to the left along the frequency axis.

During the experiments, the dynamic mechanical testing was conducted using a custom-built DMA suitable for tensile tests on small, soft samples[15]. In the DMA, each resilin sample, synthesized from the recombinant proteins, was attached in a butt joint configuration to the pin head of an insect pin using a cyanoacrylate adhesive and accelerator (Loctite Super Glue and Loctite 712, Loctite, USA) and then the pin shaft was clamped to the shaft of an electromagnetic oscillator (2160B, Data Physics Corporation, UK). The other end of the resilin sample was then attached in a similar fashion to the head of a second pin attached to a force gage (Futek, USA). Some nominal force was applied to avoid slackness during the dynamic testing. A custom-made transducer was used to measure the displacement, where the oscillator shaft was attached to a stainless steel cantilever beam instrumented with two strain gages in a half-bridge configuration[15]. The dynamic mechanical properties of the resilin were measured by driving the oscillator with a custom, swept sine LabVIEW program (National Instruments, Austin), and the inducing force, and resulting displacements were recorded with a data acquisition card (PCI-4461, National Instruments, Austin) which is capable of simultaneous sampling. Both the displacement gage and force gage signals were amplified through an amplifier (PA30E, Data

Physics Corporation, UK) and then sent to the data acquisition card. A schematic diagram of the experimental setup[15] can be found in Fig. 2-1. A custom-made environmental chamber (water bath) was used to immerse the resilin sample in liquid for the duration of the testing, and also to control the temperature. A slit was made on each end of the water bath, sufficiently wide so the insect pins could move without friction, yet narrow enough so the surface tension would hold the water inside the chamber without leaking. Usually, surface tension can hold the water if the slit is less than 1.2 mm wide. However, the surface tension of ethanol is lower than the water. Consequently, ethanol started to leak through these slits, and leakage increased with increasing concentrations of ethanol. To prevent leakage of ethanol solutions, added high vacuum grease (Dow Corning, USA) was added to the outside the chamber slits, thereby leakage stopped around the slits without introducing friction on the insect pins during the dynamic testing. Accuracy of the instrument was verified by conducting an experiment on a silicone rubber sample both in this custom made unit and in a commercial DMA (TA Instruments Q800, New Castle, DE). The modulus from the custom made DMA was within 2.9% of the results from the commercial DMA at room temperature. Moreover, experiments conducted in both air and water for the silicone rubber using the custom made DMA to test the water drag and the moduli were within 2.3% at room temperature (supplementary information, Fig. A.1). Also, the effect of possible friction of the moving pin against the environmental chamber slit was tested by conducting two experiments, with and without the chamber in place. The resulting moduli were within 2.5%, suggesting that the effect of friction was insignificant (supplementary information, Fig. A.2).

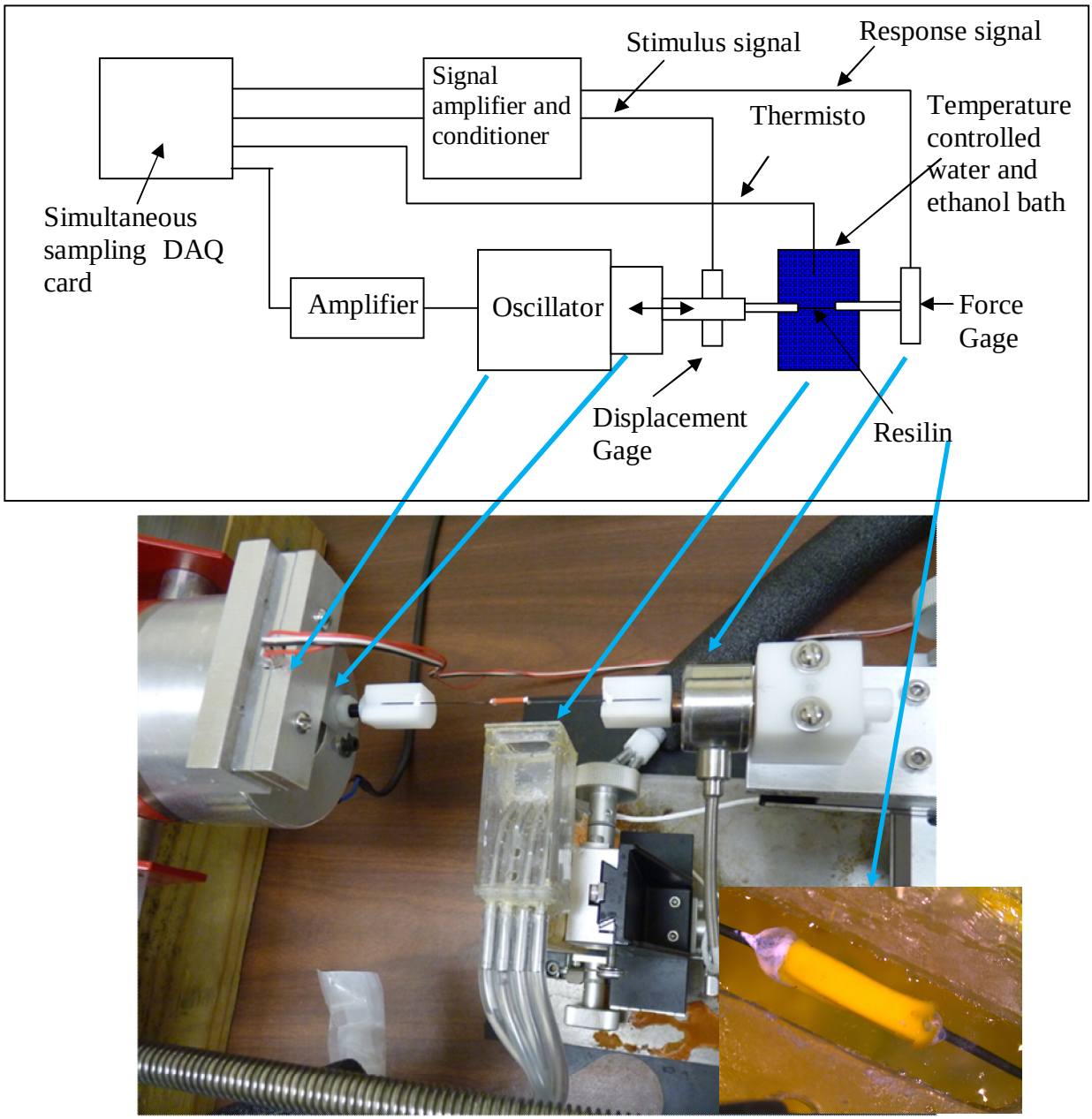

Fig. 2-1. Schematic and top view of the dynamic Mechanical Analyzer setup. The LabVIEW program drives the oscillator and converts the outputs from force and displacement gages to viscoelastic moduli. The water bath is shifted out of the way to see load train. A mounted resilin specimen is shown in the inset.

Data was collected by varying the temperature, frequency and ethanol concentration. Higher ethanol concentrations usually shift the master curve to the left so that the glass transition frequency moves into the measurable range[23]. Temperatures of the specimen chamber, also called water bath, were controlled by circulating an antifreeze-based coolant through four stainless steel tubes passing through the chamber. Coolant temperatures were controlled by a LAUDA RE206 temperature bath. Temperature in the water bath was recorded using a bead thermistor (Honeywell, USA). Multi-frequency data was taken at intervals every 5-6˚C apart within the range -5 to 65˚C, at constant ethanol concentration. It would be useful to conduct experiments at lower temperature, but due to instrument limitations, temperatures below -5˚C were not attempted.

During the experiment, temperature was increased from 2.3˚C to 57.4˚C for 0% ethanol and multi-frequency data was collected for every 5-6˚C interval. For 40% ethanol, water was replaced by 40% ethanol of room temperature in the chamber and allowed to reach thermal equilibrium at 57.4˚C, and then data was collected while temperature was decreased towards -1˚C. Similarly, temperature was changed from low to high for 65% ethanol, high to low for 73% ethanol and again low to high for 85% ethanol while multi-frequency data was collected at similar intervals of temperature. Though unconventional, this eliminated time required to return the re-circulating water bath to a fixed temperature. Anomalies could have resulted from this procedure, though no attempt was made to address this possibility.

At each temperature, data was recorded at discrete varying frequencies ranging from 1 Hz to 120 Hz at every 2 to 5 Hz. Ethanol concentration was diluted using distilled water, and we considered six different ethanol concentrations for our experiment: 0%, 40%, 65%, 73%, 85% and 95%. Stresses were calculated by dividing the load output by the cross sectional area

(measured while immersed in water at room temperature) of each sample, and measured actuator displacement were divided by the initial distance between pin heads to calculate the strains. Moduli were calculated from the ratio of stress and strain amplitudes during cyclic loading, and phase differences were obtained from the phase difference between displacement and load signals. Storage modulus, loss modulus and tan δ were calculated at each corresponding frequency and temperature. Master curves of the recombinant resilin were generated from the experimental data using time-temperature and time-concentration superposition to determine the properties of recombinant resilin over a wide range of frequencies. The results were compared with master curves obtained from the natural resilin of cockroaches[16] and dragonflies[15].

2.4 Results and Discussions

2.4.1 Plasmid Construction and Protein Purification. Total RNA was purified successfully from the pupae stage of Drosophila, the stage when the resilin was expressed[13]. Using RT-PCR, clone-1 (exon-1 + exon-2) was amplified and cloned in the T-A cloning vector pGEM followed by subcloning into the expression plasmid PColdI. After transforming the plasmid PColdI into *E. coli* strain BL21, and growing for 24 h at 15 °C, affinity chromatography with Ni-NTA was used to purify soluble protein. Following SDS-PAGE of clone-1, a single protein of approximately 47 kDa was observed (Fig. 2-2), which is similar to that obtained by Elvin et al. for exon-1[13]. The purity level of recombinant clone-1 resilin was very high as evident from the lack of substantial amounts of other proteins in lane 2.

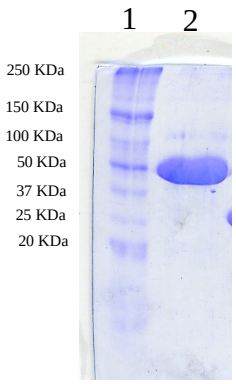

Fig. 2-2. Ni-NTA affinity purified resilin. Molecular masses of standards (lane 1) are shown at left of gel. Lane 2, highly purified resilin (15 μg) is visible at approximately 47 kDa.

2.4.2 Mass Spectrometry. Correct protein expression was verified on the protein gel using matrix-assisted laser desorption ionization-mass spectrometry (MALDI-MS). During the process, the SDS-PAGE was stained with Coomassie blue, and then the band was digested with trypsin. Analysis by MALDI-MS yielded detectable peaks shown in Fig. 2-3 and the peaks correspond to the peptide fragments shown in table 2.1, which were fragments of the expected amino acid sequence.

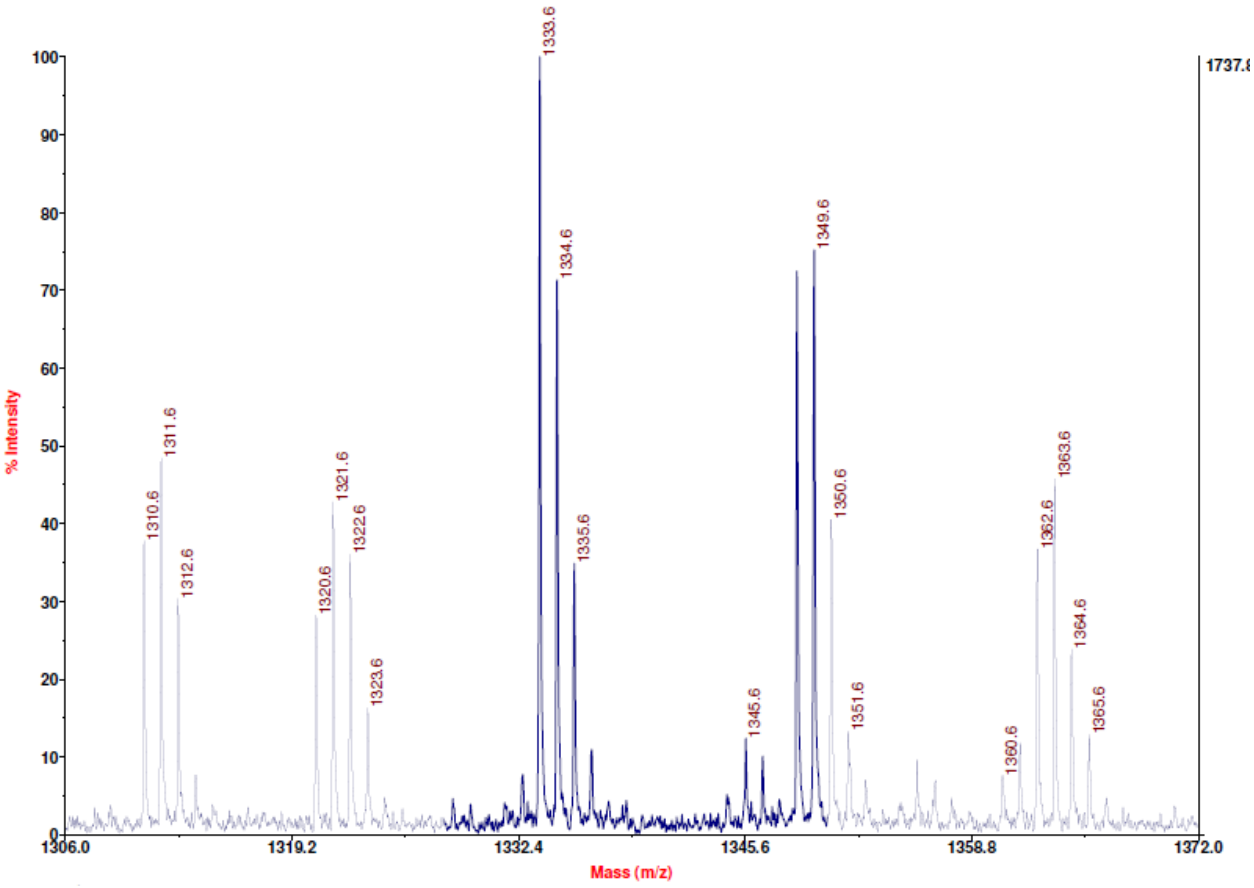

Fig. 2-3. Mass spectrum of peptides from mass spectrometry. From the different mass spectra, peptide sequences can be obtained.

Table 2-1. Protein sequence results from mass spectrometry. Range of amino acid residue indicates fragment under consideration with the corresponding mass/charge ratio and amino acid sequence shown in last column. The dots indicate the cleavage site of trypsin.

Range of amino acid residues of resilin	Monoisotropic mass, mass/charge (u/e)	Amino Acid Sequence
168-182	1310.6	R.SSSSYGAPGGGNGGR.P
101-115	1320.6	R.PSSSYGAPGGGNGGR.P
214-228	1320.6	R.PSSSYGAPGGGNGGR.P
296-310	1333.6	R.PSSSYGAPGSGPGGR.P
266-278	1348.6	R.PSDSYGAPGQNQK.P
45-59	1348.6	R.PSDSYGAPGGGNGGR.P
116-130	1362.6	R.PSDTYGAPGGGNGGR.P
183-197	1362.6	R.PSDTYGAPGGGNGGR.P

2.4.3 Crosslinking. A pilot study of chemical crosslinking was conducted on the soluble protein using the horseradish peroxidase. Crosslinking was verified by performing SDS-PAGE, as shown in Fig 2.4. Crosslinked protein was excluded from the gel due to increase in overall size of crosslinked protein. Crosslinked proteins also emitting blue light in response to exposure to UV light (data not shown), which was evidence of di-tyrosine crosslinking according to Elvin et al[13]. We tested crosslinking with and without superoxide dismutase which usually increases the crosslinking density[13], also with different concentration of proteins, and for all cases we got similar results. After the pilot study, solid hydrogel was cast in a 1mm x 1.5mm x 8mm PTFE mold.

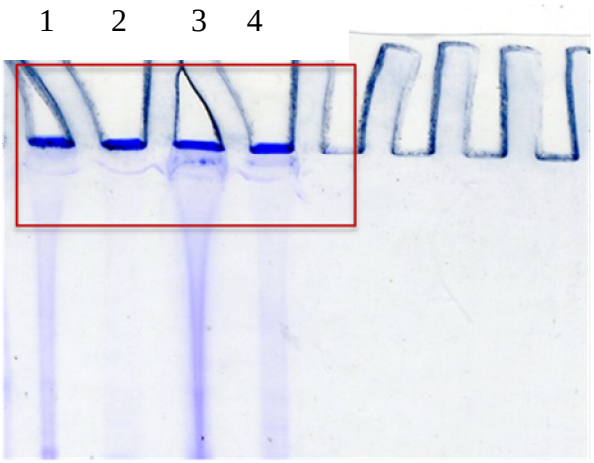

Fig. 2-4. Crosslinked resilin retained in wells of SDS-polyacrylamide gel. Lane 1, Resilin crosslinked without SOD (15 µg). Lane 2, Resilin crosslinked with SOD (15 µg). Lane 3, Resilin crosslinked without SOD (15 µg). Lane 4, Resilin crosslinked with SOD (15 µg).

2.4.4 Thermogravimetric Analysis (TGA). We conducted a thermogravimetric analysis on the resilin sample to calculate the water content. Our preparation of crosslinked resilin was approximately 80 wt% water based on the observed decrease from 100 wt% to the 20 wt% under the increasing temperature (Fig. 2-5). This value agrees with the theoretical calculations (weight of the solid hydrogel ≈ 20.56 mg, protein concentration = 200 mg/ml, volume of soluble protein used = 20 µl, and amount of protein added for crosslinking = 200mg/mg * 20 µl = 4 mg, resulting in a wt% of protein = (4* 100 /20.56) ≈ 19.45 %). There was another small drop from 20 wt% to 10 wt% above 250˚C (much larger than the water vaporization temperature), likely due to the dissociation of carbon bonds.

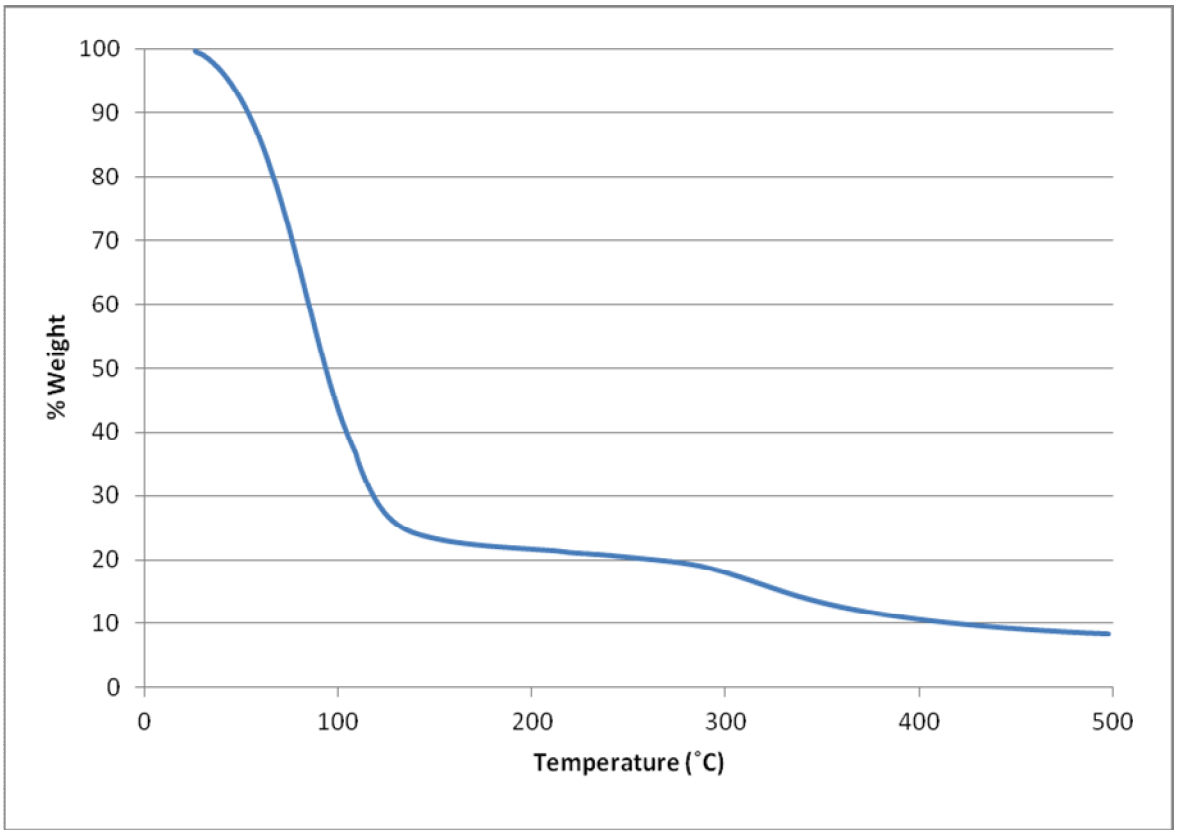

Fig. 2-5. Thermogravimetric analysis of solid resilin-like hydrogel suggested a water content of approximately 80 wt%.

2.4.5 Adhesive Properties. In some cases, adhesion of measurable strength is formed when a polymer above its glass transition temperature is brought into contact with a surface [26]. This adhesion property depends mainly on the interfacial and surface tensions, and viscoelastic properties of the polymer[27]. One of the common criteria for a material to show adhesive properties, known as Dahlquist criterion, is that the material's elastic modulus at an appropriate time scale needs to be on the order of 100 kPa[21] or less for a polymer to exhibit tack. A sufficiently high segmental mobility, and capability for large deformation to store and dissipate large amount of energy are also among the requirements to show good tack behavior[28]. However, even though some of the polymers meet the Dahlquist criterion, they don't necessarily show

adhesive behavior[29]. Another determining factor of adhesion is surface energy. If the surface energy of the substrate is low, it may not adequately wet a surface nor form strong adhesive bonds[30].

We measured the contact angle of the water drop on the surface of the hydrogel-like sample and calculated the work of adhesion from the contact angle and surface energy using Young-Dupre equation shown in the table 2.2. Values of the contact angles indicated that the surface of the hydrogel was hydrophilic in nature.

Table 2-2. Contact angle and work of adhesion for water droplet on the wet and dry sample, and Hexadecane drops on the dry sample.

Surface energy of water[31]			71.97	mJ/m^2 at 25˚C
Surface energy of Hexadecane[31]			27.05	mJ/m^2 at 25˚C
Wet sample in water				
Trials	Left angle	Right angle	Mean	W_{adh}, mJ/m^2
1	31.4˚	37.3˚	34.4˚	131.35
2	30.4˚	36.4˚	33.4˚	132.05
Dry sample				
Trials	Left angle	Right angle	Mean	W_{adh}, mJ/m^2
1	83.2˚	87.4˚	85.3˚	77.85
2	84.1˚	83.6˚	83.8˚	79.73
Dry sample in Hexadecane drops				
Trials	Left angle	Right angle	Mean	W_{adh}, mJ/m^2
1	8.1˚	9.8˚	9.0˚	53.77
2	8.1˚	10.6˚	9.4˚	53.74

Since the elastic modulus of the resilin-like hydrogel was below 100 kPa, satisfying the Dahlquist criterion, one would expect that resilin should be tacky, but the sample didn't show any sign of tack when probed with a stainless steel tweezer while in water, as well as on a sample freshly removed from water. One of the reasons might be due to the high water content in the sample (80wt%). So, whenever another surface is brought into contact with the sample, a water interlayer is energetically favored, preventing tack. According to Neuendorf et al.[32], due to the hydrophilic nature of the some polymer and significant degradation of the bond between the polymer and substrate occurring in an aqueous environment, these polymers don't exhibit adhesive properties. Reduction in bond strength of 80-90% was observed between the adhesive biopolymer and organic or inorganic substrate interfaces under prolonged presence of water vapor. Resilin-like hydrogels had 80wt% water and also hydrophilic in nature, as a result they might not form noticeable adhesive bonds.

2.4.6 Dynamic Mechanical Analysis. Using the experimental results of different ethanol concentrations, temperatures and frequencies from the DMA, we calculated the storage modulus (E'), loss modulus (E") and tan δ, and plotted against log of frequency. The master curves, obtained from these calculated values using TTSP, showed the effect of ethanol concentration, temperature and frequency on the viscoelastic properties of resilin (clone -1).

2.4.6.1 Temperature Shift. For 0% ethanol (100% water), we conducted the experiments every 5 to 6˚C within the temperature range from 3 to 59˚C, and plotted against the log of the frequencies. To develop the master curves, the data were shifted horizontally by distances corresponding to thermal shift factors, a_T, based on a reference temperature of 24.5˚C, following the principle of TTSP according to the Ferry[33], and the resulting master curve is shown in Fig. 2-6. With less than perfect data due to the small delicate samples and instrument, the E'

and E" curves were shifted simultaneously, visually monitoring both curves to obtain a compromise shift factor. Vertical shifts based on the ratio of absolute temperatures would result in a 15% (less than 0.07 decade) maximum shift, so were not deemed sufficient to necessitate their use. Density change shifts would be inappropriate, as the same number of chains pass through a given cross section regardless of temperature[34]. Still when vertical shift was considered using the temperature ratios, master curves did not show significant differences with confidence (Fig. A.4).

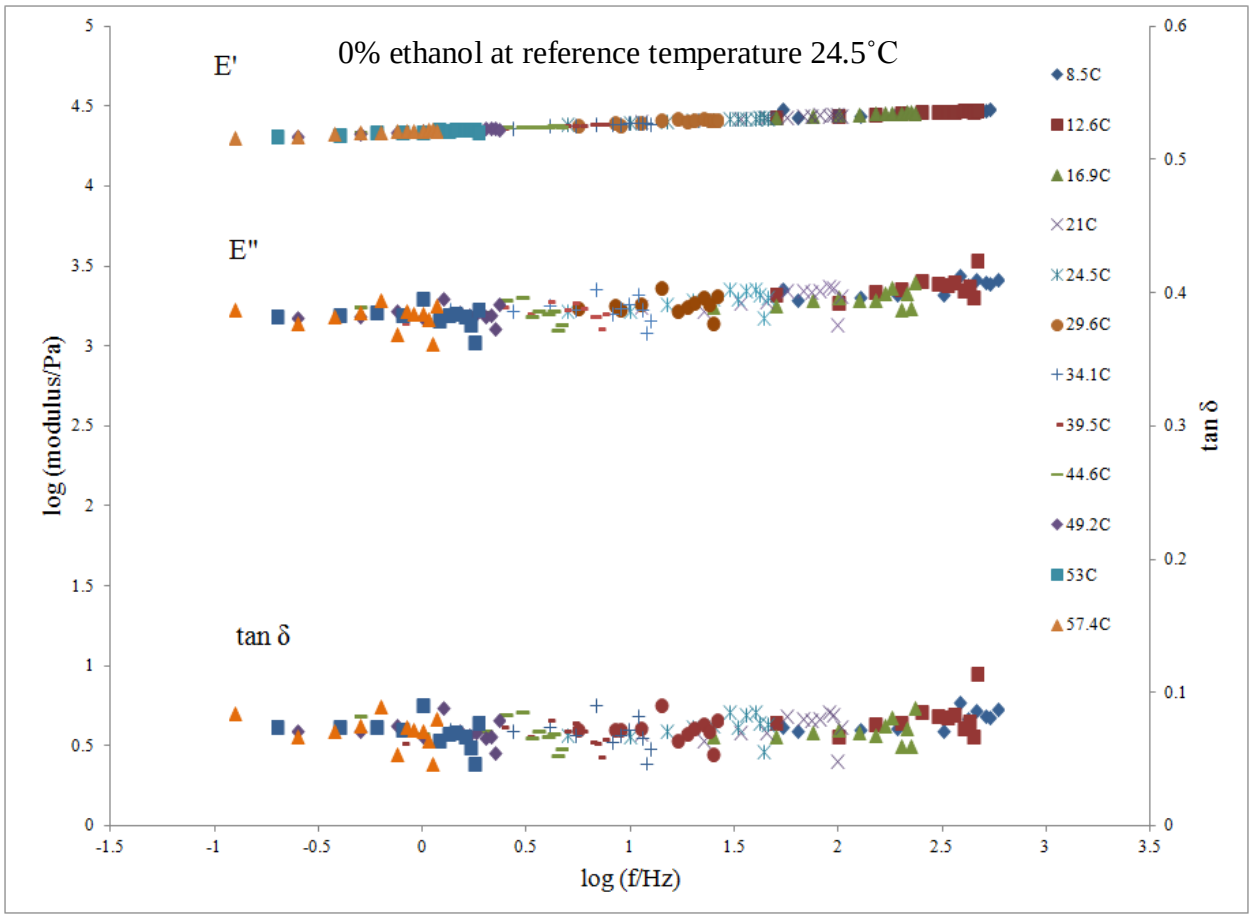

Fig. 2-6. Master curve obtained using the TTSP for storage modulus, loss modulus and tan δ at a reference temperature 24.5˚C for data obtained at 0% ethanol.

It was clear from the Fig. 2-6 that the resilin sample did not show any significant transition at 0% ethanol concentration over the temperature and frequency ranges tested, and substantially lower temperatures could not be imposed without freezing the surrounding water. The storage modulus was on the order of 26 kPa, well within the rubbery plateau with the reference temperature at 24.5˚C. The Williams-Landel-Ferry (WLF) equation was used to fit a_T at different temperatures and experimental results were consistent with the WLF equation for C_1 = 12, C_2 = 200˚C (Fig. 2-7). We also applied the Arrhenius equation to fit the shift factors and found a similar quality fit with an activation energy, E_a =98 kJ/mol (Fig. 2-7).

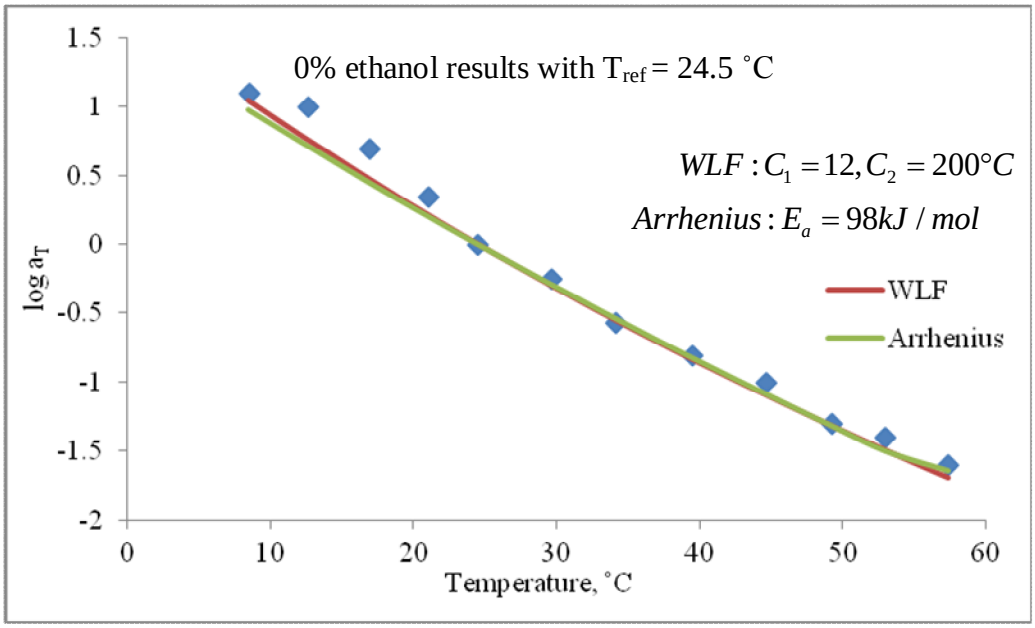

Fig. 2-7. Thermal shift factor, plotted against temperature for 0% ethanol, and WLF fit with the values C_1 = 12 and C_2 = 200˚C and Arrhenius fit with activation energy, E_a = 98 kJ/mol at reference temperature 24.5˚C.

As water freezes below 0˚C, and also due to some limitations of our experimental setup, the experiments could not be performed at sub-zero temperatures to characterize the transition from the rubbery to glassy state. Considering the temperature limitations, this superposition

technique can be extended by varying the diluent concentration without lowering the temperature[15, 25]. To determine the transition, additional experiments were conducted on the same specimen[1] as above, but immersed in 40%, 65%, 73%, 85% and 95 vol% of ethanol, and applied TTSP was applied to each case. As different concentrations of ethanol were used, the reduced water concentration in the water bath might draw water from the hydrogel, though no attempt was given to quantify this. Also, absorbed ethanol might act as a plasticizer or anti-plasticizer in the hydrogel, though no attempt was made to evaluate these possibilities, as the work was premised on successful shifting reported in the literature[15, 25]. The storage modulus data for 0%, 65%, 73% and 85% ethanol concentration cases are shown in Fig. 2-8. Results indicate that the resilin sample became stiffer with the increase of ethanol concentration and E' increased from 26 kPa at 0% ethanol to around 12.8 MPa at 85% ethanol, a change of nearly three orders of magnitude.

[I] Several specimens were used to debug the methods and once method was defined, complete frequency, thermal, and ethanol concentration scan experiments were conducted on the same sample. Thus, all results presented herein correspond to data obtained from one single specimen.

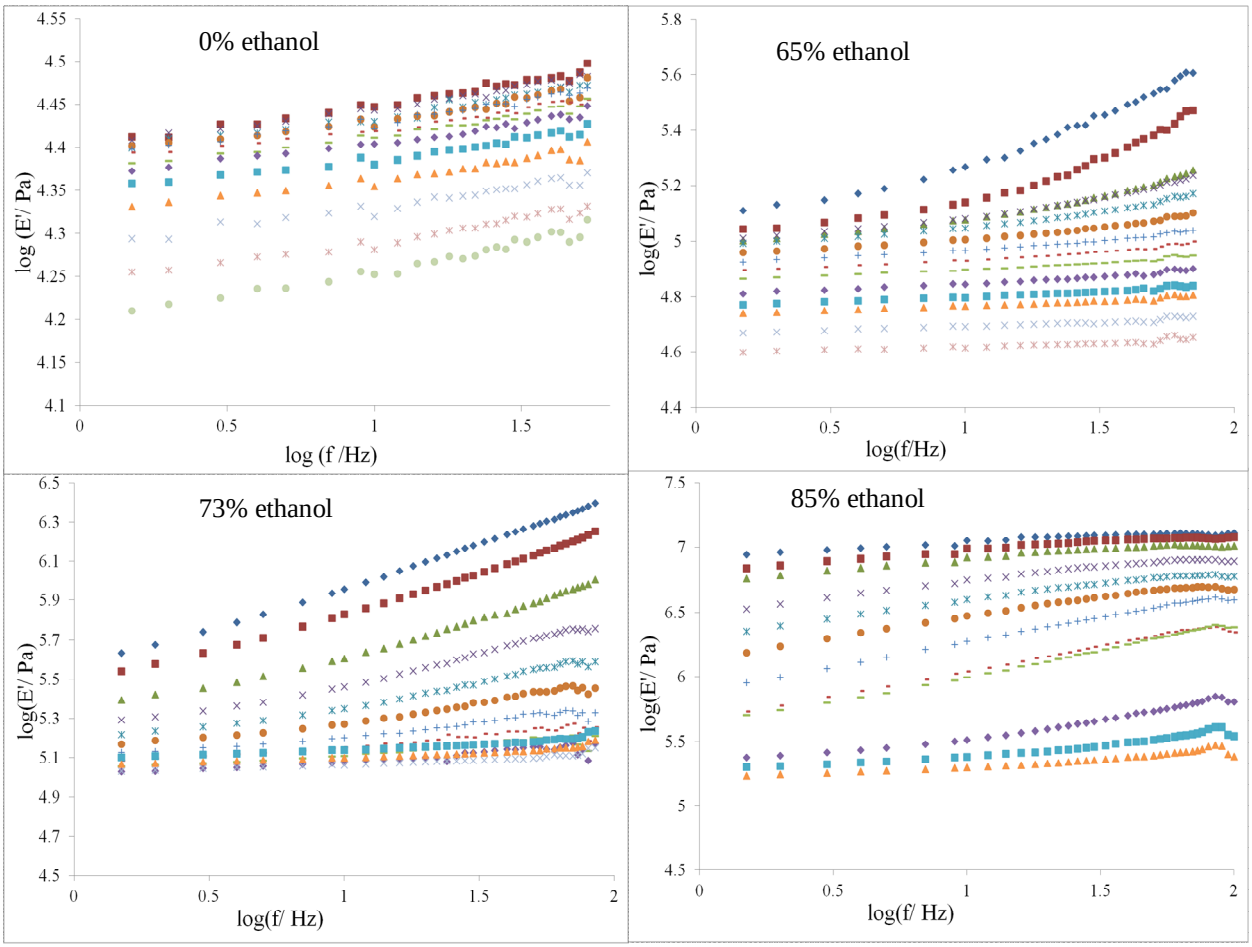

Fig. 2-8. Storage modulus against frequency plot for different ethanol concentrations in log-log scale for resilin-like hydrogel of clone-1.

From Fig. 2-8, it can be seen that there was a significant change in viscoelastic properties within the range of frequency and temperature tested associated with the change in ethanol concentration. Thermally shifted master curves were developed for each case using the TTSP by horizontally shifting E' and E" simultaneously to determine the appropriate thermal shift factors, a_T. Data above 70 Hz for some tests were erratic, perhaps due to resonance limitations with the instrument, so these results were not used nor retained in the shifted master curves. There were noticeable tan δ peaks only for the 73% and 85% ethanol cases. No vertical shifts were used for

reasons explained earlier, though potential volume changes associated with the varied ethanol content did raise potential issues. Master curves for 85% ethanol are shown in Fig. 2-9 with the reference temperature of 23.5˚C, and tan δ peak can be approximately identified around $10^{1.28}$ Hz with a storage modulus of 1.1 MPa. However, the modulus at the upper plateau seems two orders of magnitude lower than expected glassy plateau for a solid polymer. Two possible interpretations will be discussed below.

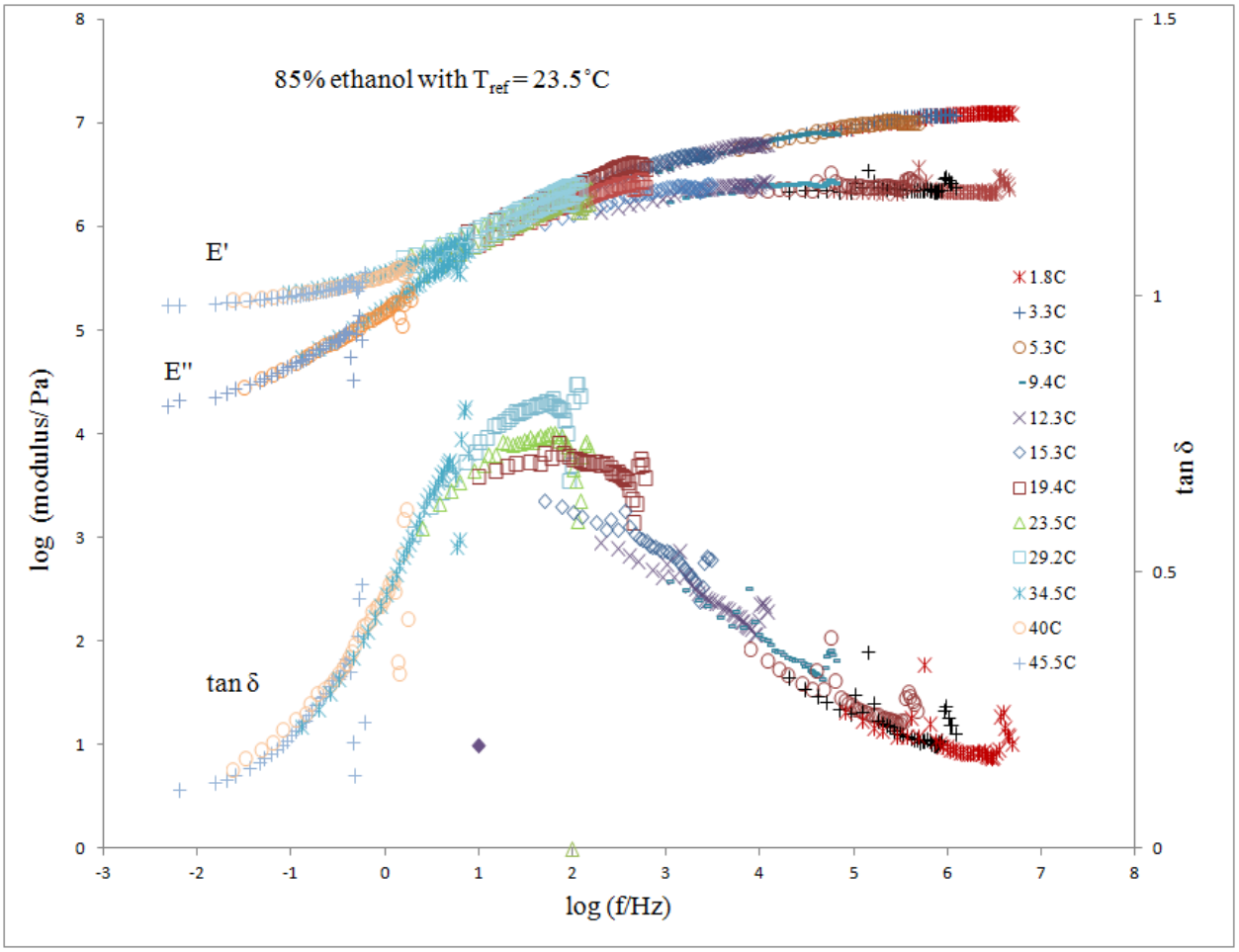

Fig. 2-9. Master curves of storage modulus, loss modulus and tan δ for 85% ethanol concentration using TTSP with the reference temperature 23.5˚C for clone-1.

Thus, it is clear from Fig 2.9 that high ethanol concentrations can drive the resilin sample to go through some transition. Master curves were generated for each ethanol-water combination using TTSP, and in every case the thermal shift factor was well fit with appropriate choices of constants for the respective WLF and Arrhenius equation fits of the data. Table 2.3 shows the values of C_1 and C_2 for WLF equation fits and activation energies for Arrhenius fits of the thermal shift factors, along with frequencies at the approximate peak of the tan δ plots.

Table 2-3. WLF constant values and activation energy for different ethanol concentrations and peak frequency from the tan δ plots which involve transitions from one state to another for resilin-like hydrogels of clone-1.

% Ethanol	Temp. range (˚C)	C_1	C_2 (˚C)	Arrhenius E_a (kJ/mol)	Ref Temp. (˚C)	tan δ peak (Hz)
0	2.3 to 57.4	12	200	98	24.5	
65	-1 to 48	25	175	217	23.9	
73	2 to 46.1	11.2	112.8	183	26.4	$10^{4.5}$
85	1.8 to 45.5	8.9	70.1	240	23.5	$10^{1.3}$

The master curves, obtained from the different ethanol concentrations including the peak values determined by TTSP, were based on the ethanol concentration only. To determine the resilin properties similar to their native state, we developed one single doubly-shifted master curve using all the ethanol concentration data and applied time concentration superposition[35] based on the 0% ethanol (i.e. 100% hydration in water) results with a reference temperature of 24˚C (Fig. 2-10). Combined shift factors ($a_{Tc} = a_T \cdot a_c$) for different ethanol concentrations are shown in Fig. 2-11, where a_T corresponds to the temperature shift factor and a_c corresponds to concentration shift factor. From the Fig. 2-10, we can see that the tan δ peak is approximately at 10^{15} Hz with a storage modulus of 1.1 MPa. The modulus at the stiffer plateau is much lower

compared to the accepted modulus for this transition to be the glass transition[36]. This transition occurs multiple decades beyond the natural frequencies of the resilin in insect usage, as shown in the doubly-shifted master curve using TTCSP (Fig 2.10). The highest frequency reported for resilin usage in insects was measured for Cicada at 13 kHz[9], while for the clone-1 transition occurs at 10^{15} Hz in room temperature, which means the resilin operates at frequencies well below the measured transition frequency, at least at room temperature. Results indicate that the functioning temperature affects the mechanical properties of resilin. However, the glass transition frequency is about 11 decades beyond the highest operation frequency reported for natural resilin. According to Fig. 2.7, the maximum shift from 24.5˚C to 0˚C would be about 2 decades. Therefore, even near freezing temperatures, the transition frequency would still be 9 decades beyond the use frequencies, assuming hydrated conditions, leaving resilin well within the rubbery regime and allowing it to function over a range of temperatures for insects without significant effect on the mechanical properties.

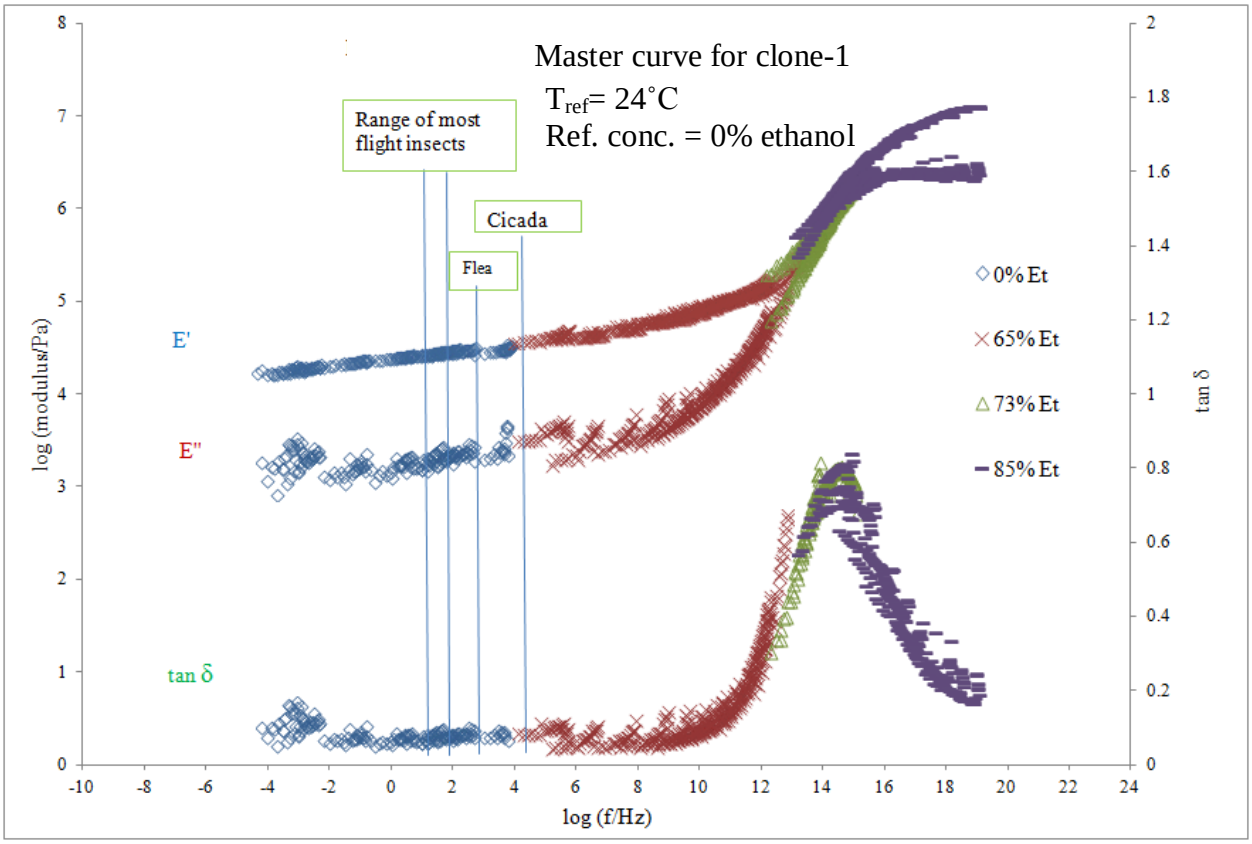

Fig. 2-10. Doubly shifted master curve of storage modulus, loss modulus and tan δ for clone-1 of resilin based on 0% ethanol concentration (100% water) using TTCSP with the reference temperature 24˚C.

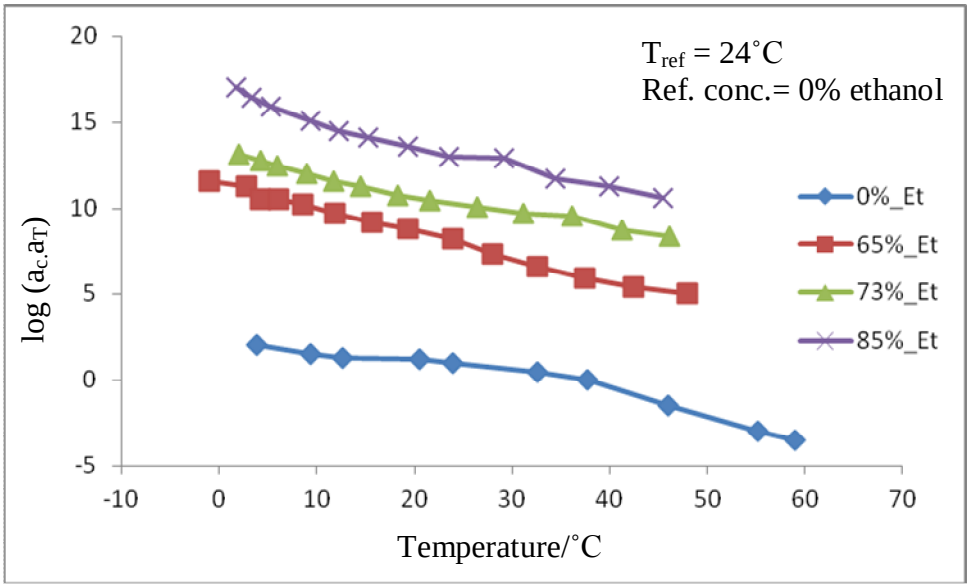

Fig. 2-11. Total shift factor $a_c.a_T$ plotted against temperatures for different ethanol concentrations for clone-1 with T_{ref} = 24˚C.

As there is a peak in the doubly-shifted tan δ plot, the resilin sample was clearly going through a transition from one state to another state. According to Mullar et al.[37], materials with viscoelastic properties sometimes exhibit thermorheologically complex behavior due to some additional relaxation process caused by reversible hydrogen bonds, and can display a transition within the rubbery plateau. Also, during our previous molecular simulation study on the repeating motifs of resilin[38-39], it was observed that intramolecular hydrogen bonds might influence the properties of resilin in different functions[39]. Adhikary et al.[40] and Takano et al.[41] also reported the contribution of the intramolecular hydrogen bonds on the stability of protein conformations. Thus, one explanation for the transition experienced by resilin during our experiments could result from disruption of intramolecular hydrogen bonds. On other hand, even though the plateau modulus is much smaller than expected for glassy behavior, the transition involved a modulus increase on the order of three decades, which is typical of glass transitions.

This would make this consistent with the transition corresponding to a T_g, and is considerably larger than mentioned by Muller et al.[37] for hydrogen bonds, where the storage modulus increased by only one order of magnitude. Another interpretation is that this transition corresponds to the glass transition frequency, with the abnormally low modulus resulting from the swelling due to the very high water content (ca. 80%).

Diluent molecules can diffuse into a polymer and effectively plasticize the material by increasing the free volume, though in some cases diluents can act as an anti-plasticizer due to the strong interactions with specific functional groups[42]. As the diluent concentration increases, however, the additional effect of additional diluent is often reduced, as diluent molecules are partially shielded from the polymer molecules by the strongly bound diluent molecules and become loosely bound. At sufficiently high concentrations, as reported by Roy et al.[43] for proton exchange membranes, some water molecules effectively act as free water, occupying free volume or even voids within materials. Thus, initial diluent molecules are often very effective as plasticizing a polymer, though has less effect on swelling, whereas additional diluent at higher concentrations yields less plasticization but more efficient swelling.

With 80% water, these resilin-like hydrogels samples were highly swollen, thus reducing the number of polymer molecules per unit area, resulting in a lower modulus than would be expected for a solid polymer[44]. According to Okay[45] and Schausberger et al.[46], the modulus of the diluted polymer (E_{dp}) can be described using a power law relationship between modulus of the undiluted polymer (E_{up}) and the volume fraction of the entangled or crosslinked polymer (υ_p) within the rubbery state ($E_{dp}/ E_{up} = \upsilon_p^x$, where the exponent x determines the dependence of modulus on polymer fraction. For Okay[45], x=2.1±0.1 & Schausberger et al.[46], x = 2). For diluted polymers, the exponent was much higher than linear dependency (x=1) on the polymer fraction

predicted according to theory of linear elasticity[47]. Considering 20% polymer fraction in the hydrogel, the modulus would be only 3.4% of the expected modulus ((polymer fraction)$^{2.1}$x 100% = 3.4%), and this effectively closes the modulus discrepancy. It is not clear, however, how relevant the power law relationship and exponents are as one goes from the rubbery to the glassy state, so the validity of this extension is questionable. If one assumes the observed transition results from intramolecular hydrogen bonds within the rubbery plateau, then there would be another transition from the rubbery state to glassy state and shift, likely resulting in a much higher than expected modulus of a solid polymer in the glassy state (typically about 3GPa[36])).

ChBD (exon-2) usually forms β-plated sheets[48], while exon-1 is mostly unstructured[11]. Another possible explanation for the observed transition is that, due to the presence of ethanol, the secondary structure of the chitin binding domain (ChBD) in the clone might change, taking on more ordered conformations that could restrict molecular mobility as increasing crystallinity does in semi-crystalline polymers. Moreover, ethanol is less cohesive than water and could cause additional intramolecular hydrogen bonds in the hydrogel; exon-1 might change the secondary structure from random coil to more ordered conformation[49]. Consequently, the observed transition could possibly occur due to the effects of increased order organization within the hydrogel. The current study does not permit definitive determination of the mechanism(s) responsible for the observed transition and more study is needed to understand the very pronounced temperature and rate-dependent transition observed at increased ethanol concentrations.

2.4.6.2 Effect of Ethanol. According to Lillie et al.[25], the higher ethanol concentration results in only a shift of the master curve to the left, moving the glass transition frequency into the experimentally measurable frequency range. During the experiments, we observed different

sections of what became the master curves with an increase of ethanol concentration and consequently the sample became stiffer (Fig. 2-10) within the experimental frequency and temperature window. In an attempt to better understand effects on specimen dimensions and mechanisms responsible for the retarding effect of ethanol, the static loads were measured at every temperature for each ethanol concentration. Fig. 2-12 reveals that static loads increased with increasing ethanol concentration, apparently offsetting specimen shrinkage since the ends of the hydrogels were attached to fixed ends. (As the length was kept constant, the stress-free gage length of the specimen could have decreased with ethanol-induced shrinkage, effectively increasing the actual strains beyond the nominal applied strain amplitude. Failure to capture the relevant experimental details prevented any corrections in the reported moduli, and these are expected to be small based on the relatively modest increases in static load levels, especially at higher test temperatures.) Moreover, the amplitudes for 73% and 85% ethanol concentrations at lower temperature were lower than the applied amplitude during the dynamic mechanical testing due to increased modulus of hydrogels and instrument capabilities, but these actual measured amplitudes were used to calculate the moduli.

The addition of ethanol caused reduced water concentrations in the water bath and this might draw some water from the resilin-like hydrogel and change the stiffness of the hydrogel, though the percent of change in absorbed water content was not determined. The static loads increased significantly with a decrease in temperature at all ethanol concentrations tested (Fig. 2-12), which was in stark contrast to the 0% ethanol case. This could suggest a change in interactions of ethanol with the protein's functional groups and/or a change in solubility of water and/or ethanol within the hydrogel as a function of temperature. The ethanol might also act as

either a plasticizer or an anti-plasticizer within the hydrogel, which would change the modulus of the sample. Again, no definitive role has been determined.

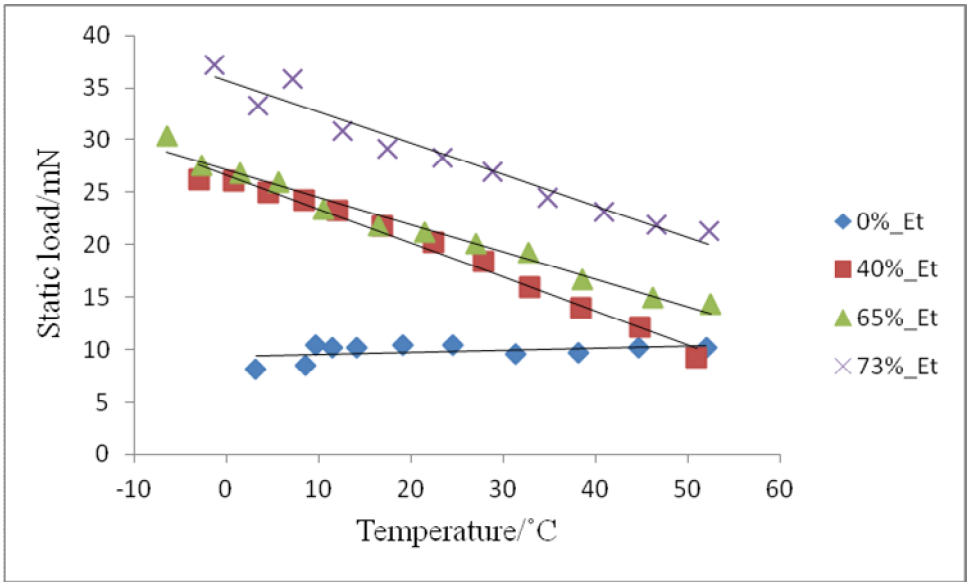

Fig. 2-12. Static loads at different temperature and ethanol concentration. Static load changed drastically at different ethanol concentrations.

2.4.6.3 Comparison with the Natural Resilin. The properties of recombinant resilin were compared with similar properties of natural resilin obtained from locusts[6] and dragonflies[15] in water (Fig. 2-13). Andersen et al.[6] reported that resilience of the locusts prealar arm resilin were 95% at 15 Hz, while according to King[15], dragonflies resilin's resilience were 99% at 15 Hz, and we found that the resilience of recombinant resilin from clone-1 was 90% at 15 Hz (tan δ = 0.07) in water at room temperature (According to Ferry[33], Resilience, $R = e^{-(\pi/2)\tan\delta}$). The storage modulus of recombinant resilin from clone-1 was almost 1.5 decades lower than that of locusts and dragonflies resilin. But, the loss modulus of the clone-1 resilin was higher than the dragonfly but lower than the locust resilin, while the lowest tan δ was observed for dragonfly resilin. The clone-1 resilin structure was more similar to locust than dragonfly resilin, because both clone-1

and locust resilin had ChBD within their amino acid sequence, whereas dragonfly resilin does not. The stiffness of ChBD is much higher than resilin, and the resulting resilin-like hydrogel behaves like a composite with the ChBD[14]. The loss modulus (E') and tan δ for the clone-1 resilin was constant over the measured frequency range in water, while they were increasing for locust resilin, and that might be due to the absence of exon-3 in the clone-1 resilin.

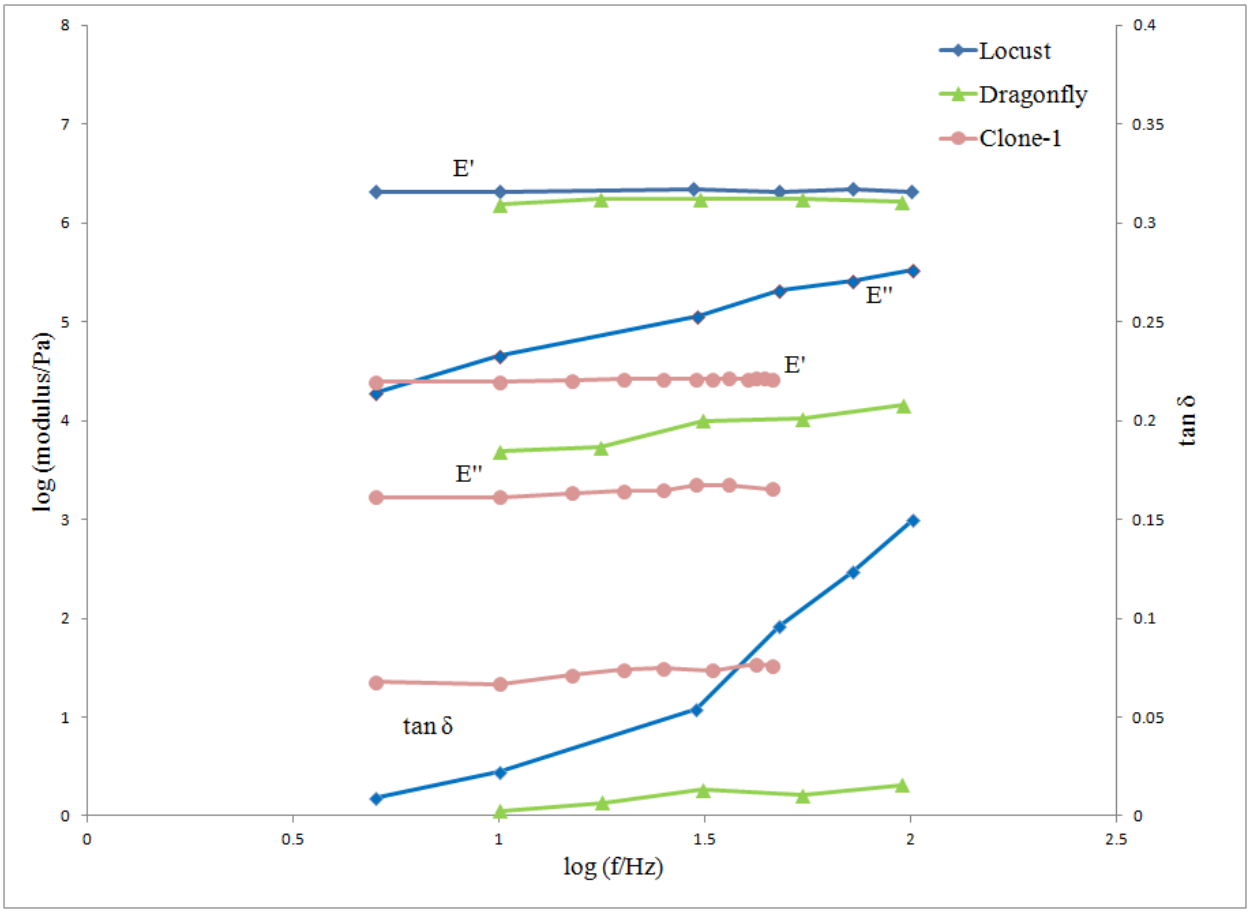

Fig. 2-13. Comparison of E', E" and tan δ between the locust, dragonfly and recombinant resilin (Clone-1) between 5 to 100 Hz in water.

We compared the master curve for the storage modulus of clone-1 resilin with the master curve of natural dragonfly resilin (both at 65% ethanol concentration[15]), and with the master

curve of a cockroach's natural resilin (both at 73% ethanol concentration[16]). The storage modulus for the clone-1 resilin was almost 1.5 decades lower than that of natural dragonfly resilin (Fig. 2-14(a)). The storage modulus of clone-1 was also around 1.5 decades lower than cockroach resilin at low frequencies, but at higher frequencies, the values became more similar (Fig. 2-14(b)). The structure of clone-1 is similar with natural resilin from cockroaches and locusts resilin, in that all three have ChBD in the protein sequence.

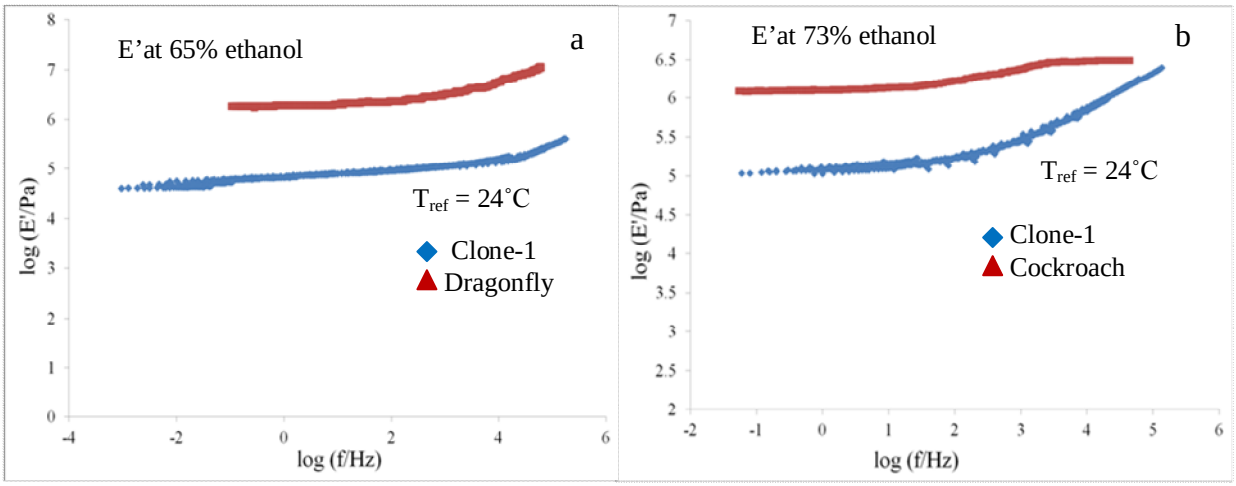

Fig. 2-14. Comparison of the storage modulus master curves between (a) Clone-1 and dragonfly resilin at 65% ethanol concentration (b) Clone-1 and cockroach resilin at 73% ethanol concentration.

2.4.7 Experimental Limitations. There were some concerns about the experiments. One of them was the noise in the data, and that might be due to some electric noise or other sources. Another concern was the high evaporation rate of ethanol. We used an open system for our experiment, and due to the high evaporation rate, there was a concern with maintaining the constant ethanol concentration, especially at 85% and 90% concentrations. This was partly reduced by covering most of the environment chamber. Future studies should carefully track the

stress-free length of the specimen to further elucidate dimensional changes in the presence of ethanol.

2.5 Conclusion

Recombinant resilin from clone-1 (exon-1 + exon-2) was successfully synthesized, crosslinked, and characterized. TGA results showed that the crosslinked sample contained 80wt% water. The hydrophilic nature and high water content may have precluded appearance of tack, as surface energetics may not have favored wetting of a probe, even though the material was soft enough to satisfy the Dahlquist criterion. DMA was conducted on the recombinant resilin sample to determine the dynamic mechanical properties, comparing these results with those of natural resilin from locust, dragonfly and cockroach. Doubly shifted master curves, based on application of the time temperature concentration principle (TTCSP), were formed with data collected over a frequency range at selected temperatures and ethanol concentrations. DMA results showed that the storage modulus was about 1.5 orders lower than that of natural resilin, and the master curves were more similar to locust and cockroach resilin properties, perhaps because the clone is more similar to these materials (which all contain ChBD) than to dragonfly resilin. The resilience of the resilin-like hydrogel sample was around 90% at 15Hz in water, and that was close to that reported for natural resilin from locust.

In the master curves developed from the DMA results, a pronounced transition was seen based on the peak of tan δ plot and over 100-fold increase in the storage modulus. Although prior literature has referred to this as a glass transition in resilin, other explanations may also be considered. Because the storage modulus at the stiffer plateau is much lower than the accepted modulus of glassy polymers, one possibility is that this transition is associated with the intramolecular hydrogen bonds predicted in molecular simulation of the repeat motif of resilin[39],

and also Mullar et al.[37] noticed a similar kind of transition due to the hydrogen bonds on polybutadiene within the rubbery plateau. On the other hand, the transition involved a storage modulus change spanning at least two orders of magnitude, which could suggest a true glass transition, albeit with the upper plateau modulus substantially lowered (modulus as low as 3.4% of that of the undiluted polymer) because of reduced chain density due to swelling at such high water content in the resilin-like hydrogel[45-46]. Moreover, if there exist another transition from rubbery to glassy state, modulus could be higher than accepted glassy moduli. Another possibility is that due to the presence of the less cohesive ethanol absorbed in the specimen, ChBD and exon-1 might change the secondary structure, increasing the modulus through more organized conformations or crystalline effects. More experiments are needed to conclusively determine the specific mechanism(s) responsible for the pronounced transition. Nonetheless, these findings of the recombinant resilin and comparable results with the other natural resilin may provide a better understanding of the structure and properties, which could eventually lead to tailoring the properties for specific biomedical applications.

References

1. T. Weis-Fogh, A rubber-like protein in insect cuticle. *Journal of Molecular Biology*, 1960, **37**, 889-907.
2. T. Weis-Fogh, Molecular interpretation of the elasticity of resilin, a rubber-like protein. *Journal of Molecular Biology*, 1961, **3**, 648-667.
3. R. E. Lyons, Lesieur, E., Kim, M.,Wong, D.C.C., Huson, M.G., Nairn, K. M., Brownlee, A. G., Pearson, R. D., Elvin, C. M., Design and facile production of recombinant resilin-like polypeptides: gene construction and a rapid protein purification method. *Protein Engineering, Design & Selection*, 2007, **20**, 25-32.
4. D. Young and H. C. Bennet-Clark, The role of tymbal in cicada sound production. *Journal of Experimental Biology*, 1995, **198**, 1001-1019.
5. S. J. Edwards, Predation and digestion in assassin bugs (Heteroptera, Reduviidae. University of Cambridge, UK, 1960.
6. S. O. Andersen and T. Weis-Fogh, Resilin. A rubber-like protein in arthropod cuticle. *Advances in Insect Physiolology*, 1964, **2**, 1-65.
7. D. Neff, S. F. Frazier, Identification of resilin in the leg of cockroach, Periplaneta americana: confirmation by a simple method using pH dependence of UV fluorescence. *Arthropod Structure and Development*, 2000, **29**, 75-83.
8. R. Kram, B. Wong, Three-dimensional kinematics and limb kinetic energy of running cockroaches. *Journal of Experimental Biology*, 1997, **200**, 1919-1929.
9. H. C. Bennet-Clark, Daws, A. G., Transduction of mechanical energy into sound energy in the cicada Cyclochila australasiae. *The Journal of Experimental Biology*, 1999, **202**, 1803-1817.

10. N. Skals, Surlykke, A., Sound production by abdominal tymbal organs in two moth species: the green silver-line and the scarce silver-line (Noctuoidea: Nolidae: Chloephorinae). *Journal of Experimental Biology*, 1999, **202**, 2937-2949.
11. G. Qin, Hu, X., Cebe, P. and Kaplan, D. L., Mechanism of Resilin Elasticity. *Nature Communication*, 2012, **3**, 1-18.
12. G. F. Elliott, A. F. Huxley and T. Weis-Fogh, On the structure of resilin. *Journal of Molecular Biology*, 1965, **13**, 791-795.
13. C. M. Elvin, A. G. Carr, M. G. Huson, J. M. Maxwell, R. D. Pearson, T. Vuocolo, N. E. Liyou, D. C. C. Wong, D. J. Merritt and N. E. Dixon, Synthesis and properties of crosslinked recombinant pro-resilin. *Nature*, 2005, **437**, 999-1002.
14. G. Qin, S. Lapidot, K. Numata, X. Hu, S. Meirovitch, M. Dekel, I. Podoler, O. Shoseyov and D. L. Kaplan, Expression, Cross-Linking, and Characterization of Recombinant Chitin Binding Resilin. *Biomacromolecules*, 2009, **10**, 3227–3234.
15. R. King, Dynamic Mechanical Properties of Resilin. Master's, Virginia Polytechnic Institute and State University, 2010.
16. U. Choudhury, Dynamic Mechanical Properties of Cockroach (Periplaneta americana) Resilin. Master's Thesis, Virginia Polytechnic Institure and State University, 2012.
17. F. W. Studier, Protein production by auto-induction in high density shaking cultures. *Protein Expression & Purification*, 2005, **41**, 207–234.
18. D. A. Malencik and S. O. Anderdon, Dityrosine Formation in Calmodulin: Cross-Linking and Polymerization Catalyzed by *Arthromyces* Peroxidase. *Biochemistry*, 1996, **35**, 4375-4386.

19. D. A. Fancy and T. Kodadek, Chemistry for the analysis of protein- protein interations : rapid and efficient cross-linking triggered by long wavelength light. *PNAS*, 1999, **96**, 6020-6024.
20. S. S. Nielsen, Food Analysis. 4th edn., Springer, 2010.
21. C. Creton, Pressure-Sensitive Adhesives: An Introductory Course. *MRS Bulletin*, 2003, **28**, 434-439.
22. M. E. Schrader, Yound-Dupre Revisited. *Langmuir*, 1995, **11**, 3585-3589.
23. Y. I. Matveev, V. Y. Grinberg, I. V. Sochava and V. B. Tolstoguzov, Glass transition temperature of proteins. Calculation based on the additive contribution method and experimental data. *Food Hydrocolloids*, 1997, **11**, 125-133.
24. J. M. Gosline and C. J. French, Dynamic mechanical properties of elastin. *Biopolymers*, 1979, **18**, 2091-2103.
25. M. A. Lillie and J. M. Gosline, The effects of hydration on the dynamic mechanical properties of elastin. *Biopolymers*, 1990, **29**, 1147-1160.
26. A. Zosel, Adhesion and Tack of Polymers: Influence of Mechanical Properties and Surface Tensions. *Colloid & Polymer Science*, 1985, **263**, 541-553.
27. A. Zosel, Adhesive Failure and Deformation Behaviour of Polymers. *Journal of Adhesion*, 1989, **30**, 135-149.
28. C. Gay, Stickiness – Some Fundamentals of Adhesion. *Integrative and Comparative Biology*, 2002, **42**, 1123-1126.
29. A. M. Grillet, N. B. Wyatt and L. M. Gloe, ed.^eds., InTech Europe, Dr. Juan De Vicente (Ed.) edn., 2012, p.^pp.

30. M. Barquins and J. Cognard, Adhesion Characteristics of Gold Surfaces. *GoldBull*, 1986, **19**, 82-86.
31. G. Storm, M. Fredriksson and P. Stenium, Contact Angles, Work of Adhesion, and Interfacial Tensions at a Dissolving Hydrocarbon Surface. *Journal of Colloid and Interface Science*, 1986, **119**, 352-361.
32. R. E. Neuendorf, E. Saiz, A. P. Tomsia and R. O. R.O. Ritchie, Adhesion between biodegradable polymers and hydroxyapatite: Relevance to synthetic bone-like materials and tissue engineering scaffolds. *Acta Biomaterialia*, 2008, **4**, 1288–1296.
33. J. D. Ferry, Viscoelastic Properties of Polymers. Wiley, New York, 1980.
34. Y. Wada and H. Hirose, Glass Transition Phenomena and Rheological Properties of Petroleum Asphalt. *Journal of Physical Society of Japan*, 1960, **15**, 1885–1894.
35. K. A. Patankar, D. A. Dillard, S. W. Case, M. W. Ellis, Y. H. Lai and C. S. Gittleman, Linear Hygrothermal Viscoelastic Characterization of Nafion NRE 211 Proton Exchange Membrane. *Fuel Cells*, 2012, **12**, 787-799.
36. D. Roylance, ed.^eds., Cambridge, 2001, p.^pp. Massachusetts Institute of Technology: MIT OpenCourseWare.
37. M. Muller, U. Seidel and R. Stadler, Influence of hydrogen bonding on the viscoelastic properties of thermoreversible networks: analysis of the local complex dynamics. *Polymer*, 1995, **36**, 3143-3150.
38. M. S. Khandaker, D. M. Dudek, E. P. Beers, D. A. Dillard and D. R. Bevan, Molecular Modeling on the Elastomeric Properties of Repeating Motifs of Disordered Elastomeric Proteins. in prep.

39. M. S. Khandaker, D. M. Dudek, D. A. Dillard, E. P. Beers and D. R. Bevan, Molecular Modeling of the Elastomeric Properties of Repeating Units and Building Blocks of Resilin, a Disordered Elastic Protein. *Journal of the Mechanical Behavior of Biomedical Materials*, in review.

40. R. Adhikary, J. Zimmermann, J. Liu, R. P. Forrest, T. D. Janicki, P. E. Dawson, S. A. Corcelli and F. E. Romesberg, Evidence of an Unusual N−H···N Hydrogen Bond in Proteins. *Journal of Americal Chemical Society*, 2014, **136**, 13474−13477.

41. K. Takano, Y. Yamagata, J. Funahashi, Y. Hioki, S. Kuramitsu and K. Yutani, Contribution of intra- and intermolecular hydrogen bonds to the conformational stability of human lysozyme. *BioChemicstry*, 1999, **38**, 12698-12708.

42. E. B. Stukalin, J. F. Douglas and K. F. Freed, Plasticization and antiplasticization of polymer melts diluted by low molar mass species. *Journal of Chemical Physics* 2010, **132**.

43. A. Roy, M. A. Hickner, T. Glass, Y. Li, B. Einsla, K. B. Wiles, X. Yu and J. E. McGrath, States of water- investigating the water-polymer interactions and transport phenomenon in proton exchange membranes. *Preprints of Symposia - American Chemical Society*, 2005, **50**, 699-700.

44. A. Roy, Structure Property Relationships of Proton Exchange Membranes. Virginia Poylechnic Institute and State University, 2008.

45. O. Okay, in *Hydrogel Sensors and Actuators*. eds. G. Gerlach and K. F. Arndt, Springer Berlin Heidelberg, 2010, vol. 6, pp. 1-14.

46. A. Schausberger and I. V. Ahrer, On the time-concentration superposition of the linear viscoelastic properties of plasticized polystyrene melts using the free volume concept. *Macromolecular Chemistry and Physics*, 1995, **196**, 2161-2172.

47. P. J. Flory, Principles of Polymer Chemistry. First edn., Cornell University Press, Ithaca, United States 1953.

48. S. J. Hamodrakas, J. H. Willis and V. A. Iconomidou, A structural model of the chitin-binding domain of cuticle proteins. *Insect Biochemistry and Molecular Biology*, 2002, **32**, 1577–1583.

49. L. Li, T. Luo and K. L. Kiick, Temperature-triggered phase separation of a hydrophilic resilin-like polypeptide. *Macromolecule Rapid Communications*, 2015, **36**, 90-95.

Chapter 3: Investigation on the Functions of Exons and Chitin Binding Domain (ChBD) on the Mechanical Properties of Resilin

3.1 Abstract

The results are reported from an investigation of the functions of the different exons on the mechanical properties of resilin which can be found in insect cuticles where high resilience and low stiffness are required. Various segments of the fruit fly resilin gene are cloned and recombinant proteins are purified from different exons of the fruit fly resilin gene, including the full length resilin. Doubly-shifted, complex moduli master curves are developed from dynamic mechanical analysis (DMA) results of resilin-like hydrogels using the time-temperature superposition principle (TTSP) and time-temperature concentration superposition principle (TTCSP), and compared to results reported for natural resilin. The resulting master curves show that the resilin-like hydrogels of each clone undergo a significant transition, though moduli at the highest frequencies are low compared to accepted moduli glassy polymers of solid polymers. This transition could be associated with intramolecular hydrogen bonds, the moduli ranges across these transitions span on the order of three decades for clone-3 and clone-4, while clone-5 span for 1.5 decades. Thus, the prominent transitions exhibited by each clone can also associated with glass transitions, though swelling due to high water content dilutes the polymer chain density so that the upper storage moduli plateau are on the order of 1 to 26 MPa. Moreover, due to the presence of less cohesive ethanol, secondary structure of exon-1, exon-3 and ChBD (exon-2) can change and transition might be due to the crystalline effects. Results from the clones with and without chitin binding domains (ChBD) indicate that the transition occurs at lower frequencies for the clone without ChBD than for the clones with the ChBD, perhaps due to the

disordered nature of the clone without ChBD. For all the clones, transitions were at least few decades beyond the working frequency range of natural resilin at room temperature.

Keywords: Resilin; Molecular cloning; Doubly-shifted modulus master curve; Glass transition temperature; Recombinant resilin; Hydrogen bonds; Temperature dependence, Concentration dependence, Hydrogel.

3.2 Introduction

Resilin was first discovered in 1960 by Weis-Fogh[1] during studies of flight mechanisms of locusts and dragonflies. Elastomeric in nature, resilin can be found within the structures of insects where long range elasticity and energy storage is required, including the salivary feeding pump of assassin bugs[5], cicadas tymbal mechanism[4] for sound production, and structural support at leg joints in cockroaches[6]. The working frequency range of resilin is from 6 Hz in cockroaches locomotion[7-8] to 13 kHz in cicadas[9] and moths[10] sound production.

Resilin contains distinct repetitive motifs like other elastomeric proteins (gliadin, elastin, and spider silks) in its polymeric sequence to confer elastic properties, and forms a rubber-like network through crosslinking of tyrosine residues, forming di- and tri-tyrosine[50]. Resilin in each species has its own form, likely matched to its specific function[15].

Generally, insect resilin genes have three protein coding regions, or exons (Fig. 3-1). Both exon 1 and 3 contain elastomeric repetitive motifs and are mostly disordered in nature while exon 2 is more ordered in nature and known as chitin binding domain (ChBD)[11]. Ardell and Andersen[51] identified that fruit fly resilin has two significant elastic repeat motifs; 18 pentadecapeptide repeats (GGRPSDSYGAPGGGN) in exon 1 and 11 tridecapeptide repeats (GYSGGRPGGQDLG) in exon 3. At exon 2, ChBD of type R&R-2 (PAKYEFNYQV EDAPSGLSFGHSEMRDGDFTTGQYNVLLPDGRKQIVEYEADQQGYRPQIRYEGDANDG

SGPSGP) binds with the cuticle polysaccharide chitin and forms a high performance protein carbohydrate composite material[14].

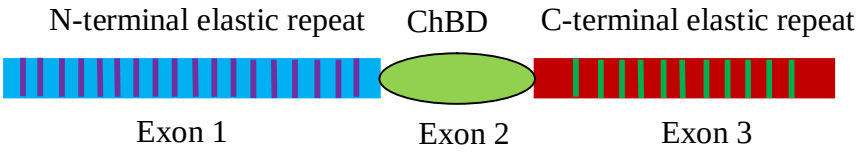

Fig. 3-1. Exons in insect resilin. Exon 2 is known as ChBD, which binds the chitin and helps the process of construction of the cuticle composite, while exon 1 and exon 3 contain elastomeric repetitive motifs.

To implement any of the unique properties of resilin in biomedical applications, it's important to synthesis recombinant resilin of comparable properties. Elvin et al.[13] was the first to synthesize recombinant resilin-like hydrogels of 1st exon, and later Qin et al.[14] and others successfully synthesized recombinant resilin. The mechanical properties of recombinant resilins were not as good as natural resilin in terms of the stiffness and resilience. Also, previous works did not investigate and compare the dynamic mechanical properties with natural resilin to our knowledge.

During our previous work[52], a resilin-like hydrogel was synthesized from clone-1 (exon 1 + exon 2) and water content and dynamic mechanical properties were determined, along with estimating the surface energies relevant to adhesion. To understand the structural and functional properties of native resilin more completely, we cloned and expressed recombinant proteins from different exons as well as full length fruit fly resilin. Resilin-like hydrogels were individually prepared from each clone using photochemical crosslinking. The dynamic mechanical properties of each clone were determined in water (fully hydrated) and at different ethanol concentrations, used to effectively measure any possible transition within the measurable frequency range.

Finally, doubly-shifted master curves were developed by applying TTSP and TTCSP for the storage modulus (E'), loss modulus (E") and tan δ, and compared with a reported master curve of natural resilin from cockroach.

3.3 Material and Methods

Total RNA was extracted from light colored *Drosophila melanogaster* pupae of the Canton S strain (obtained from Dr. Philip's lab, Biological Sciences, Virginia Tech). Different clones were amplified following the same procedures as chapter 2[52] using the following primers: clone-3 (exon 3 only) (For primer 5'-CTGGAGCCCGCCAAGTACGAATTTAA-3', Rev primer 5'-CTCCAGCTAGTACCGATAACCGCTGCCAT-3'); clone-4 (exon 2 + exon 3) (For primer 5'-CTCGAGGGAGGTCCTGGCGGTCAGAAT-3′, Rev primer 5'-CTCCAGCTAGTACCGATA ACCGCTGCCAT-3'); clone-5 (exon 1 + exon 2 + exon 3) (For primer 5′-CTCGAGCCGGA GCCACCAGTTAACTCGTA-3′, Rev primer 5'-CTCCAGCTAGTACCGATAACCGCTG CCAT-3'). PCold I (TaKaRa Bio Inc., NJ, USA) was used as expression vector and same procedures were followed for plasmid construction, protein expression, protein purification, scale up and lyophilization as chapter 2[52].

Photochemical crosslinking[18] was used to prepare the resilin-like hydrogels for each clone and a custom-made dynamic mechanical analyzer (DMA) was used to characterize the recombinant resilin following the procedures of our previous work[52]. Dynamic mechanical testing was conducted in water and 0%, 40%, 65%, 73%, 85%, and 95% ethanol concentrations to develop master curves using TTSP and TTCSP within the temperature range -5.6˚C to 56˚C (details in chapter 2[52]). Ethanol concentrations were chosen based on the work performed by King[15] and Choudhury[16] on natural resilin. According to Lillie et al.[25], increased ethanol concentrations move the master curves to the left along the frequency axis and bring the

transition within the measureable frequency range. Master curves were generated by shifting the curves horizontally only along the log frequency axis. As the number of chains passing through a given cross section remains constant, density-based vertical shift seems inappropriate and also the ratio of the absolute temperature would result maximum shift of 15% which is equivalent to less than 0.07 decade. Other mechanisms capable of requiring vertical shifts are also possible, but were not explored. No vertical shifts were used to develop the master curves. Static loads were measured for each temperature and ethanol concentration during the DMA evaluation to investigate the effect of ethanol concentrations on the resilin samples.

3.4 Results and Discussions

3.4.1 Expression and Synthesis of Resilin-like Hydrogels. Plasmids of all the clones were constructed from the total RNA using gene specific primers. Through enzymatic digestion, the plasmid PCold I was constructed containing all the clones and transformed into *E. coli* strain BL21, and allowed to grow for 24 h at 15˚C. PCold I is a cold shock expression vector. It works only at 15˚C, while expressions of all the other proteins are halted, which favored growth of the target protein. The proteins were purified in soluble form using a Ni-NTA column. The SDS-PAGE gel picture of all the clones is shown in Fig. 3-2, which was generated during the pilot study. The expression and purity levels of all three clones were very high, and purity was evident from the lack of a substantial amount of other proteins for the other clones. Correct protein expression was verified using mass spectrometry. Photochemical crosslinking resulted in resilin-like hydrogels for all the clones from the soluble recombinant proteins.

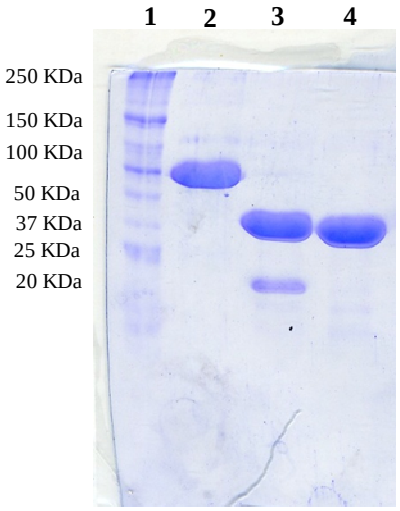

Fig. 3-2. Ni-NTA affinity purified resilin. Lane 1, Molecular masses of standards; Lane 2, clone-1 (15 μg); Lane 3, clone-3 (15 μg); Lane 4, clone-2 (15 μg).

3.4.2 Water Content. During our previous work[52], thermogravimetric analysis (TGA) was conducted on the resilin-like hydrogel of clone-1 (exon-1 + exon-2), and results indicated that there was 80 wt% water in the hydrogel[52]. The water content agreed with the theoretical calculation based on the amount of lyophilized protein used to form the resilin-like hydrogel. Equal ratios of lyophilized proteins were used to conduct the crosslinking for all the clones, resulting in resilin-like hydrogels for each case.

3.4.3 Characterization. DMA was conducted on the resilin-like hydrogels of clone-3, clone-4 and clone-5 to determine the mechanical properties at different temperature and frequencies. As the hydrogels required hydration all the time, experiments on water-immersed specimens could not be conducted at sub-zero temperatures to determine the glass transition temperature (T_g) or other possible transitions. To generate the master curves exhibiting pronounced transitions, experiments were also conducted at different ethanol concentrations (40%, 65%, 73%, 85% and 95 vol%) within the temperature range of -5.6˚C to 56˚C. Similar to studies on clone-1, experiments were not conducted at lower temperatures due to instrument limitations. The higher ethanol concentrations shift the curve to the left along the log frequency axis, bringing the

transition within the measurable frequency range of the instrument[25]. Increasing ethanol content reduced the water concentration in the environmental chamber, drawing water from the hydrogel. According to Gosline et al.[24], the stiffness of elastin, a resilin-like elastomeric material, increases from as little as 10% water loss, effectively retarding the viscoelastic response and shifting the curves to the left along the frequency axis.

3.4.3.1 DMA on Clone-3 (Exon-3). We showed in chapter 2 that the master curve generated in water (0% ethanol) for clone-1 using TTSP did not show any noticeable transition. The storage modulus was within the rubbery plateau at the reference temperature of 24.5˚C. The master curve at 0% ethanol for clone-3 followed a similar trend with no significant transition. The resilience of clone-3 in 0% ethanol was around 85% at 10Hz at room temperature, based on the measured tan $\delta = 0.11$ and the relationship reported in Ferry[33] that resilience, $R = e^{-(\pi/2)\tan\delta}$. Thus, experiments were conducted at different ethanol concentrations and a horizontal doubly-shifted master curve was generated using TTCSP with the reference temperature of 24˚C and reference concentration of 0% ethanol (Fig. 3-3). Total shift factors used for TTCSP are shown in Fig 3.4, where a_c represents the shift factor due to ethanol concentration and a_T represents the thermal shift factor. Similar to the previous work on clone-1[52], insufficient information about the volumetric changes with increasing ethanol concentration and the relatively small vertical shifts anticipated based on the ratio of absolute temperatures, no vertical shifting was applied for clone-3 during the TTCSP.

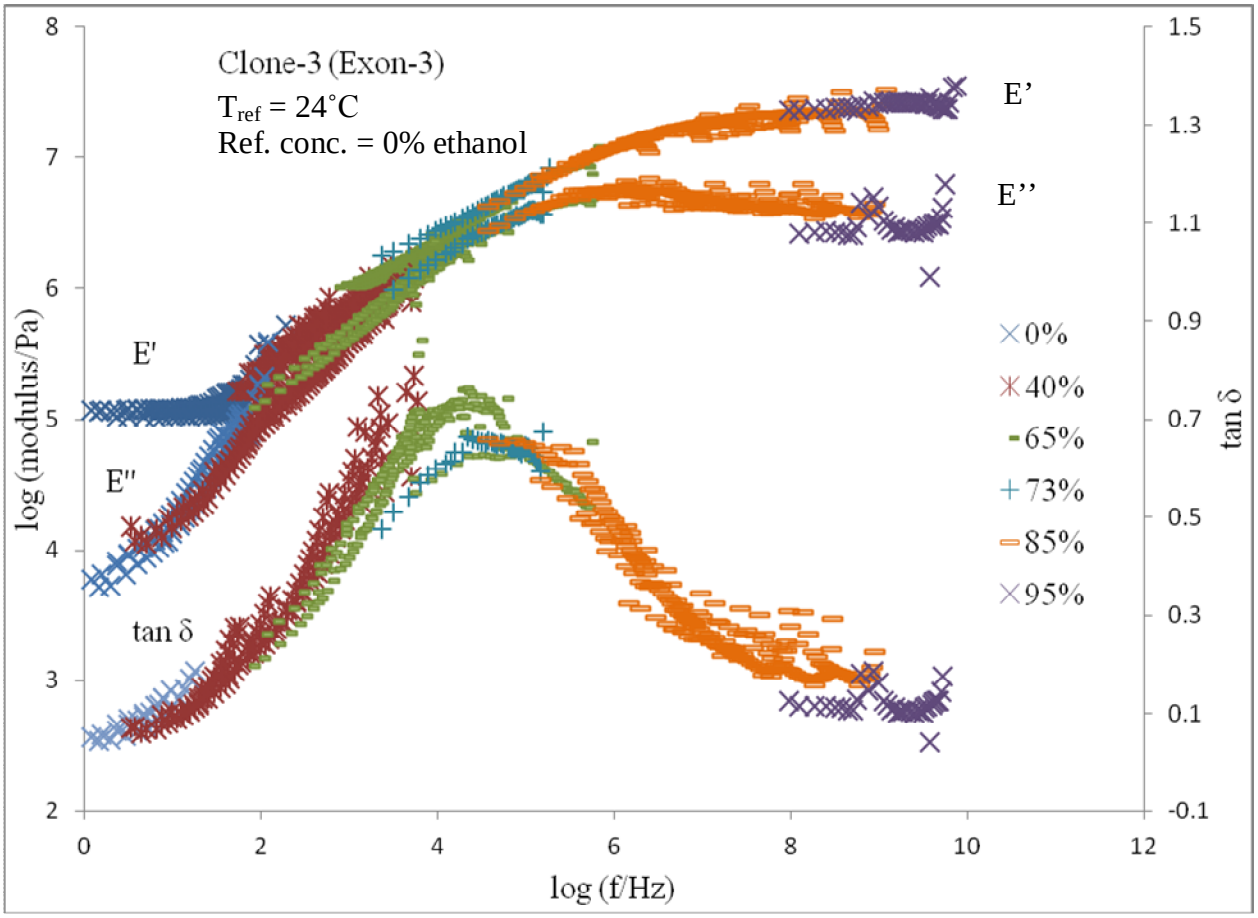

Fig. 3-3. Doubly-shifted master curve of storage modulus, loss modulus and tan δ for clone-3 of resilin based on a reference temperature of 24˚C and reference concentration of 0% ethanol (100% water) formed using TTCSP.

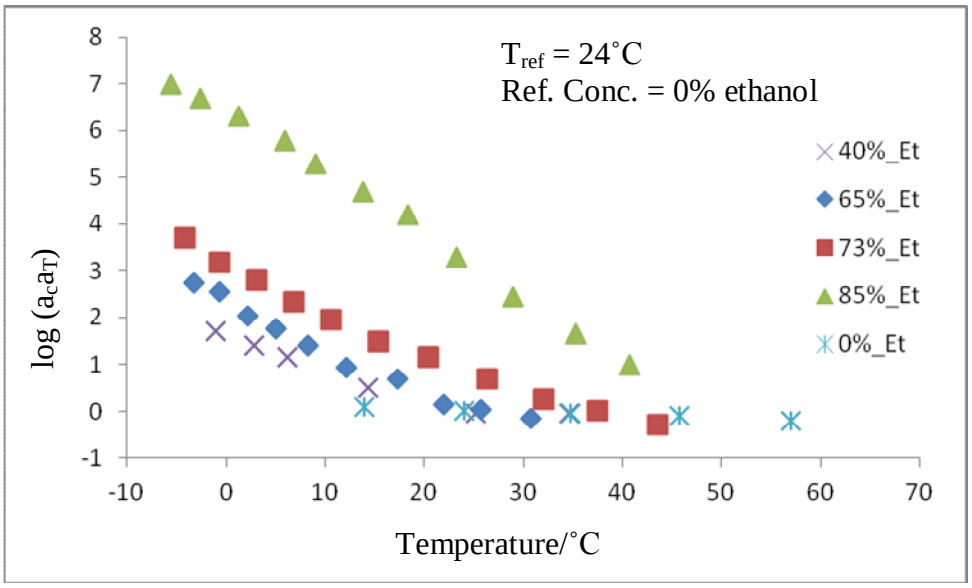

Fig. 3-4. Total shift factors $a_c.a_T$ plotted against temperatures for different ethanol concentrations for clone-3 with reference temperature of 24˚C and reference concentration of 0% ethanol.

In Figure 3.3, the tan δ peak is around $10^{4.5}$ Hz with a storage modulus of 4.4 MPa for clone-3. Similar to the clone-1 results shown in chapter 2, the upper storage modulus plateau of clone-3 appears to be too small for the transition to be considered a glass transition[36], so other explanations are possible. In addition to the rubber to glass transition, the formation of intramolecular hydrogen bonds or changes in secondary structure could also lead to transitions, as described in previous work[52]. Such behavior could result from increased conformational order of the exons due to the presence of less cohesive ethanol. On the other hand, the glassy plateau modulus could be lower than expected for amorphous polymers because of the significant swelling due to the high water content. High water content causes loosely bound water molecules

in the hydrogels[44] (details in chapter 2) and reduce the modulus to only 3.7% of the expected modulus of a solid polymer[53].

The effect of ethanol concentrations on the static loads of clone-3 is shown in Fig 3.5. As observed in our previous work on clone-1[52], the static loads increased with increased ethanol concentration for the clone-3 specimen, held at what is believed to be a constant length imposed on the mounted specimen by the load train. Different ethanol concentrations provided different sections of the master curve and eventually a complete master curve was obtained (Fig. 3-3). The effects of ethanol on the resilin-like hydrogen synthesized from on clone-3 were similar to that from clone-1[52]. Also, for clone-3 measured amplitudes of strain at different ethanol concentrations, the same length and cross sectional area (as used for 0% ethanol) were used for all the calculations to determine the moduli, effectively assuming that no shrinkage of the specimen occurred with the introduction of ethanol.

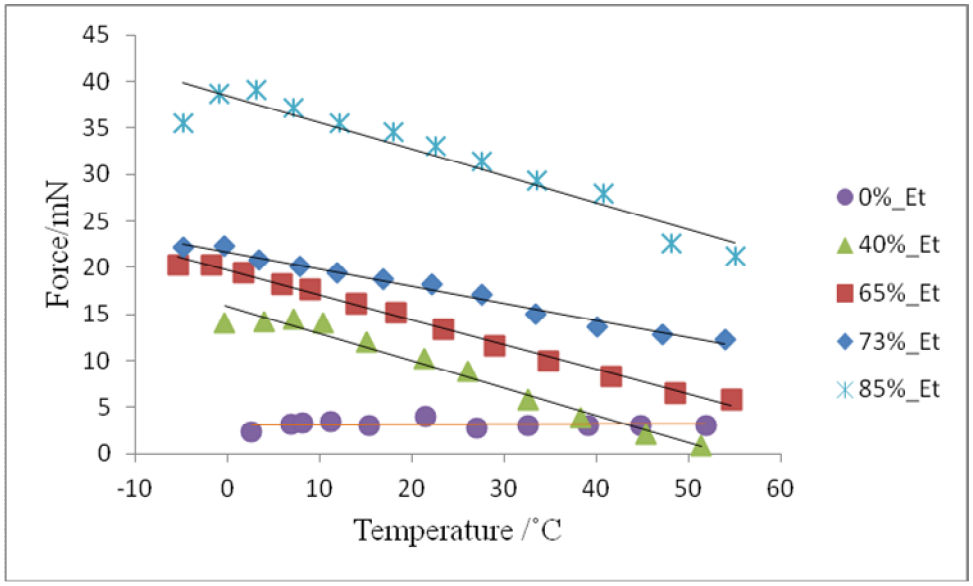

Fig. 3-5. Static loads at different temperature and ethanol concentration due to the change in ethanol concentration for clone-3.

Thermally shifted master curves of the resilin-like hydrogel of clone-3 were developed for each ethanol concentration to determine the transition frequency using the TTSP, and the shift factors were well fit with both the WLF equation and Arrhenius equations. The tan δ peak frequency, and WLF constants and activation energies for different ethanol concentrations are shown in Table 3.1. Results showed that the approximate tan δ peak is shifting to the left along the frequency axis with the increase of ethanol concentration.

Table 3-1. WLF constant values and activation energy for different ethanol concentrations and peak frequency from the tan δ plot which refers to transition from one state to another for resilin-like hydrogel of clone-3.

% Ethanol	Temp. range (˚C)	WLF C_1	WLF C_2 (˚C)	Arrhenius E_a, (kJ/mol)	Ref Temp. (˚C)	tan δ peak (Hz)
0	2.5 to 57	5	370	12	24	
40	-1.1 to 54.8	15	260	136	25.2	
65	-3.2 to 56.3	18	240	138	25.4	$10^{4.2}$
73	-4.2 to 55.3	20	245	142	26.3	$10^{3.8}$
85	-5.6 to 40.7	14	150	216	23.3	$10^{1.7}$

3.4.3.2 DMA on Clone-4 (Exon-2 + Exon-3). Clone-4 is the combination of clone-3 and ChBD. Similar experiments were conducted at different ethanol concentrations on the resilin-like hydrogel of clone-4, and doubly shifted master curves were generated using TTCSP with reference temperature of 24.2˚C (Fig. 3-6). Total shift factors used for TTCSP are shown in Fig 3.7. The resilience of clone-4 were 93% at 10 Hz (tan δ =0.04) (according to Flory[47], resilience, $R = e^{-(\pi/2).\tan\delta}$) at room temperature. The tan δ peak was approximately at 10^8 Hz with storage modulus of 3.2 MPa. The transition occurred at much higher frequency for clone-4 compared to clone-3, which might be due to the presence of ChBD in clone-4. This transition might be also due to the intramolecular hydrogen bonds or glass transition. Similar to clone-1 and clone-3, the transition might be the glass transition, with the relatively low upper plateau modulus resulting from the highly diluted state of the hydrated hydrogel or could be due to formation of intramolecular hydrogen bonds or increasing structural order. There were some discontinuities on the E' plot between 0% and 65% ethanol concentrations, though the E" plot was continuous. If vertical shifts were considered for different ethanol concentrations to construct a continuous E'

master curve, this would probably lead to a discontinuous E” curve, as both are similarly affected by vertical shifts.

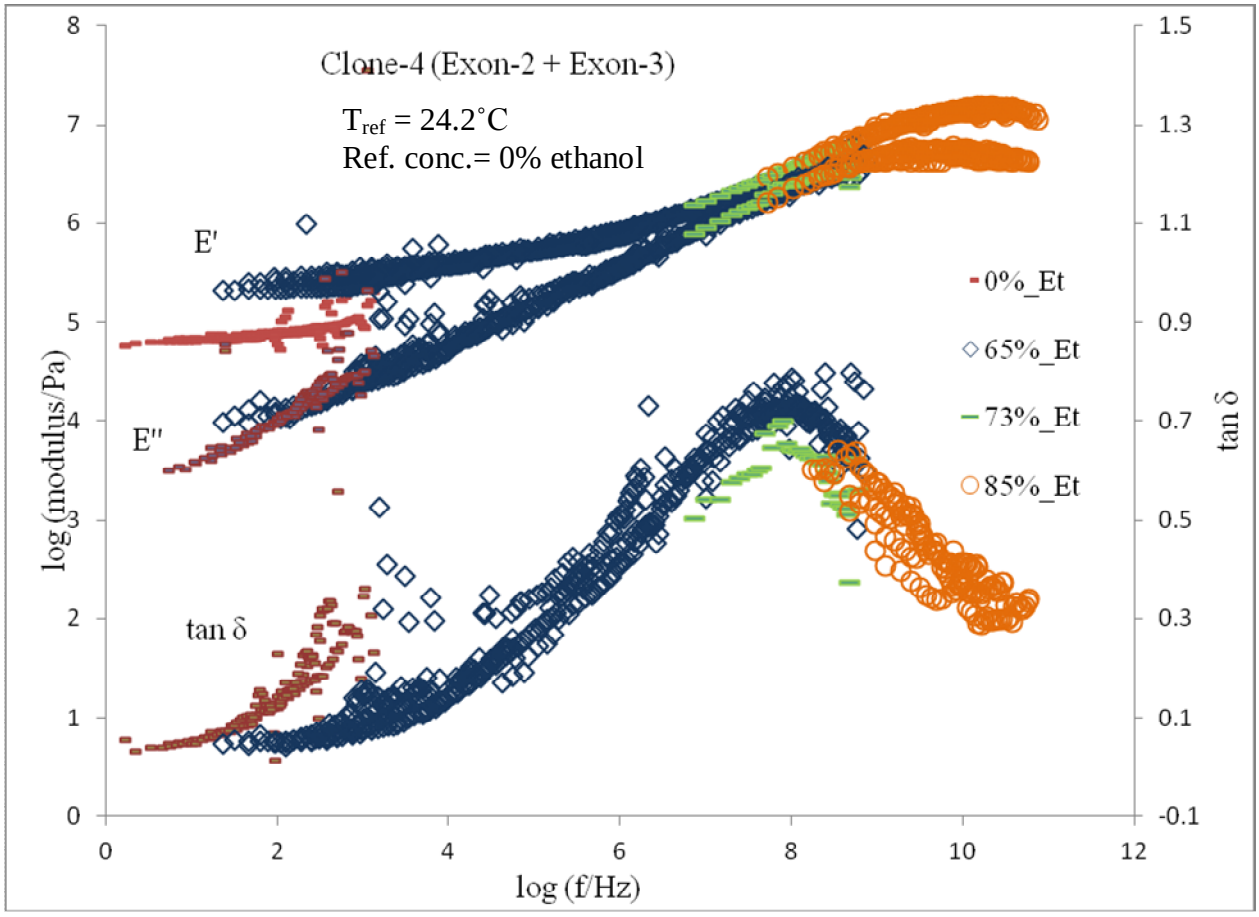

Fig. 3-6. Doubly-shifted master curve of storage modulus, loss modulus and tan δ for resilin-like hydrogel of clone-4 based on a reference temperature of 24.2˚C and reference concentration of 0% ethanol (100% water) formed using TTCSP.

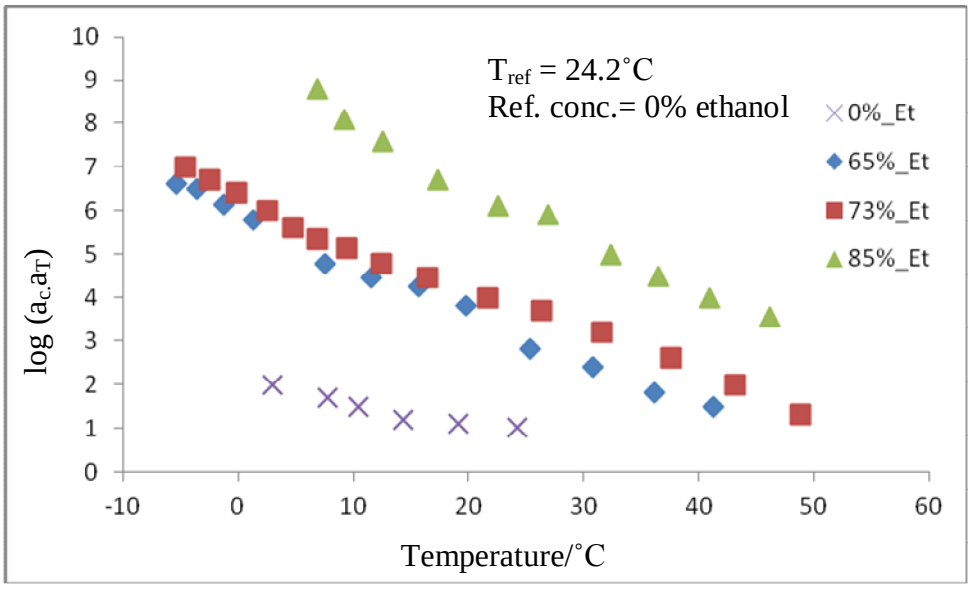

Fig. 3-7. Total shift factors plotted for different ethanol concentrations for clone-4 against temperature for a reference temperature of 24.2˚C and reference concentration of 0% ethanol (100% water).

The master curve of clone-4 for each ethanol concentration was generated to identify the transition using the TTSP, and the shift factors were again well fit with Arrhenius and WLF equations. The estimated WLF constants and activation energies for different ethanol concentrations are shown in Table 3.2. Results showed that the tan δ peak is shifting to the left along the frequency axis, similar to the clone-3, with increasing ethanol concentration.

Table 3-2. The tan δ peak frequency and WLF constant values for different ethanol concentrations resilin-like hydrogel of clone-4.

% Ethanol	Temp. range (˚C)	WLF C_1	WLF C_2 (˚C)	Arrhenius E_a, (kJ/mol)	Ref Temp. (˚C)	tan δ peak (Hz)
0	3 to 51.1	11	280	93	24.2	
65	-5.4 to 41.3	26	235	262	25.4	$10^{5.3}$
73	-4.6 to 48.8	22	240	229	26.4	$10^{4.2}$
85	1.7 to 46.2	26	229	318	26.9	$10^{1.7}$

3.4.3.3 DMA on Clone-5. In fruit fly resilin, there were two exons with two distinct repetitive motifs and ChBD was located between the exons[14]. Full length resilin-like hydrogels were synthesized from the recombinant proteins and conducted DMA's to develop master curves. Similar to clone-3 and clone-4, DMA's were conducted in different concentrations of ethanol to shift the curve to the left along the frequency axis and to determine any possible transition, and TTCSP were applied to develop a doubly shifted mater curve with reference temperature of 22.7˚C (Fig. 3-8). For clone-5, the tan δ peak was very wide and storage modulus around the wide peak was about 0.16 MPa. Moreover, the transition was only one order of magnitude similar to the reported results by King[15] and Choudhury[16] for native resilins and results obtained by Muller et at.[37] for polybutadiene, and suggested that this transition might be due to intramolecular hydrogen bonds within the rubbery plateau similar to clone-3 and clone-4. Even though, the transition was observed for only for one order similar for hydrogen bonding, it did not reach to the plateau yet. This clone might have broader plateau than the other clones. Thus, similar to clone-3 and clone-4, the transition for clone-5 could potentially be due to intramolecular hydrogel bonds, glass transition, increasing structural order, or crystallization

effects. The master curves at each ethanol concentration also did not show any specific tan δ peak, though a very broad peak is suggested in the doubly-shifted master curve.

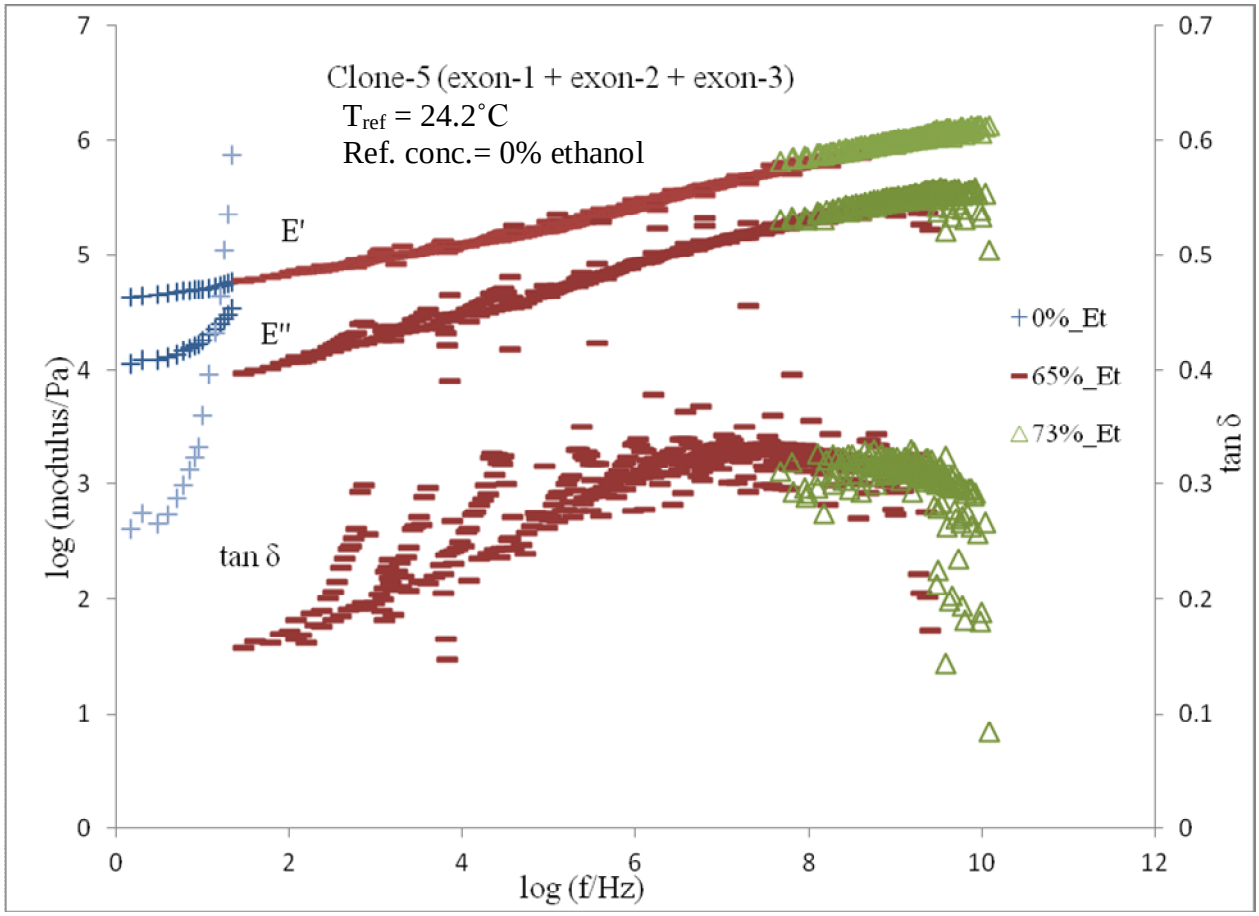

Fig. 3-8. Doubly shifted master curve for resilin-like hydrogel of clone-5 of E', E" and tan δ with the reference temperature 24.2˚C at 0% ethanol concentration (100% water) using TTCSP.

3.4.3.4 Comparison between Different Clones and Native Resilin. Doubly shifted master curves for E' using TTCSP from all the clones were plotted with the master curve of native resilin from cockroach[16] (Fig. 3-9). Cockroach resilin has three exons where ChBD (exon-2) is in the middle, similar to the synthesized recombinant full length resilin (clone-5). From the figure, the storage modulus of clone-5 is several orders of magnitude lower than that of native

resilin of cockroach. Most insects use resilin within the frequency range of 10-100 Hz, and, at room temperature, the transitions might arise from hydrogen bonds or glass transition or crystalline effect, and were several decades beyond this range for all the clones from recombinant proteins and for native resilin. The highest reported natural frequency of resilin measured is for Cicada for sound production, at 13 kHz[9], and other than clone-3, the transition frequency for each of the other clones was multiple decades higher than 13 kHz. The E' is much lower at working range in nature compared to native cockroach resilin. Compared to other clones and native resilin, clone-1 displays a transition at much higher frequency and it has lower storage modulus compared to others before transition. As described in the previous chapter for clone-1, if temperature decreases from room temperature to 0˚C, which is equivalent to 2 decades, the transition frequency will be still be multiple decades beyond the working frequency for all the clones other than clone-3 and the resilin-like hydrogels would still behave similarly as at room temperature. Thus mechanical function of resilin with insects is not expected to be significantly affected by temperature within their operational temperature range.

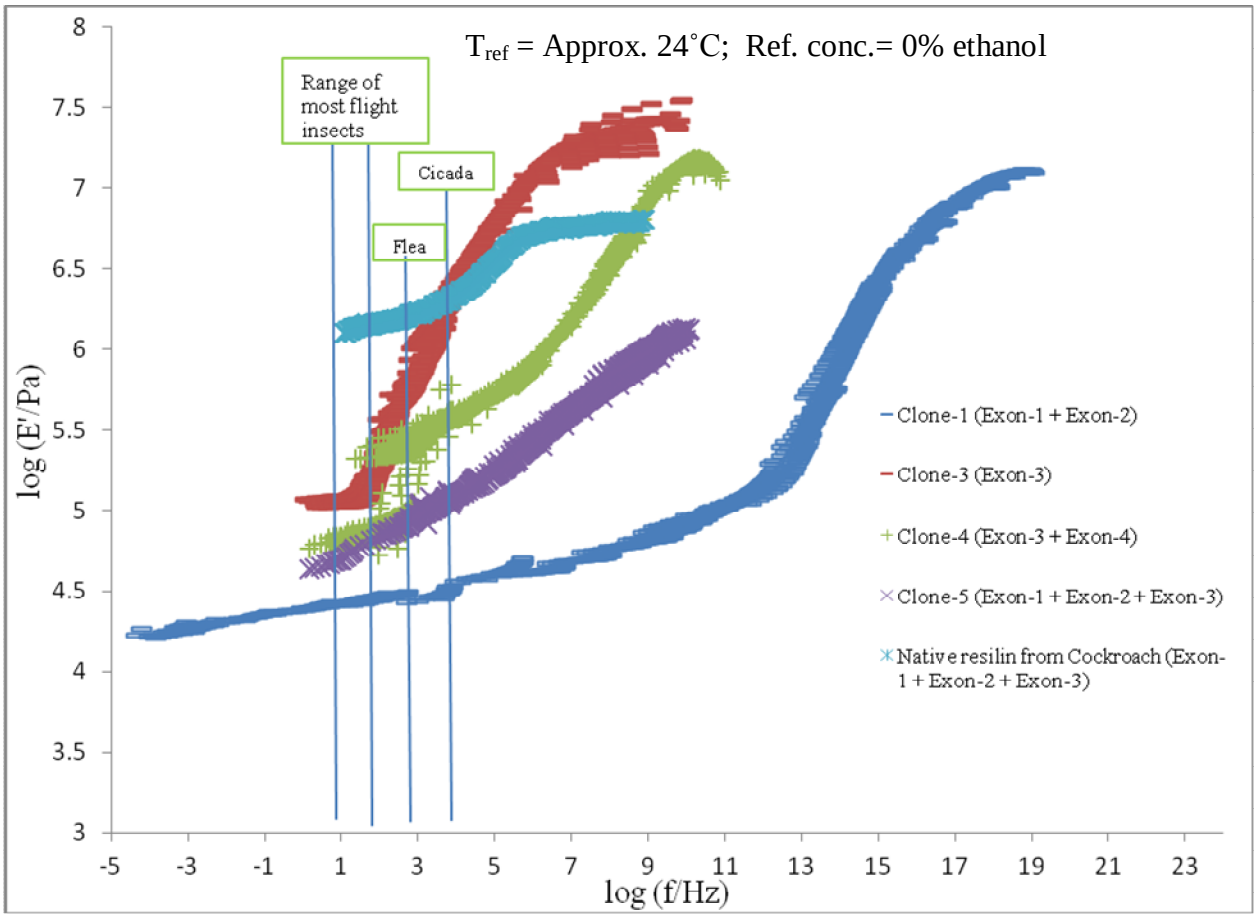

Fig. 3-9. Comparison between the doubly shifted master curves of E' for different clones and native resilin from cockroach at 0% ethanol concentration (100% water) using TTCSP.

3.4.3.5 Effect of ChBD. Most insect resilins have ChBD (exon-2), which allows strong interaction and binding between chitin and resilin during the process of resilin deposition and construction of cuticle composite[14]. ChBD is more ordered in nature compared to exon-1 and exon-3, which are mostly unstructured proteins. From Fig. 3-9, it is evident that the transition for the clones with ChBD was at frequency multiple decades higher than the clone without ChBD (clone-3). This might be due to the fact that the clone-3 is unstructured and amorphous in nature,

compared to all the other clones and native resilin. Thus, the transition can occur at a lower frequency compared to other clones which have ordered ChBD.

3.5 Conclusion

Recombinant resilin-like hydrogel was synthesized and then characterized from exon-3 (clone-3), exon-2 and exon-3 (clone-4), and full length resilin (clone-5). DMA was conducted on each resilin-like hydrogel at different temperatures and ethanol concentrations, and master curves were developed for each concentration by TTSP. Doubly shifted master curves were generated using TTCSP at the selected temperatures and ethanol concentrations. Results showed a transition in the master curves for each clone. As the storage modulus after the transition was not large enough to consider this transition as glass transition for each case, the transition might be within the rubbery plateau and due to the intramolecular hydrogen bonds. On the other hand, as the transition for all the clones occurred for multiple orders of magnitude and another transition for glass transition will cause the modulus to reach much higher than reasonable value. Another possibility is that the transition might be due to crystalline effect which occurred due to the change in the secondary structure of the exons due to less cohesive ethanol. Results from clone-3 and clone-4 indicated that transition occurred at lower frequency than the clone with ChBD (clone-4), and that may be due to disordered nature of the clone. All these new biomaterials synthesized from different clones could be a good candidate for different biomedical applications, even though they are not as good as natural resilin. Moreover, these findings provide insights which could be used to develop new biomaterials for specific biomedical applications.

References

1. T. Weis-Fogh, A rubber-like protein in insect cuticle. *Journal of Molecular Biology*, 1960, **37**, 889-907.
2. T. Weis-Fogh, Molecular interpretation of the elasticity of resilin, a rubber-like protein. *Journal of Molecular Biology*, 1961, **3**, 648-667.
3. R. E. Lyons, Lesieur, E., Kim, M.,Wong, D.C.C., Huson, M.G., Nairn, K. M., Brownlee, A. G., Pearson, R. D., Elvin, C. M., Design and facile production of recombinant resilin-like polypeptides: gene construction and a rapid protein purification method. *Protein Engineering, Design & Selection*, 2007, **20**, 25-32.
4. D. Young and H. C. Bennet-Clark, The role of tymbal in cicada sound production. *Journal of Experimental Biology*, 1995, **198**, 1001-1019.
5. S. J. Edwards, Predation and digestion in assassin bugs (Heteroptera, Reduviidae. University of Cambridge, UK, 1960.
6. S. O. Andersen and T. Weis-Fogh, Resilin. A rubber-like protein in arthropod cuticle. *Advances in Insect Physiolology*, 1964, **2**, 1-65.
7. D. Neff, S. F. Frazier, Identification of resilin in the leg of cockroach, Periplaneta americana: confirmation by a simple method using pH dependence of UV fluorescence. *Arthropod Structure and Development*, 2000, **29**, 75-83.
8. R. Kram, B. Wong, Three-dimensional kinematics and limb kinetic energy of running cockroaches. *Journal of Experimental Biology*, 1997, **200**, 1919-1929.
9. H. C. Bennet-Clark, Daws, A. G., Transduction of mechanical energy into sound energy in the cicada Cyclochila australasiae. *The Journal of Experimental Biology*, 1999, **202**, 1803-1817.

10. N. Skals, Surlykke, A., Sound production by abdominal tymbal organs in two moth species: the green silver-line and the scarce silver-line (Noctuoidea: Nolidae: Chloephorinae). *Journal of Experimental Biology*, 1999, **202**, 2937-2949.
11. G. Qin, Hu, X., Cebe, P. and Kaplan, D. L., Mechanism of Resilin Elasticity. *Nature Communication*, 2012, **3**, 1-18.
12. G. F. Elliott, A. F. Huxley and T. Weis-Fogh, On the structure of resilin. *Journal of Molecular Biology*, 1965, **13**, 791-795.
13. C. M. Elvin, A. G. Carr, M. G. Huson, J. M. Maxwell, R. D. Pearson, T. Vuocolo, N. E. Liyou, D. C. C. Wong, D. J. Merritt and N. E. Dixon, Synthesis and properties of crosslinked recombinant pro-resilin. *Nature*, 2005, **437**, 999-1002.
14. G. Qin, S. Lapidot, K. Numata, X. Hu, S. Meirovitch, M. Dekel, I. Podoler, O. Shoseyov and D. L. Kaplan, Expression, Cross-Linking, and Characterization of Recombinant Chitin Binding Resilin. *Biomacromolecules*, 2009, **10**, 3227–3234.
15. R. King, Dynamic Mechanical Properties of Resilin. Master's, Virginia Polytechnic Institute and State University, 2010.
16. U. Choudhury, Dynamic Mechanical Properties of Cockroach (Periplaneta americana) Resilin. Master's Thesis, Virginia Polytechnic Institure and State University, 2012.
17. F. W. Studier, Protein production by auto-induction in high density shaking cultures. *Protein Expression & Purification*, 2005, **41**, 207–234.
18. D. A. Malencik and S. O. Anderdon, Dityrosine Formation in Calmodulin: Cross-Linking and Polymerization Catalyzed by *Arthromyces* Peroxidase. *Biochemistry*, 1996, **35**, 4375-4386.

19. D. A. Fancy and T. Kodadek, Chemistry for the analysis of protein- protein interations : rapid and efficient cross-linking triggered by long wavelength light. *PNAS*, 1999, **96**, 6020-6024.
20. S. S. Nielsen, Food Analysis. 4th edn., Springer, 2010.
21. C. Creton, Pressure-Sensitive Adhesives: An Introductory Course. *MRS Bulletin*, 2003, **28**, 434-439.
22. M. E. Schrader, Yound-Dupre Revisited. *Langmuir*, 1995, **11**, 3585-3589.
23. Y. I. Matveev, V. Y. Grinberg, I. V. Sochava and V. B. Tolstoguzov, Glass transition temperature of proteins. Calculation based on the additive contribution method and experimental data. *Food Hydrocolloids*, 1997, **11**, 125-133.
24. J. M. Gosline and C. J. French, Dynamic mechanical properties of elastin. *Biopolymers*, 1979, **18**, 2091-2103.
25. M. A. Lillie and J. M. Gosline, The effects of hydration on the dynamic mechanical properties of elastin. *Biopolymers*, 1990, **29**, 1147-1160.
26. A. Zosel, Adhesion and Tack of Polymers: Influence of Mechanical Properties and Surface Tensions. *Colloid & Polymer Science*, 1985, **263**, 541-553.
27. A. Zosel, Adhesive Failure and Deformation Behaviour of Polymers. *Journal of Adhesion*, 1989, **30**, 135-149.
28. C. Gay, Stickiness – Some Fundamentals of Adhesion. *Integrative and Comparative Biology*, 2002, **42**, 1123-1126.
29. A. M. Grillet, N. B. Wyatt and L. M. Gloe, ed.^eds., InTech Europe, Dr. Juan De Vicente (Ed.) edn., 2012, p.^pp.

30. M. Barquins and J. Cognard, Adhesion Characteristics of Gold Surfaces. *GoldBull*, 1986, **19**, 82-86.
31. G. Storm, M. Fredriksson and P. Stenium, Contact Angles, Work of Adhesion, and Interfacial Tensions at a Dissolving Hydrocarbon Surface. *Journal of Colloid and Interface Science*, 1986, **119**, 352-361.
32. R. E. Neuendorf, E. Saiz, A. P. Tomsia and R. O. R.O. Ritchie, Adhesion between biodegradable polymers and hydroxyapatite: Relevance to synthetic bone-like materials and tissue engineering scaffolds. *Acta Biomaterialia*, 2008, **4**, 1288–1296.
33. J. D. Ferry, Viscoelastic Properties of Polymers. Wiley, New York, 1980.
34. Y. Wada and H. Hirose, Glass Transition Phenomena and Rheological Properties of Petroleum Asphalt. *Journal of Physical Society of Japan*, 1960, **15**, 1885–1894.
35. K. A. Patankar, D. A. Dillard, S. W. Case, M. W. Ellis, Y. H. Lai and C. S. Gittleman, Linear Hygrothermal Viscoelastic Characterization of Nafion NRE 211 Proton Exchange Membrane. *Fuel Cells*, 2012, **12**, 787-799.
36. D. Roylance, ed.^eds., Cambridge, 2001, p.^pp. Massachusetts Institute of Technology: MIT OpenCourseWare.
37. M. Muller, U. Seidel and R. Stadler, Influence of hydrogen bonding on the viscoelastic properties of thermoreversible networks: analysis of the local complex dynamics. *Polymer*, 1995, **36**, 3143-3150.
38. M. S. Khandaker, D. M. Dudek, E. P. Beers, D. A. Dillard and D. R. Bevan, Molecular Modeling on the Elastomeric Properties of Repeating Motifs of Disordered Elastomeric Proteins. in prep.

39. M. S. Khandaker, D. M. Dudek, D. A. Dillard, E. P. Beers and D. R. Bevan, Molecular Modeling of the Elastomeric Properties of Repeating Units and Building Blocks of Resilin, a Disordered Elastic Protein. *Journal of the Mechanical Behavior of Biomedical Materials*, in review.

40. R. Adhikary, J. Zimmermann, J. Liu, R. P. Forrest, T. D. Janicki, P. E. Dawson, S. A. Corcelli and F. E. Romesberg, Evidence of an Unusual N−H···N Hydrogen Bond in Proteins. *Journal of Americal Chemical Society*, 2014, **136**, 13474−13477.

41. K. Takano, Y. Yamagata, J. Funahashi, Y. Hioki, S. Kuramitsu and K. Yutani, Contribution of intra- and intermolecular hydrogen bonds to the conformational stability of human lysozyme. *BioChemicstry*, 1999, **38**, 12698-12708.

42. E. B. Stukalin, J. F. Douglas and K. F. Freed, Plasticization and antiplasticization of polymer melts diluted by low molar mass species. *Journal of Chemical Physics* 2010, **132**.

43. A. Roy, M. A. Hickner, T. Glass, Y. Li, B. Einsla, K. B. Wiles, X. Yu and J. E. McGrath, States of water- investigating the water-polymer interactions and transport phenomenon in proton exchange membranes. *Preprints of Symposia - American Chemical Society*, 2005, **50**, 699-700.

44. A. Roy, Structure Property Relationships of Proton Exchange Membranes. Virginia Poylechnic Institute and State University, 2008.

45. O. Okay, in *Hydrogel Sensors and Actuators*. eds. G. Gerlach and K. F. Arndt, Springer Berlin Heidelberg, 2010, vol. 6, pp. 1-14.

46. A. Schausberger and I. V. Ahrer, On the time-concentration superposition of the linear viscoelastic properties of plasticized polystyrene melts using the free volume concept. *Macromolecular Chemistry and Physics*, 1995, **196**, 2161-2172.

47. P. J. Flory, Principles of Polymer Chemistry. First edn., Cornell University Press, Ithaca, United States 1953.
48. S. J. Hamodrakas, J. H. Willis and V. A. Iconomidou, A structural model of the chitin-binding domain of cuticle proteins. *Insect Biochemistry and Molecular Biology*, 2002, **32**, 1577–1583.
49. L. Li, T. Luo and K. L. Kiick, Temperature-triggered phase separation of a hydrophilic resilin-like polypeptide. *Macromolecule Rapid Communications*, 2015, **36**, 90-95.
50. S. O. Andersen, The cross links in resilin identified as dityrosine and trityrosine. *Biochimica et Biophysica Acta*, 1964, **93**, 213-215.
51. D. H. Ardell and S. O. Andersen, Tentative identification of a resilin gene in Drosophila melanogaster. *Insect Biochemistry and Molecular Biology*, 2001, **10**, 965-970.
52. M. S. Khandaker, D. M. Dudek, E. P. Beers and D. A. Dillard, Expression, Crosslinking and Developing a Modulus Master Curve of Recombinant Resilin. in prep.
53. M. S. Khandaker, D. M. Dudek, E. P. Beers and D. A. Dillard, Expression, Crosslinking and Developing a Modulus Master Curve of Recombinant Resilin. *in prep.*

Chapter 4: Molecular Modeling of the Elastomeric Properties of Repeating Units and Building Blocks of Resilin, a Disordered Elastic Protein

Md Shahriar K. Khandaker, Daniel M. Dudek, Eric P. Beers, David A. Dillard and David R. Bevan (in review)

4.1 Abstract

The mechanisms responsible for the properties of disordered elastomeric proteins are not well known. To better understand the relationship between elastomeric behavior and amino acid sequence, we investigated resilin, a disordered rubber-like protein, found in specialized regions of the cuticle of insects. Resilin of *Drosophila melanogaster* contains Gly-rich repetitive motifs comprised of the amino acids, PSSSYGAPGGGNGGR, which confer elastic properties to resilin. The repetitive motifs of insect resilin can be divided into smaller partially conserved building blocks: PSS, SYGAP, GGGN and GGR. Using molecular dynamics (MD) simulations, we studied the relative roles of SYGAP, and its less common variants SYSAP and TYGAP, on the elastomeric properties of resilin. Results showed that SYGAP adopts a bent structure that is one-half to one-third the end-to-end length of the other motifs having an equal number of amino acids but containing SYSAP or TYGAP substituted for SYGAP. The bent structure of SYGAP forms due to conformational freedom of glycine, and hydrogen bonding within the motif apparently plays a role in maintaining this conformation. These structural features of SYGAP result in higher extensibility compared to other motifs, which may contribute to elastic properties at the macroscopic level. Overall, the results are consistent with a role for the SYGAP building block in the elastomeric properties of these disordered proteins. What we learned from simulating the repetitive motifs of resilin may be applicable to the biology and mechanics of

other elastomeric biomaterials, and may provide us the deeper understanding of their unique properties.

Keywords: Resilin; Repetitive motifs; Hydrogen bonds; Molecular modeling; Disordered protein; Elastomeric proteins; Foldamers.

4.2 Introduction

Elastomeric proteins are present in a wide range of living organisms[1]. Despite their ubiquity, we have little understanding about the affect of molecular variations on macroscopic material properties. Typically, the secondary structures of these unstructured proteins are in dynamic equilibrium between folded (mainly β-turn) and extended (poly-proline II(PPII) and β-strands conformations[2]. To improve the understanding of structural and functional properties, amino acid sequences of disordered proteins are needed to be investigated[3]. Probable disorder-promoting residues are aspartic acid, methionine, lysine, arginine, serine, glutamine, proline and glutamic acid. The majority of these disorder-promoting residues are polar, often charged, and commonly found on the surface of the proteins[4]. Disordered proteins usually show low sequence complexity and have significant amino-acid compositional bias. Glycine and proline often appear in the sequence of disordered proteins, and both contribute to disorder, though for opposite reasons[5]. Proline is conformationally restricted due to its cyclic side chain, promotes the formation of PPII structures, and reduces the ability to form hydrogen-bonded secondary structure[1]. On the other hand, glycine is so flexible due to the absence of a side chain that order is entropically unfavorable[5].

Resilin is first discovered by Weis-Fogh in 1960[6]. It is one of the disordered proteins in a family with similar functionalities which includes elastin, abductin, and spider silks etc. Resilin has remarkable diverse function and that includes role in feeding (salivary pump of assassin

bugs[7]), sound production (cicada tymbal mechanism[8]), hind coxae of the froghopper[9] and structural support at leg joints (cockroach[10]). Resilin is also structurally diverse. It is pure polymer in dragonfly tendons and composite of resilin and chitin in fruit flies, locusts[11]. Resilin is believed to be highly unstructured with no α-helices or β-sheets[11-12]. They form a rubber network due to crosslinking of tyrosine residues forming di- and tri-tyrosine[13]. Unlike the other elastomeric proteins, resilin sequences have both non-conserved and conserved domains, and the conserved domains usually participate in crosslinking.

Most insect resilin genes are comprised of three protein coding regions, or exons. Both exon 1 and exon 3 contain elastomeric repetitive units while exon 2 is designated the chitin binding domain (ChBD)[14]. Resilin contains distinct repetitive units, PSSSYGAPGGGNGGR in exon 1 and GYSGGRPGGQDLG in exon 3, that appear to confer elastomeric properties to proteins in ways similar to other elastomeric proteins like elastin, spider silk and gliadin[15].

MD simulations are useful in developing an atomic-level description which are not conformational disorder, although the scope is limited to small oligopeptides[16] and short time scales[17]. To understand the extraordinary properties of resilin, a bottom-up approach can be employed by atomistic modeling[12, 18-19]. Steered molecular dynamics (SMD) and moving constraints are two extensions of MD that allow for constant velocity pulling (e.g., moving constraints and constant velocity SMD) or constant force pulling (e.g., constant force SMD)[20]. In both constant velocity SMD and moving constraints scenarios, the center of mass of a group of atoms or each pulled atom is connected through a virtual spring (k = stiffness) to a virtual atom that moves at a constant velocity (v = velocity)[21]. The purpose of virtual atoms and virtual springs is to provide an analog to position-controlled atomic force microscopy (AFM) to compare with the experimental results[22]. Constant velocity SMD is one of the techniques that has

been used to simulate the mechanical functions of proteins and protein unfolding pathways[23], and to predict Young's modulus[24].

The pulling velocity and the stiffness of the virtual springs influence the constant velocity pulling simulations. For instance, faster pulling rates can lead to over-estimated mechanical properties as they do not provide enough time for the protein to reorganize[25]. Though it is unclear whether this is a numerical artifact or associated with some rudimentary time dependence, the effect of pulling velocity on results for a molecule surrounded by water is not believed to be relevant to actual polymer viscoelasticity effects. Thus, a sufficiently reduced pulling velocity is employed in simulations to obtain limiting or equilibrium behavior[19]. However, there is a balance, which must be sought when choosing a pulling velocity, since a reduced pulling velocity necessitates a greater number of simulation time steps to reach the same level of deformation, which will be computationally expensive.

Moreover, periodic boundary conditions need to be applied to reduce computation time and keep the number of atoms constant in the system. If the box enclosing the protein in a solvent, is too large, most of the time will be spent on solvent interactions while a smaller box will cause boundary effects[19].

Petrenko et al.[19] used the NAMD2.6 molecular dynamics (MD)[26] package for their simulations to assess the flexibility of simulated peptides. Using constant velocity SMD, constrained/unconstrained MD (k = 10 kcal/mol/A^{o2}, v = 0.1 m/s), the CHARMM force field[27] for peptides, and the TIP3P model[28] for water, they reported a high level of disorder due to a lack of stable secondary structure and lack of stable intra-protein hydrogen bonds. Even when their simulations included 12% of tyrosine residues involved in crosslinks to form dityrosine, Petrenko et al.[19] found no significant decrease in crosslinking due to peptide fluctuations which

was consistent with the experimental work that peptide dynamics does not change with the level of crosslinking at 16% in AN16 peptides[29].

In another study, Kappiyoor et al.[12] used the GROMACS package[30-31] and the OPLS AA force field[32] for simulating the effect of polarity on the elastic properties of resilin found in different insects using constant velocity SMD (k = not reported, v = 0.1 m/s). To determine the effect of polarity, charges were varied to zero and one-half of the natural value, and all the polar amino acids were replaced with non-polar amino acids in three different simulations. Results showed that increased polarity led to higher extensibility and lower stiffness. Natural resilin is hydrophilic, and able to adsorb water to transfer deformation energy to improve elasticity while the non-polar, half charge and zero charge counterparts had higher elasticity for their hydrophobic side chains[12].

Previous MD studies of resilin have not considered the function of the resilin repeating motifs or their building blocks on the elasto-mechanical properties. One work explored the effect of polarity on the elastomeric properties[12] even though all natural repeating motifs in the resilin sequence have same charges while other work looked only at the absence of secondary structure[19]. Consequently, MD simulations were conducted on the most frequent repeating motifs from exon 1 (PSSSYGAPGGGNGGR) compared to other repeating motifs in terms of elastomeric properties to understand their contribution to the mechanical properties of resilin. We used MD simulation to test the effects of the SYGAP (and divergent SYSAP and TYGAP) building block alone or in combination with other building blocks of the resilin repetitive motifs, e.g., SYGAP, PSSSYGAP, PSSSYGAPGGN, and PSSSYGAPGGGNGGR, to understand their effects on conformation and mechanical properties of resilin. During the process, we also studied different pulling velocities on these repeating units to choose a suitable velocity to avoid

computationally expensive simulations, and to our knowledge this is the first study on the effect of the velocity on repetitive pentadecapeptide motifs of resilin.

The purpose of this work was to take advantage of the natural diversity of resilin to develop a fundamental understanding of the elastomeric disordered protein using MD simulations. The simulations applied to these diverse repetitive motifs will advance our understanding of the molecular mechanisms responsible for the remarkable behavior exhibited by insect resilin.

4.3 Materials and Methods

A bottom-up approach was employed to understand the mechanism of the elastomeric properties of resilin. The molecular models were constructed using the computer programs Discovery Studio Visualizer[33] and Visual Molecular Dynamics (VMD)[34]. The MD package NAMD2.6[26] was used for all simulations. The all-atom CHARMM22 force field[27] was used for peptides and the TIP3P model was used for water[28]. Covalently linked hydrogen atoms were constrained to fixed lengths with the SHAKE algorithm[35] which allowed us to use an integration time step of 2 fs. For the van-der-Waals interactions, the switching function started at 10 Å while the cutoff distance was 12 Å bringing the interactions to zero at the cutoff distance. The system coordinates were saved every 0.01 ns for later analysis. To calculate long-range electrostatic forces the particle-mesh Ewald (PME)[36] method was used. Depending on the periodic cell size, the grid point spacing for PME was adjusted to be approximately 1 Å.

Peptides were immersed in a water box with padding of at least 10 Å on all sides. Simulations were conducted using a leapfrog time integration scheme with a time step of 0.002 picoseconds (ps). All systems were simulated using the following steps: (i) energy minimization, (ii) heating to 310 K (iii) a canonical NPT (constant Number of particles, Pressure, and

Temperature) ensemble-based simulation performed with temperature controlled at 310K for 5×10^6 time steps, (iv) an NVE (constant Number of particles, Volume, and Energy) equilibration, during which the motif was allowed to move freely for 5×10^6 time steps. Periodic boundary conditions were applied to keep the number of atoms constant in the system throughout the simulation.

After the NVE, instead of continuing the simulations on the final conformation, clustering was conducted on all the conformations observed during the MD using GROMACS. A cutoff of 0.10-0.20 nm was used for clustering analysis[37]. Further simulations were continued on the most favorable conformation, i.e. frequency was 60% or more during the NVE. We extended the MD runs out to 100 ns to verify the equilibrium and we observed similar results (Results not shown). Once the most favorable conformation was defined, a water box was generated that was large enough to conduct the steered molecular dynamics (SMD). Minimization, heating, NPT ensemble and NVE ensemble were conducted on the system again following the same procedure as before, while the position of the protein was fixed to prepare the system for SMD. Finally, SMD pulling was carried out on the protein where the N-terminus of the motif (the amide group attached to the alpha carbon of the first amino acid) was held fixed while pulling on the C-terminus (the carboxyl group attached to the alpha carbon of the final amino acid) at a constant velocity of 0.1 m/s. This velocity was determined by running simulations on three different motifs at different velocities (0.1, 0.5, 1, 5, 10 and 50 m/s). Although 0.1, 0.5 and 1 m/s gave similar results, the velocity chosen for the SMD was 0.1 m/s, because according to Gautieri et al.[25], modulus converges to constant value for pulling velocity less than 0.5 m/s.

The extended structure after SMD was put into a water box and the MD simulation was continued by releasing the N- and C-termini for a total 60 ns to compare the collapsed structure

with the structure obtained after clustering. Structures were aligned using the Chimera 1.9 visualization program[38].

Secondary structure assignments were performed using the Xtlsstr program[39]. Even though DSSP[40] is a widely used program, Xtlsstr was chosen due to its ability to identify polyproline II (PPII) type helices in addition to other secondary structures. The simulations were repeated to determine the effect of entropy on the protein. The force field was modified by switching off the attractive part of the Lennard-Jones (LJ) interactions (C6) and all electrostatic interactions, leaving only the repulsive part of the Lennard-Jones interactions (C12) and bonded interactions as described by Grater et al.[41]. The resulting model is only restricted by local steric repulsion of the atoms and the bonded interactions, mainly the dihedral potentials along the protein backbone. Hydrogen bonds within the motif were predicted using the molecular visualization software RasTop 2.2 (http://www.geneinfinity.org/rastop/).

4.4 Results and Discussion

4.4.1 Equilibrium

Analysis of unrestrained MD simulations based on root-mean-square deviation (RMSD) revealed that the systems changed quickly from their initial structures but then remained relatively unchanged out to 100 ns (supplementary information, Fig. C.1). Although substantial fluctuations were observed since these peptides are relatively small and disordered, systematic changes in RMSD were not apparent.

4.4.2 Clustering

A clustering analysis[37] of the MD simulations was conducted based on the backbone atoms to determine the most favorable conformation within each simulation. During the MD simulation, conformations were recorded at every 500 time-steps, followed by clustering on all the

conformations. Using a cutoff of 0.15-0.20 nm, frequencies of the most favorable conformational cluster were 61% for PSSSYGAPGGGNGGR, 59% for PSSSYSAPGGGNGGR, 66% for PSSTYGAPGGGNGGR and 74% for PSSTYSAPGGGNGGR. The latter peptide is not found among reported sequences for natural resilin but is a composite synthetic sequence representing both the SYSAP and TYGAP variants of SYGAP. The representative structure for each peptide from the clustering is shown in Fig. 4-1. Notably, due to the bend between tyrosine (TYR) and alanine (ALA) for PSSSYGAPGGGNGGR, the end-to-end distance of this motif (20Å) was about one-half that of the other motifs (Table 4.1).

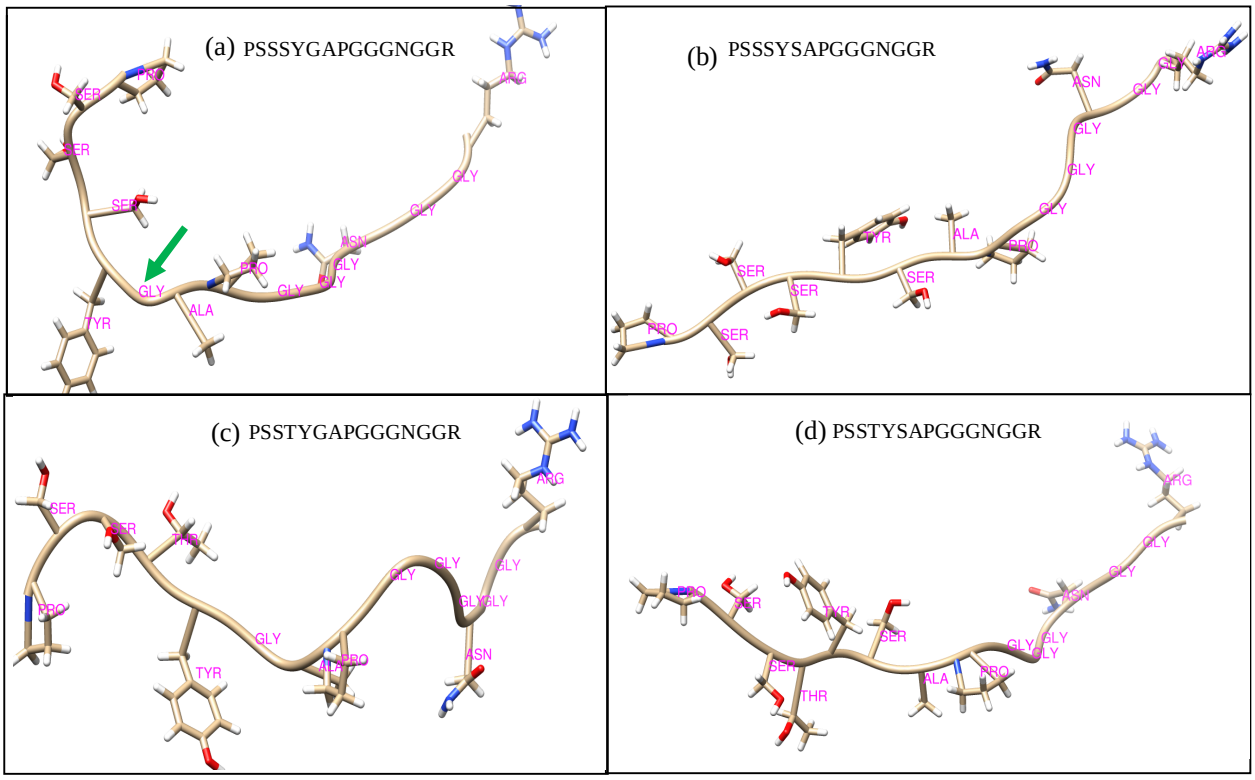

Fig. 4-1. Structure of the four peptides after clustering of MD results (a) PSSSYGAPGGGNGGR, (b) PSSSYSAPGGGNGGR, (c) PSSTYGAPGGGNGGR and (d) PSSTYSAPGGGNGGR. Due to the bend between tyrosine (TYR) and alanine (ALA) for PSSSYGAPGGGNGGR, at arrow in (a), the end--to-end distance of the motif is smaller (20 A˚) compared to the other motifs.

Table 4-1. Energies and non-bonded interactions between protein and water of the repeating motifs. The most common repeating motif of Drosophila melanogaster, PSSSYGAPGGGNGGR, has the highest extensibility and least stiffness compared to others.

Fragments	Bond Energy (kcal/mol)	van der Waals Energy (kcal/mol)	Total Energy (kcal/mol)	Potential Energy (kcal/mol)	Force at 55% strain (pN)	non-bonded interaction between protein & water, (kcal/mol)	Length at Equilibrium (Å)
PSSSYGAPGGGNGGR	5500	7800	-41430	-53710	22	-710	20.68
PSSSYSAPGGGNGGR	6860	9850	-52300	-67540	2902	-700	40.04
PSSTYGAPGGGNGGR	7070	10130	-53870	-69630	2250	-690	38.33
PSSTYSAPGGGNGGR	7960	11450	-60800	-78460	1620	-710	37.68

4.4.3 Pulling Velocity Influenced the Force Required for Displacement

Using the representative structures from the unrestrained MD simulations, pulling simulations were conducted. The effect of pulling velocity, over a range including v = 50, 10, 5, 1, 0.5, and 0.1 m/s, was examined initially. Using the peptide PSSSYSAPGGGNGGR, there are only small qualitative differences in the forces at velocities between 1, 0.5, and 0.1 m/s, but there are notable differences for the higher velocities (Fig. 4-2). Similar results were also obtained for other peptides. This effect of pulling velocity on force is similar to that obtained for collagen by Kwansa et al.[20] and Gautieri et al.[24]. According to Gautieri et al.[24], the apparent modulus of tropocollagen converges to a constant value for pulling rates below 0.5 m/s because force vs strain plots are similar for 0.5 m/s or lower pulling rates. These similar outcomes from pulling simulations of different peptides may result from compatible interactions between the amino acids and their surroundings. In our studies, bond energy, van der Waals energy, potential energy, total energy, and non-bonded interaction energy between water and protein were almost

identical for all the velocities, which implied these energies do not make much contribution to the variations at different velocities.

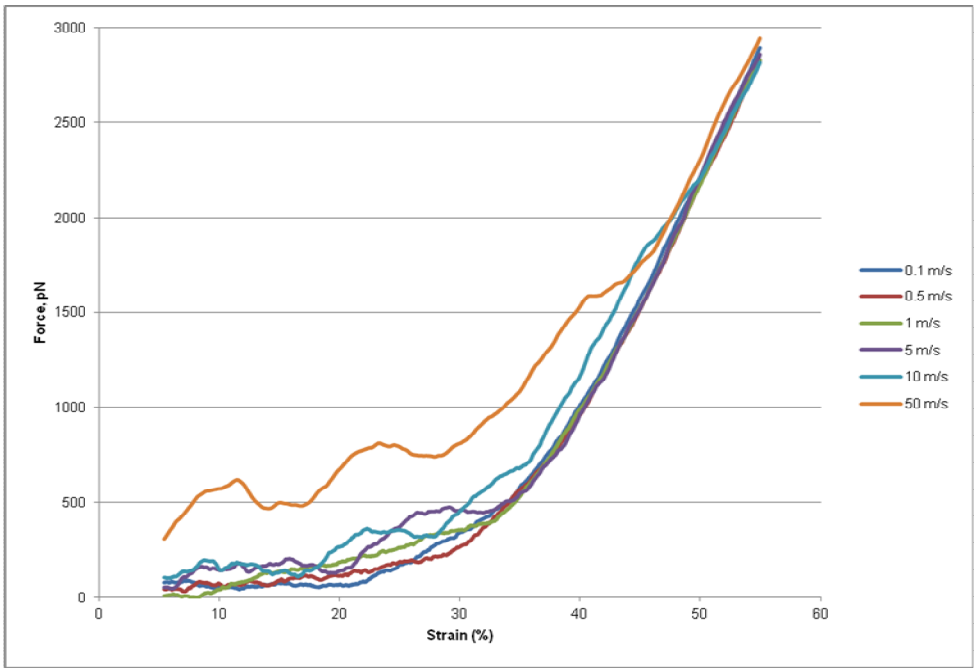

Fig. 4-2. Force vs Strain plot for different pulling velocitites on peptide PSSSYSAPGGGNGGR. Strain represents engineering strain of the 40.04 Å long molecular model and was defined as the change of length over the initial length (end-to-end distance).

4.4.4 Repeating Motifs in Exon-1

The *Drosophila* exon 1 resilin domain has PSSSYGAPGGGNGGR as the most common repetitive motif [15]. During our work, we have considered four sequence motifs PSSSY**G**APGGGNGGR, PSSTY**G**APGGGNGGR, PSSSY**S**APGGGNGGR and PSSTY**S**APG GGNGGR to understand whether the most frequent motif has any significance over others. From the force versus strain curves obtained from the repeating motifs shown in Fig. 4-3, the PSSSYGAPGGGNGGR motif has lowest stiffness. The force required to pull this motif is very

small compared to other motifs for equal strain. The fluctuations of force for PSSSYGAP GGGNGGR are probably due to the interactions with the surrounding water and among the amino acids. Similar fluctuations can be obtained for all the plots in Fig. 4-3, if all of them are plotted at the same scale (supplementary information, Fig. C.2). Results show that the force required to deform 55% of the initial end-to-end distance is much smaller for the most common repetitive motif compared to others as shown in Table 4.1.

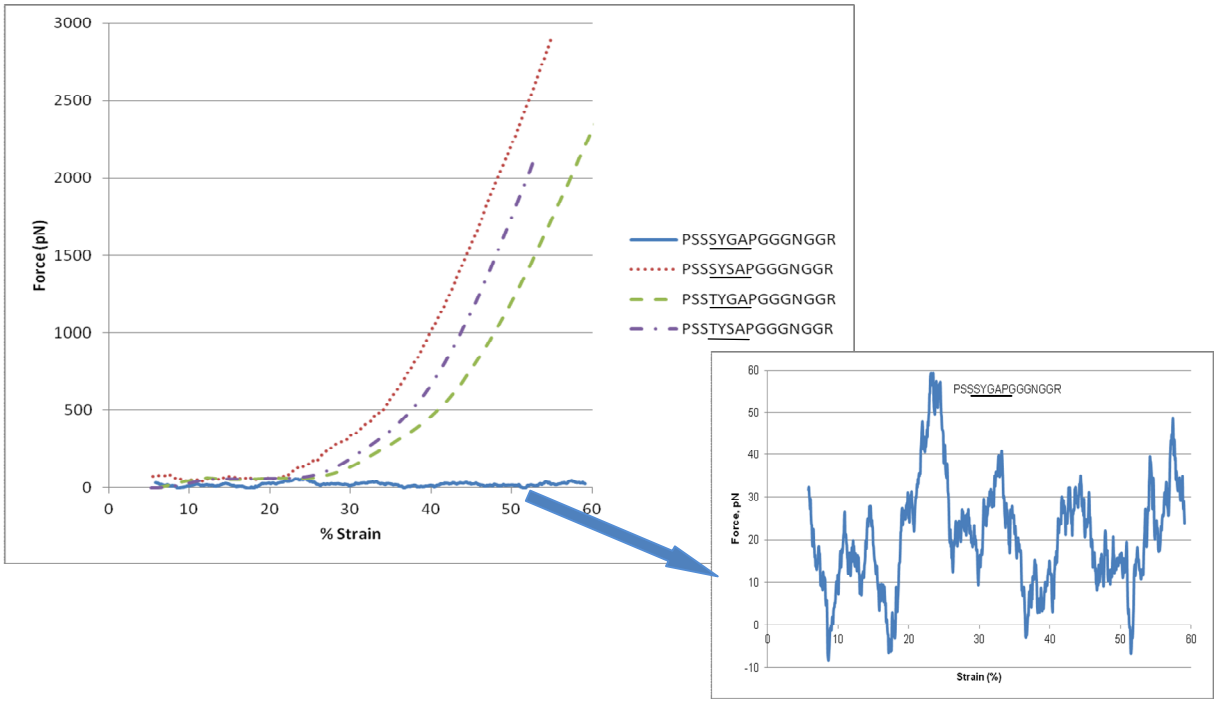

Fig. 4-3. Force-displacement plot for PSSSYGAPGGGNGGR, PSSSYSAPGGGNGGR, PSSTYGAPGGGNGGR and PSSTYSAPGGGNGGR. Among the motifs, PSSSYGAPGG GNGGR has highest extensibility and this is the most frequently represented repetitive motif in all insect resilin (Inset fig figure is provided at smaller scale). The Fluctuations are probably due to the interactions with the surrounding water and among the amino acids.

Referring back to the structures in Fig. 4-1, we see that PSSSYGAPGGGNGGR has the smallest length (Table 4.1), which results from a bend at the glycine residue between tyrosine

and alanine (Fig. 4-2a). This bend may be favored not only by the lack of a side chain on glycine, but also due to the presence of serine before tyrosine instead of threonine which has an extra methyl group which can create steric hindrance. The MD simulation was repeated three times and the same bend at the glycine was observed each time. All of the other motifs have a bend at the GGGN and GGR building blocks, but those bends do not influence the end-to-end distance to the same extent, as is shown in Table 4.1. Bent motifs could offer increased flexibility over more linearly arranged motifs if the bend can change shape when loaded, and if this elongated motif can come back to its initial bent conformation when force is removed, then this bent conformation may contribute to the macroscopic elastomeric properties.

4.4.5 Secondary Structure Analysis

Resilin is a disordered elastomeric protein in which there is no secondary structure like α-helix or β-sheet. However, resilin may possess polyproline II (PPII) helices[3] or β-turns[1, 14] which may influence its properties. According to Teule et. al.[42], central PG residue in a consensus motif favors the formation of type II β-turns. We have examined all four motifs using Xtlsstr software for PPII helix and results are shown in Table 4.2. The most frequent motif, PSSSYGAPGGGNGGR, has the fewest number of amino acids participating to form PPII, which might influence formation of a bent structure because these amino acids will not participate to form secondary structure.

Table 4-2. Polyproline II (PPII) helix in the four motifs. PSSSYGAPGGGNGGR has fewest numbers of amino acids that can adopt phi, psi values characteristic of PPII helix. Both PSSSYSAPGGGNGGR and PSSTYSAPGGGNGGR also have β-strand structure in addition to PPII while PSSTYGAPGGGNGGR only has PPII. Lowercase letters in the Xtlsstr assignment denote the end residues of secondary structure stretches.

Sequence	PPII	Pattern[a]	Location
PSSSYGAPGGGNGGR	2	------Pp-------	7,8
PSSTYGAPGGGNGGR	4	--PPp-Pp-------	3,4,5,7,8
PSSSYSAPGGGNGGR	5	---PpEe----Pp--	4,5,12,13
PSSTYSAPGGGNGGR	4	EEe-PPPP-NNN---	5,6,7,8

[a]Secondary structures disordered (-, N); poly-proline II-helix (P, p); β-strand (E, e)

4.4.6 Effects of Building Blocks

Exon-1 of resilin from *D. melanogaster* has PSSSYGAPGGGNGGR as the most frequent repetitive motif[15]. This motif can be subdivided into small building blocks: PSS, SYGAP, GGGN and GGR. Among the building blocks, most insects have SYGAP though some also have SYSAP and TYGAP. To gain further insight regarding the aforementioned bend in PSSSYGAPGGGNGGR, which resulted in a much shorter end-to-end distance compared to other motifs, and to determine whether the flanking building blocks (PSS, GGGN and GGR) influence the bend, we analyzed the following partial versions of the resilin pentadecapeptide: SYGAP, PSSSYGAP, PSSSYGAPGGGN. Similar building block combinations were constructed for all variations of the repetitive motifs under investigation here. MD simulations yielded results comparable to those for the full-length pentadecapeptide, i.e. motifs containing the repeat SYGAP exhibited the characteristic bending between tyrosine (Y) and alanine (A), and end-to-end distance is smaller compared to motifs with SYSAP, TYGAP and TYSAP (Table 4.3). As building blocks PSS, GGGN and GGR had very little influence on the bend, we

reasoned that a further comparison of SYGAP, SYSAP, TYGAP and TYSAP might yield new insight on the diverse functions of resilins and the distinct bend in SYGAP-containing peptides.

Table 4-3. End-to-end distances of fragments of the resilin motif comprised of varying building blocks. End-to-end distances of fragments containing SYGAP (in bold) are always the shortest within each fragment class.

Fragments	End-to end distance (Å)	Fragments	End-to end distance (Å)	Fragments	End-to end distance (Å)
SYGAP	4.85	PSSSYGAP	8.28	PSSSYGAPGGGN	11.38
SYSAP	12.01	PSSSYSAP	17.14	PSSSYSAPGGGN	20.81
TYGAP	14.25	PSSTYGAP	21.29	PSSTYGAPGGGN	23.89
TYSAP	15.4	PSSTYSAP	24.55	PSSTYSAPGGGN	30.79

We have calculated all energy contributions and interaction energies between peptide and water, as shown in Table 4.4. All the energies for the various repeating fragments are almost the same. The only difference among these four fragments is their length after equilibrium and before SMD. The length of SYGAP is 4.852 Å, which is less than half of the length of the other fragments. We performed the MD simulations three times with identical results. Among the four fragments, SYGAP and TYGAP have glycine in the central position, which provides conformational freedom for protein folding, but TYGAP has threonine instead of serine at the beginning of this sequence. The larger size of the threonine side chain may produce steric hindrance that disfavors the bending seen for SYGAP. On the other hand, SYSAP and TYSAP do not contain glycine, so they cannot bend like SYGAP. Our synthetic composite peptide assembled for this study, TYSAP, has both threonine and serine. Its higher steric hindrance than the naturally occurring peptides may explain both its lack of bending and possibly its apparent absence from the repertoire of naturally occurring resilins.

Table 4-4. Energies and non-bonded interactions between peptide and water of the repeating fragments. Force at 1nm elongation for every fragment is recorded. For all four repeating fragments, Forces at 1nm strain and length at equilibrium have noticeable variation as shown in the table.

Fragments	Bond Energy (kcal/mol)	Van-Der Waals Energy (kcal /mol)	Total Energy (kcal/ mol)	Potential Energy (kcal/mol)	Force at 1nm strain (pN)	non-bonded interaction between protein & water, (kcal/mol)	Length at Equilibrium (Å)
SYGAP	4990	5780	-28350	-40470	147	-408	4.852
SYSAP	4960	5800	-28630	-40620	2220	-416	12.01
TYGAP	5000	5840	-28640	-40721	3678	-372	14.25
TYSAP	5080	5910	-29020	-41331	5732	-422	15.40

Ramachandran plots[43] are used frequently to look at the distribution of the dihedral angles between the amino acids[44,45] and the effect of individual amino acids on the secondary structure of the proteins[46-47]. We have compared the dihedral angles during the MD for SYGAP, SYSAP, TYGAP and TYSAP using the Ramachandran plot at the bending location (glycine (G) for SYGAP and TYGAP, and serine (S) for SYSAP and TYSAP). We observed that the glycine of SYGAP does not have any preferred structure while the others have preferred ordered structures as shown in Fig. 4-4, which indicates the greater tendency of SYGAP to form disordered structure relative to the other peptides tested here. Theoretically, glycine might be in a βII turn conformation ($\varphi_3 = 90^\circ$ and $\psi_3 = 0^\circ$, where φ_3 and ψ_3 are the third residue of the turn as stated by Richardson[47] and Li at. al.[17]). From Fig. 4-4, we can see that the glycine of SYGAP has the tendency to form a βII-turn which is one of the characteristics of disordered proteins[1], while none of the other amino acids at the same location showed a similar tendency.

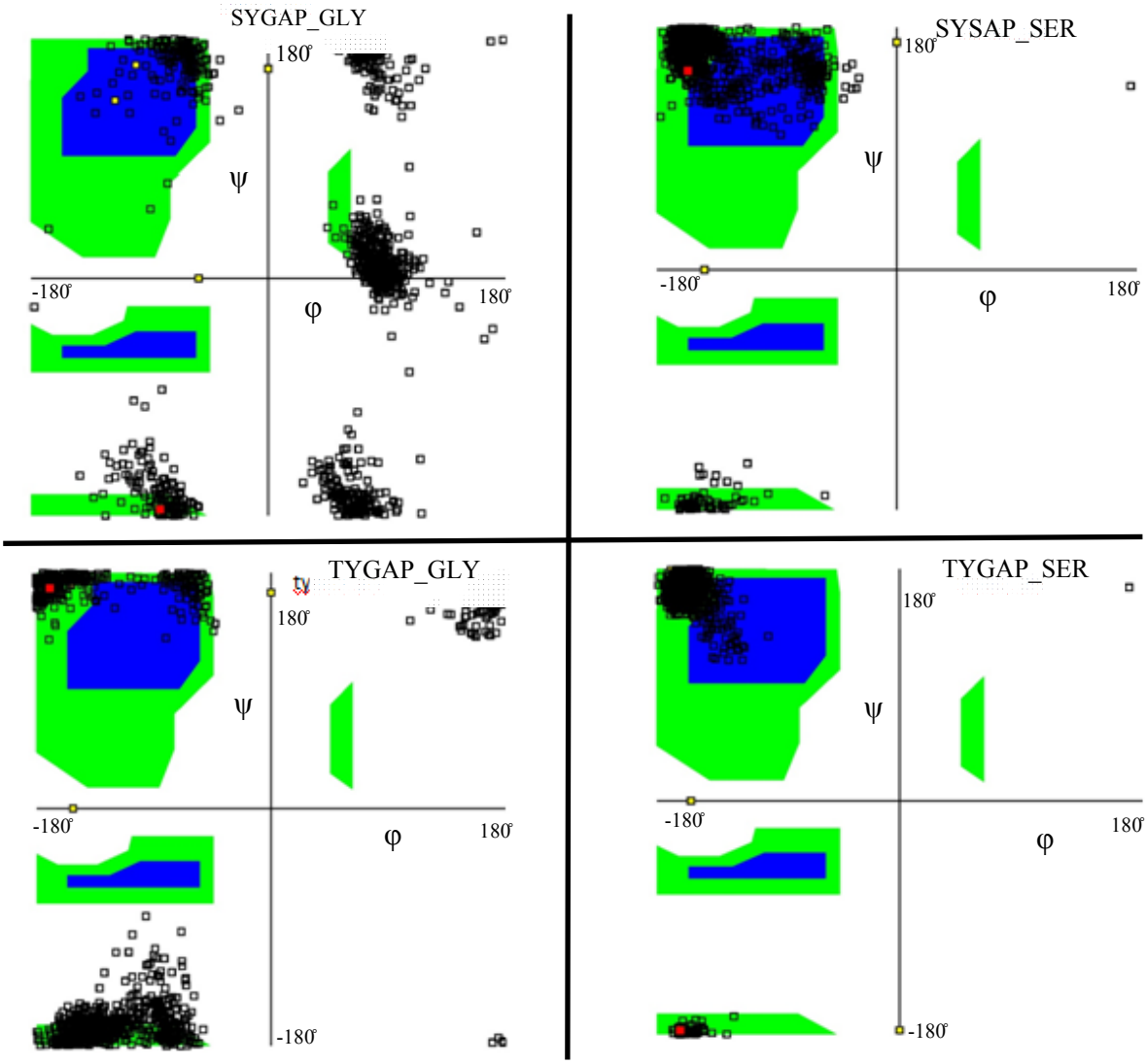

Fig. 4-4. Ramachandran plots for the fragments SYGAP, SYSAP, TYGAP and TYSAP during the MD at the third amino acid, which corresponds to the bending location of SYGAP.

The presence of a bend in SYGAP will be significant, if it can be extended and then return to its initial bent conformation when force is removed. To test this possibility, we conducted a MD simulation for 60 ns on the elongated structure of SYGAP after steered molecular dynamics (SMD), i.e. on the 1 nm elongated structure. Results showed that the

structure of the backbone of SYGAP after unrestrained MD of the extended peptide has a structure very similar to that of the starting structure prior to extension (Fig. 4-5). The backbone RMSD of these structures is 0.26 Å.

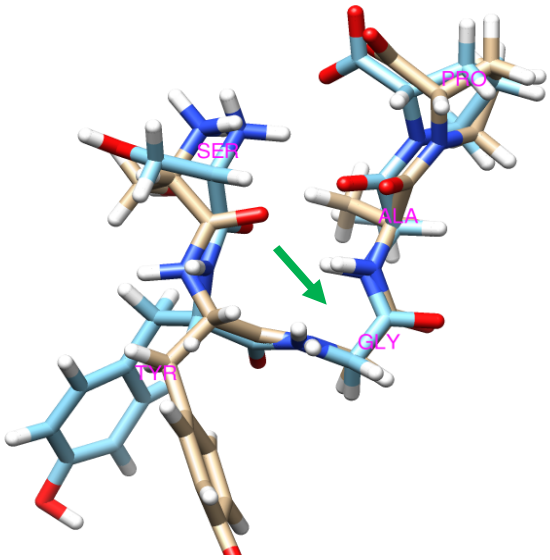

Fig. 4-5. Alignment of SYGAP structure obtained before extension by SMD (tan) and after collapse during unrestrained MD for 60 ns (blue). Both of structures have a similar bend at glycine (arrow).

To determine the entropically preferred conformation, we switched off the electrostatic interactions and the attractive portion of the Lennard-Jones (LJ) interactions leaving only bonded interactions and the repulsive part of the LJ interactions[41]. From the results, we observed that SYGAP has a comparable bent structure (Fig. 4-6), although the length (8.215 Å) is longer than when electrostatic interactions are present (Table 4.4) possibly reflecting an influence on secondary structure. On the other hand, the end-to-end distances observed for TYGAP, SYSAP and TYSAP, at 12.16, 11.67 and 13.94 Å, respectively, were similar to those in the presence of all the force field terms (Table 4.4). Cheng et al.[5] conducted a similar study on spider silk and resilin, and showed a comparably low persistence length due to the low steric hindrance of

glycines. Moreover, Dicko et al.[48] concluded that the emergence of elasticity in silks correlates highly with the glycine content. They suggested that glycine controls the soluble precursor assembly and proline governs the solid fiber behavior. According to our results, SYGAP forms a bent structure, and end-to-end distance is very short compared to the other repeats which agrees with result from Cheng et al.[5], as stated above. Resilin also has high glycine content like other elastomeric proteins and here we show that a characteristic bend occurs at the glycine of the SYGAP repeat, which may be one of the controlling factors for high elasticity.

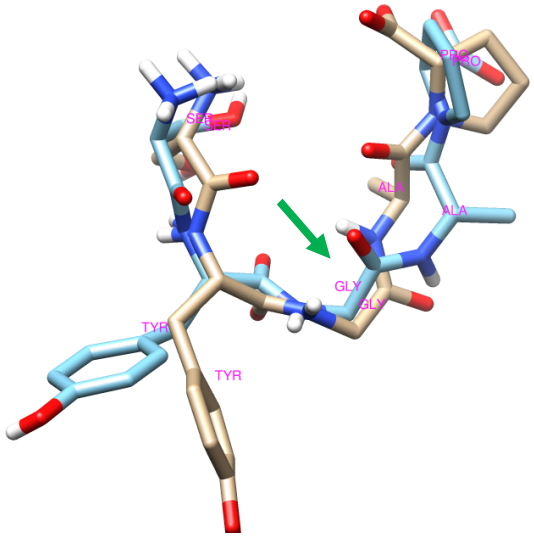

Fig. 4-6. Alignment of SYGAP structure obtained before (tan) and after switching off the electrostatic interactions and the attractive portion of the Lennard-Jones (LJ) interactions (blue). Both structures have a similar bend at the glycine residue (arrow).

We have also constructed another fragment, GYGAP to test steric hindrance, as this fragment has the least steric hindrance compared to any of the other four fragments due to the absence of side chains. The end-to-end distance for GYGAP is 14.8 Å, which is comparable to the length of SYSAP, TYGAP and TYSAP. These results indicate that bent and extended

structures resulting for these fragments at equilibrium are not only from steric hindrance, but also from the electrostatic interactions.

To clarify the possibility of charged terminal interactions between serine (S) and proline (P) in the bent conformation of SYGAP, we attached caps at both the termini. The resulting MD simulation also gave results comparable to those obtained without capping the termini (supplementary information, Fig. C.3).

From the dihedral angle results we saw that SYGAP does not have any preferred structure while the other three peptides, SYSAP, TYGAP and TYSAP, prefer some secondary structure (Table 4.2). When we consider electrostatic interactions, there are possibilities of hydrogen bonds formation in the chain. However, due to steric hindrance some of the possible H-bonds cannot be formed. During the MD simulation, the backbone rotates through different dihedral angles, as shown in the Ramachandran plots, and due to the different side groups, the peptides switch among different conformations. During the process, some residues form hydrogen bond and construct stable and preferred conformations. According to Johnson et. al.[49], an enhancement in the modulus elasticity and toughness occurs due to the tyrosine and serine stabilization through hydrogen bonding. SYGAP has four H-bonds within the backbone and the side chains, and forms the bent conformation shown in Fig. 4-7. However, for SYSAP, TYGAP and TYSAP, only one H-bond within the backbone and the side chains can be formed. According to Rauscher et al.[1], if the sequence has a higher propensity of PPII structure, the structure cannot stabilize any turns through hydrogen bonding. As a result SYSAP, TYGAP and TYSAP do not have any stable bent conformations.

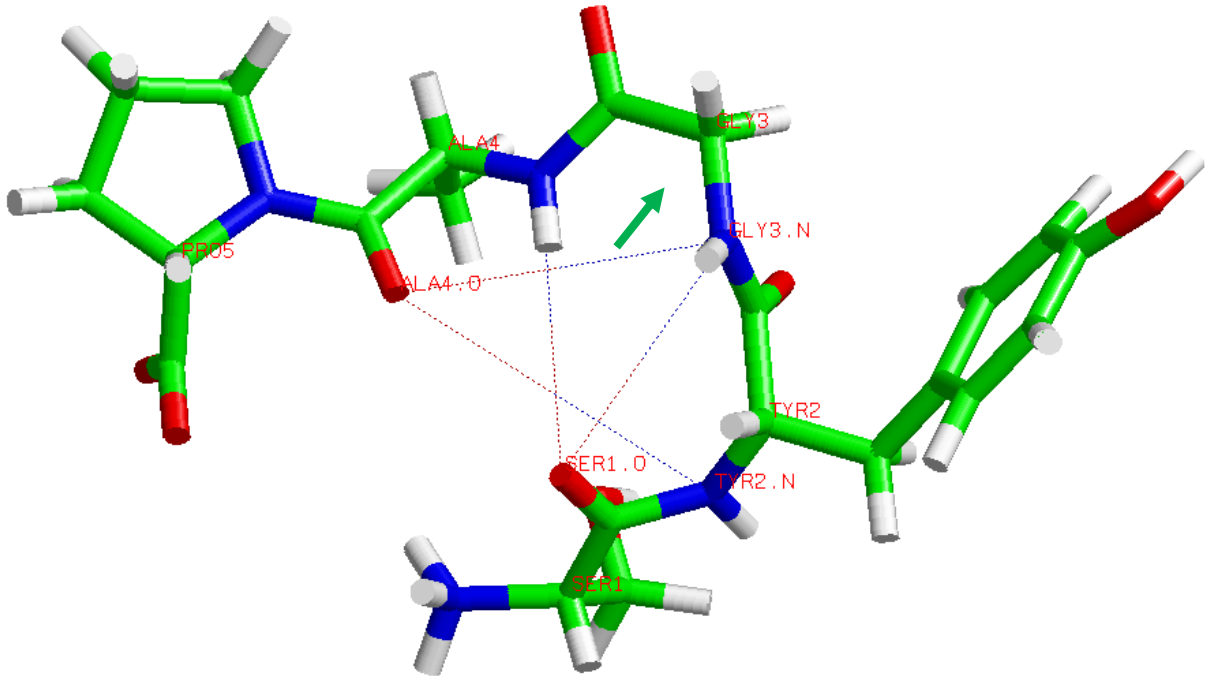

Fig. 4-7. Hydrogen bonds in the repeat motif SYGAP during bent conformation. Other than proline, all the other amino acids participate in hydrogen bonding to form the stable bent structure in addition to lack of streric hindrance at glycine (arrow).

We have also tested the order of the amino acids in the SYGAP to understand if there is any significance. We have switched alanine and proline and formed SYGPA. The MD simulation results showed that SYGPA behaves similarly to TYGAP, SYSAP and TYSAP, i.e. forming an extended structure. It does not form the bent structure and there is only one hydrogen bond within the backbone and the side chains.

The mechanisms suggested here seem related to the recently advanced concept of protein foldamers[50], which consist of relatively stiff backbones punctuated by flexible hinges that snap from one conformation to another. The motif examined herein has a bent conformation at glycine, presumably because of a lack in steric hindrance, as well as the suggestion of hydrogen bonds which could hold the bent conformation or disappear when the motif is extended. Being

conserved and repetitive in most insects' resilin gene, the motifs have potential similarity with foldamers[50], though details were not explored.

Together our results showed that the most frequent naturally occurring motif, PSSSYGAPGGGNGGR, adopts conformations that may contribute to improved elastomeric behavior compared to other related motifs. Importantly, PSSSYGAPGGGNGGR forms a bent structure, such that when we hold one end and pull the other end, the peptide unfolds, requiring very low forces to stretch in comparison to the other tested variations of this motif. When we remove the force from the PSSSYGAPGGGNGGR, it returns to its previous conformation, as was demonstrated by the collapse simulation (Fig. 4-5). From these results, we hypothesize that this ability to bend might be one of the contributing factors of the elastomeric properties of resilin.

4.5 Conclusion

Disordered elastic proteins are found throughout the animal kingdom for a variety of functions. Like other disordered elastomeric proteins (gliadin, elastin, spider silks), resilin contains distinct repetitive domains in its amino acid sequence to confer elastomeric properties[15]. In exon 1, PSSSYGAPGGGNGGR is the most frequent repetitive motif. Our objective was to determine if this repeating motif has any unique properties over other possible motifs and how this motif may thereby control the behavior of the elastomeric proteins. The results suggest that this motif makes an important contribution to the elastomeric properties of resilin by forming a favorable bent structure instead of an extended structure through a combined effect of H-bonding and lack of steric hindrance. When the protein is stretched, it moves to an extended conformation, and it comes back to the initial conformation when released due to the favorable bend. What we learned from simulating the repetitive motifs of resilin may be applicable to the biology and

mechanics of other unstructured protein domains. These findings might someday be valuable in the design and manufacture of high-performance, biocompatible rubbers with tailored mechanical properties. Moreover, we anticipate that the results will be of scientific significance in the field of biomaterials and biomedical devices.

References

1. S. Rauscher, S. Baud, M. Miao, F. W. Keeley and R. Pomes, Proline and Glycine Control Protein Self-Organization into Elastomeric or Amyloid Fibrils. *Structure*, 2006, **4**, 1667–1676.
2. B. Bochicchio, A. Pepe and T. A. M., Investigating by CD the molecular mechanism of elasticity of elastomeric proteins. *Chirality*, 2008, **20**, 985-994.
3. F. X. Theillet, L. Kalmar, P. Tompa, K. H. Han, P. Selenko, A. Keith Dunker, G. W. Daughdrill and V. N. Uversky, The alphabet of intrinsic disorder: I. Act like a Pro: On the abundance and roles of proline residues in intrinsically disordered proteins. *Intrinsically Disordered Proteins*, 2013, **1**, 1-13.
4. R. M. Williams, Z. Obradovi, V. Mathura, W. Braun, E. C. Garner, J. Young, S. Takayama, C. J. Brown and A. K. Dunker, The protein non-folding problem: amino acid determinants of intrinsic order and disorder. *Pacific Symposium on Biocomputing*, 2001, **89-100**.
5. S. Cheng, M. Cetinkaya and F. Grater, How Sequence Determines Elasticity of Disordered Proteins. *Biophysical Journal*, 2010, **99**, 3863–3869.
6. T. Weis-Fogh, A rubber-like protein in insect cuticle. *Journal of Molecular Biology*, 1960, **37**, 889-907.
7. S. J. Edwards, Predation and digestion in assassin bugs (Heteroptera, Reduviidae. University of Cambridge, UK, 1960.
8. D. Young and H. C. Bennet-Clark, The role of tymbal in cicada sound production. *Journal of Experimental Biology*, 1995, **198**, 1001-1019.
9. M. Burrows, S. R. Shaw and G. P. Sutton, Resilin and chitinous cuticle form a composite structure for energy storage in jumping by froghopper insects. *BMC Biology*, 2008, **6**.

10. S. O. Andersen and T. Weis-Fogh, Resilin. A rubber-like protein in arthropod cuticle. *Advances in Insect Physiolology*, 1964, **2**, 1-65.
11. G. F. Elliott, A. F. Huxley and T. Weis-Fogh, On the structure of resilin. *Journal of Molecular Biology*, 1965, **13**, 791-795.
12. R. Kappiyoor, Balasubramanian, G., Dudek, D. M., Puri, I.P., Elastomechanical properties of resilin. *Soft Matter*, 2011, **7**, 11006-11009.
13. S. O. Andersen, The cross links in resilin identified as dityrosine and trityrosine. *Biochimica et Biophysica Acta*, 1964, **93**, 213-215.
14. G. Qin, Hu, X., Cebe, P. and Kaplan, D. L., Mechanism of Resilin Elasticity. *Nature Communication*, 2012, **3**, 1-18.
15. G. Qin, S. Lapidot, K. Numata, X. Hu, S. Meirovitch, M. Dekel, I. Podoler, O. Shoseyov and D. L. Kaplan, Expression, Cross-Linking, and Characterization of Recombinant Chitin Binding Resilin. *Biomacromolecules*, 2009, **10**, 3227–3234.
16. M. Baer, E. Schreiner, A. Kohlmeyer, R. Rousseau and D. Marx, Inverse temperature transition of a biomimetic elastin model: reactive flux analysis of folding/unfolding and its coupling to solvent dielectric relaxation. *Journal of Physical Chemistry*, 2006, **B 110**, 3576–3587.
17. B. Li, D. O. V. Alonso and V. Daggett, The molecular basis for the inverse temperature transition of elastin. *Journal of Molecular Biology*, 2001, **305**, 581–592.
18. M. B. Charati, Ifkovits,J. L., Burdick J. A., Linhardtc, J. G., Kiick, K. L., Hydrophilic elastomeric biomaterials based on resilin-like polypeptides. *Soft Matter*, 2009, **5**, 3412–3416.

19. R. Petrenko, Computer simulations of resilin-like peptides. Doctoral Dissertation, University of Cincinnati, 2010.
20. A. L. Kwansa, Vita R. D. and J. W. Freeman, Mechanical recruitment of N- and C-crosslinks in collagen type I. *Matrix Biology*, 2014, **34**, 161-169.
21. M. Bhandarkar, A. Bhatele, E. Bohm, R. Brunner, F. Buelens, C. Chipot, A. Dalke, S. Dixit, G. Fiorin, P. Freddolino, P. Grayson, J. Gullingsrud, A. Gursoy, D. Hardy, C. Harrison, J. Hénin, W. Humphrey, D. Hurwitz, N. Krawetz, S. Kumar, D. Kunzman, C. Lee, R. McGreevy, C. Mei, M. Nelson, J. Phillips, O. Sarood, A. Shinozaki, D. Tanner, G. Zheng and F. Zhu, ed.^eds., 2011, p.^pp.
22. B. Isralewitz, Baudry, J., Gullingsrud, J., Kosztin, D., Schulten, K., Steered molecular dynamics investigations of protein function. *Journal of Molecular Graphics and Modelling*, 2001a, **19**, 13-25.
23. B. Isralewitz, Gao, M., Schulten, K., Steered molecular dynamics and mechanical functions of proteins. *Current Opinion in Structural Biology*, 2001b, **11**, 224-230.
24. A. Gautieri, M. J. Buehler and A. Redaelli, Deformation rate controls elasticity and unfolding pathway of single tropocollagen molecules. *J. Mech. Behav. Biomed*, 2009, **2**, 130-137.
25. A. Gautieri, Buehler, M.J., Redaelli, A., Deformation rate controls elasticity and unfolding pathway of single tropocollagen molecules. *Journal of the Mechanical Behavior of Biomedical Materials*, 2009, **2**, 130-137.
26. L. Kal´e, R. Skeel, M. Bhandarkar, R. Brunner, A. Gursoy, N. Krawetz, J. Phillips, A. Shinozaki and K. Varadarajan, NAMD2: Greater scalability for parallel molecular dynamics. *Journal of Computational Physics*, 1999, **151**, 283–312.

27. A. D. Mackerell, D. Bashford, Bellott, R. L. Dunbrack, J. D. Evanseck, M. J. Field, S. Fischer, J. Gao, H. Guo, S. Ha, D. Joseph-Mccarthy, L. Kuchnir, K. Kuczera, F. T. K. Lau, C. Mattos, S. Michnick, T. Ngo, D. T. Nguyen, B. Prodhom, W. E. Reiher, B. Roux, M. Schlenkrich, J. C. Smith, R. Stote, J. Straub, M. Watanabe, J. Wiorkiewicz-Kuczera, D. Yin and M. Karplus, All-atom empirical potential for molecular modeling and dynamics studies of proteins. *The Journal of Physical Chemistry B*, 1998, **102**, 3586–3616.
28. W. L. Jorgensen, J. Chandrasekhar, J. D. Madura, R. W. Impey and M. L. Klein, Comparison of simple potential functions for simulating liquid water. *The Journal of Chemical Physics*, 1983, **79**, 926–935.
29. R. E. Lyons, K. M. Nairn, M. G. Huson, M. Kim, G. Dumsday and C. M. Elvin, Comparisons of recombinant resilin-like proteins: Repetitive domains are sufficient to confer resilin-like properties. *Biomacromolecules*, 2009, **10**, 3009-3014.
30. B. Hess, C. Kutzner, D. Van Der Spoel and E. Lindahl, GROMACS 4: Algorithms for Highly Efficient, Load-Balanced, and Scalable Molecular Simulation. *Journal of Chemical Theory and Computation*, 2008, **4**, 435-447.
31. D. Van Der Spoel, E. Lindahl, B. Hess, G. Groenhof, A. E. Mark and H. J. Berendsen, GROMACS: fast, flexible, and free. *Journal of Computational Chemistry* 2005, **26**, 1701-1718.
32. G. Kaminski, R. Friesner, T.-R. J. and W. Jorgensen, Evaluation and Reparametrization of the OPLS-AA Force Field for Proteins via Comparison with Accurate Quantum Chemical Calculations on Peptides. *Journal of Physical Chemistry*, 2001, **105**, 6474 - 6487.
33. A. S. Inc, Discovery Studio Modeling Environment. (2011) Accelrys Software Inc., San Diago.

34. W. Humphrey, A. Dalke and K. Schulten, VMD: visual molecular dynamics. *Journal of molecular graph*, 1996, **14**, 33-38.

35. J. P. Ryckaert, G. Ciccotti and H. J. Berendsen, Numerical integration of the cartesian equations of motion of a system with constraints: molecular dynamics of n-alkanes. *Journal of Computational Physics*, 1977, **23**, 327–341.

36. T. Darden, D. York and L. Pedersen, Particle mesh Ewald: An N⍤ log(N) method for Ewald sums in large systems. *Journal of Chemical Physics*, 1993, **98**, 10089-10092.

37. A. Wolf and K. N. Kirschner, Principal component and clustering analysis on molecular dynamics data of the ribosomal L11·23S subdomain. *Jounal of molecular modeling*, 2013, **19**, 539-549.

38. E. F. Pettersen, T. D. Goddard, C. C. Huang, G. S. Couch, D. M. Greenblatt, E. C. Meng and T. E. Ferrin, UCSF Chimera--a visualization system for exploratory research and analysis. *Journal of Computational Chemistry*, 2004, **13**, 1605-1612.

39. S. M. King and W. C. Johnson, Assigning secondary structure from protein coordinate data. *Proteins: Structure, Function, and Genetics*, 1999, **35**, 313-310.

40. W. Kabsch and C. Sander, Dictionary of protein secondary structure: pattern recognition of hydrogen-bonded and geometrical features. *Biopolymers*, 1983, **22**, 2577–2637.

41. F. Gräter, P. Heider, R. Zangi and B. J. Berne, Dissecting entropic coiling and poor solvent effects in protein collapse. *Journal of Americal Chemical Society*, 2008, **130**, 11578–11579.

42. F. Teule, W. A. Furin, A. R. Cooper, D. J. R. and R. V. Lewis, Modifications of spider silk sequences in an attempt to control the mechanical properties of the synthetic fibers. *Journal of Material Science*, 2007, **42**, 8974–8985.

43. G. N. Ramachandran, C. Ramakrishnan and V. Sasisekharan, Stereochemistry of Polypeptide Chain Configurations. *Journal of Molecular Biology*, 1963, **7**, 95-99.

44. D. Pal and P. Chakrabarti, On residues in the disallowed region of the Ramachandran map. *Biopolymers*, 2002, **63**, 195-206.

45. M. C. Vega, J. C. Martinez and L. Serrano, Thermodynamic and structural characterization of Asn and Ala residues in the disallowed II′ region of the Ramachandran plot. *Protein Sciences*, 2000, **9**, 2322-2328.

46. B. K. Ho and R. Brasseur, The Ramachandran plots of glycine and pre-proline. *BMC Structural Biology*, 2005, **5**, 14-24.

47. J. S. Richardson, The anatomy and taxonomy of protein structure. *Advances of Protein Chemistry*, 1981, **34**, 167-339.

48. C. Dicko, D. Porter, J. Bond, J. M. Kenney and F. Vollrath, Structural disorder in silk proteins reveals the emergence of elastomericity. *Biomacromolecules*, 2008, **9**, 216-221.

49. J. C. Johnson and L. T. J. Korley, Enhanced mechanical pathways through nature's building blocks: amino acids. *Soft Matter*, 2012, **8**, 11431-11442.

50. S. H. Gellman, Foldamers: A Manifesto. *Accounts of Chemical Research*, 1998, **31**, 173-180.

Chapter 5: Molecular Modeling of Repeating Motifs of Disordered Elastomeric Proteins

5.1 Abstract

Elastomeric proteins can be found in a wide range of living organisms, and structural disorder is one of the critical features of these proteins[1]. About 40% of highly structured proteins contain disordered domains[2]. Despite their ubiquity, there is little understanding about the mechanisms responsible for the mechanical properties of these disordered elastomeric proteins. To better understand the structure-property relationship between elastomeric behavior and their amino acid sequence, we investigate the repetitive motifs from different species using molecular dynamics (MD) simulations. Repeating motifs are considered from elastin: VPGVG[3], resilin: exon-3: GYSGGRPG[4], dragline spider silk: GGYGPGS[3], flagelliform silk: GPGGY[5] and mussel byssus: GPGGG[3]. The results after clustering analyses show that all the motifs adopt a bent structure, presumably through a combined effect of intramolecular hydrogen bonding and lack of steric hindrance. These hydrogen bonds within the motifs apparently play a role in maintaining the bent conformation. During SMD pulling of these motifs, the hydrogen bonds break and they reform again when the peptides are released to move freely, returning to similar bent conformations. Adhikary et al.[6] and Takano et al.[7] also observed intramolecular hydrogen bonds which stabilizing the protein conformations. Moreover, our experimental work on recombinant resilin[8-9] and other work on natural resilin of dragonflies[10] and cockroaches[11] suggested that the measured transitions could potentially be within the rubbery plateau and due to intramolecular hydrogen bonds, though the transitions might also due to true glass transitions or altered structural organization.

Keywords: Molecular modeling; Resilin; Elastin; Spider Silk; Mussel Byssus; Elastomeric proteins; Repetitive motifs; Hydrogen bonds; Bent conformations; Foldamers.

5.2 Introduction

Spanning a broad range of material properties and functional roles[12], elastomeric proteins can be found in many bio-systems including insects, plants, fishes and humans[13]. They can be reversibly deformed to large strains with relatively small stresses and can perform biological functions with low energy loss [14]. Among the rubber-like elastomeric proteins, elastin can be found in the extracellular matrix of elastic tissues such as arteries, aorta, etc., and resilin in the specialized regions of the cuticle of insects, while both have high resilience and low stiffness[4, 14-15]. Mussel byssus, located in the hinge region of bivalves, have considerable stiffness and strength, though they are very stretchy[15]. Spiders have two different elastomeric silks in the web: flagelliform silk that forms the web orbs are soft, while dragline silk that forms the lines in the prey catching web are stiff[13]. Even though elastomeric proteins have complex domain structures, and display functional variations, they have two common features: repeating sequences and intermolecular crosslinks[3]. Due to the repetitive motifs and crosslinking, elastomeric proteins can be considered as block co-polymers[16]. It is known from rubber elasticity theory that molecular mass between the crosslinks (M_c) is the key factor controlling the shear modulus (G) of polymer networks, according to, $G = \rho RT/M_c$[17] (where T is the absolute temperature, ρ is the density, and R is the gas constant). Geometric constraints, such as chemical or physical crosslinks, rather than chemical composition, are thus predicted to play a dominant role in controlling the modulus of elastomers, according to rubber elasticity. Thus, higher crosslink density will increase the modulus of an elastomer[18]. However, repeating motifs are common features for all elastomeric proteins, independent of their properties and functions. The chemical compositions of these

repeating motifs are important in controlling the resulting viscoelastic properties, recognizing that if composition and topology increase the glass transition temperature of elastomeric proteins, they can no longer be considered as elastomers. Insight into the underlying mechanisms through which these repeating motifs affect elastomeric properties, other than through participation in the formation of crosslinks, is not clear yet[19]. During our previous molecular dynamics simulations of the repeat motif from exon-1 of resilin, we discovered that the repeat motifs favor a bent conformation instead of an extended conformation, likely through a combined effect of hydrogen bonding and lack of steric hindrance. When the protein is stretched, it moves to an extended conformation, but returns to the initial conformation when released due to the favorable bend. The flexibility may contribute to elastic flexibility at the macroscopic level[20].

The main objective of this paper was to determine if the repeating motifs from other elastomeric proteins follow the same trend to better understand the influence of structure on elastomeric properties. Here, five different repeat motifs from different elastomeric proteins are studied through a similar investigation using atomistic molecular modeling.

5.3 Methodology

MD simulations were used to simulate five repetitive motifs from proteins with elastomeric properties from different species to investigate their conformation and possible contributions to the properties. The following elastomeric proteins and repeating motifs were considered: (i) Elastin: $VPGVG^3$, (ii) Resilin exon-3: $GYSGGRPG^4$, (iii) Dragline spider silk: $GGYGPGS^3$, and Flagelliform silk: $GPGGY^5$, taken from the same insect, (iv) Mussel Byssus: $GPGGG^3$. The computer program Discovery Studio Visualizer[21] was used to construct the molecular models. Molecular modeling software GROMACS[22] was used for all simulations. The all-atom

CHARMM22 force field[23] was used for peptides and the TIP3P model was used for water[24]. The SHAKE algorithm[25] was used to constrain the covalently linked hydrogen atoms to a fixed length. The cut-off distance was 12 Å, while the switching function started at 10 Å for van-der-Waals interactions. particle-mesh Ewald (PME)[26] was used for long-range electrostatic forces, and grid point was adjusted to around 1 Å for PME based on the periodic cell size.

Peptides were immersed in a water box with padding of at least 10 Å on all sides. Simulations were conducted using a leapfrog time integration and the following steps: (a) energy minimization, (b) a canonical NVT (constant Number of particles, Volume, and Temperature) ensemble-based simulation performed with temperature controlled at 310K for 5×10^6 time steps, (c) a canonical NPT (constant Number of particles, Pressure, and Temperature) ensemble at 310K for 5×10^6 time steps using a modified Berendsen thermostat and a Parrinello-Rahman barostat, and (d) production MD where motifs were allowed to move freely for 5×10^7 time steps. Periodic boundary conditions were applied to keep the number of atoms constant in the system throughout the simulation. Van der Waals switch cutoff and columbic interactions cutoff distance were 1 nm.

The most favorable conformations for each motif were determined by clustering analysis[27] using GROMACS. A cutoff of 0.10-0.20 nm was applied for the clustering analysis. A structure is added to the cluster when its distance from any element of the cluster is less than the cutoff. The most favorable conformation was determined based on a frequency of 60% or more structures in the dominant cluster during the production MD. A larger water box was generated to conduct the steered molecular dynamics (SMD) of 1 nm elongation, so that the protein remains inside the box after the simulation. The N-terminus of the motif (the amide group attached to the alpha carbon of the first amino acid) was held fixed while the C-terminus (the

carboxyl group attached to the alpha carbon of the final amino acid) was pulled 1 nm at a constant velocity of 0.1 m/s during the SMD, similar to our previous work on repetitive motifs in exon 1 of resilin [20], with the assumption that this velocity would be suitable for the repetitive motifs of the elastomeric proteins in this study. The extended structure was released and the MD simulation was continued for 5×10^7 time steps to compare the collapsed structure with the structure obtained after clustering. Structures were aligned manually using the Chimera 1.9 visualization program[28] to compare the conformations. The molecular visualization software RasTop 2.2[29] was used to predict the existence of hydrogen bonds within the motifs.

5.4 Results and Discussion

5.4.1 Resilin

Resilin is a disordered elastomeric protein that can be found in a specialized region of insects cuticle[4]. It reportedly suffers neither from creep nor stress relaxation even after weeks of sustained straining and can be stretched to 300% of its resting length , though resolution of the instruments are not known[30-31]. Resilin reportedly has long fatigue life with resilience higher than that of synthetic polybutadiene, a high resilience rubber, though the mechanism is not clear yet [32-33]. Most insect resilin genes are comprised of three protein coding regions, or exons. Both exon 1 and exon 3 contain repeating elastomeric motifs PSSSYGAPGGGNGGR and GYSGGRPG, respectively, while exon 2 is designated the chitin binding domain (ChBD)[19]. During our previous work[20], MD simulations were conducted on PSSSYGAPGGGNGGR and a bent conformation was observed, which apparently results from a combined effect of hydrogen bonding and lack of steric hindrance, and the characteristic bending was between tyrosine (Y) and alanine (A) at glycine (G). Here, a similar investigation is conducted on the repeating motif of exon-3. After the production MD, we found a bent conformation of GYSGGRPG, and

characteristic bending occurred at the glycine that is the fifth residue in this sequence (Fig. 5-1a), where the least steric hindrance occurred, in agreement with our previous work[20]. After the SMD and release simulations, the collapsed structure was aligned with the structure obtained after clustering and they almost perfectly matched with each other (root mean square distance, RMSD = 0.55 Å). Aligned conformations are shown without the side chains for proper visualization (Fig. 5-1b). End-to-end distance of GYSGGRPG after clustering (prior to elongating) was 3.06 Å and after the second clustering upon collapse was 3.08 Å, essentially fully returned from the extended state.

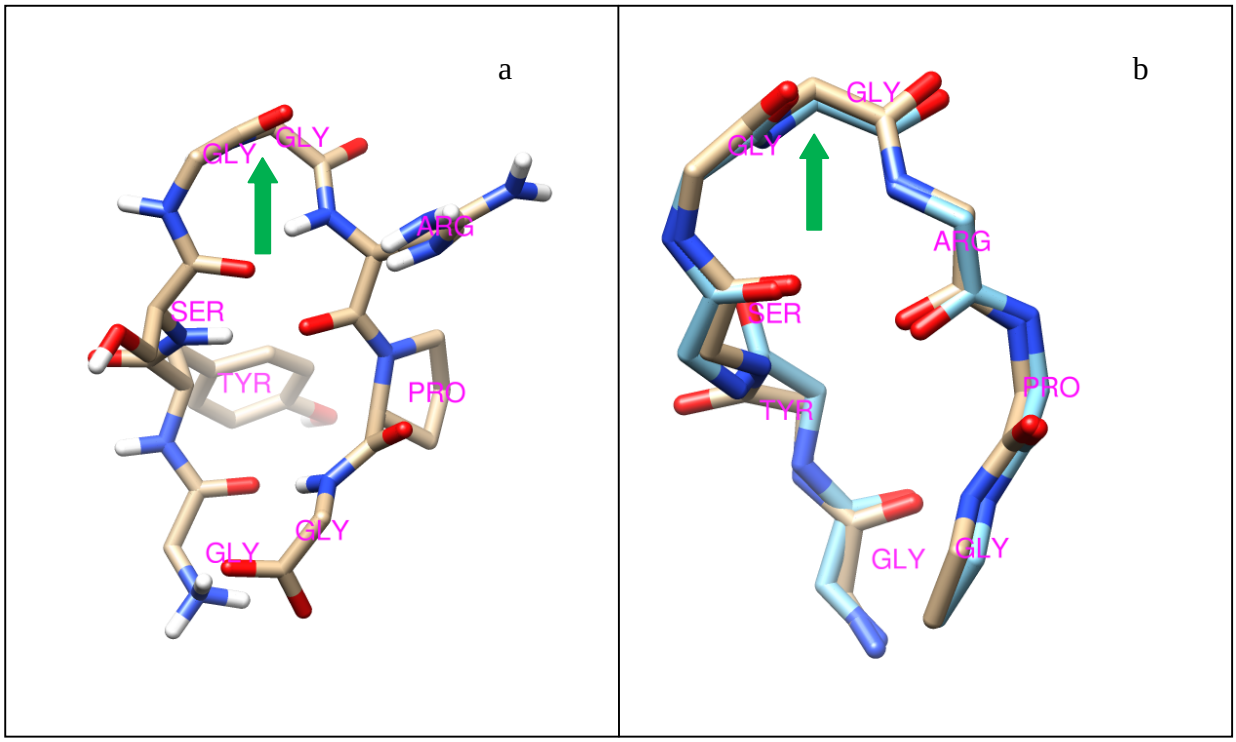

Fig. 5-1. (a) Bent conformation of GYSGGRPG after clustering with side chains shown (b) Aligned conformation of GYSGGRPG after clustering (gold) and conformation after clustering after stretching and releasing the peptide during SMD (blue).

During production MD, some residues formed hydrogen bonds and adopted stable and preferred conformations due to the formation of hydrogen bonds (Fig. 5-2a). When the motif was pulled 1 nm during the SMD pulling, some of the hydrogen bonds were broken and the protein formed an extended conformation (Fig. 5-2b), and when both the termini were released and allowed to move freely, the motif formed a bent structure (Fig. 5-2c) and the hydrogen bonds reformed.

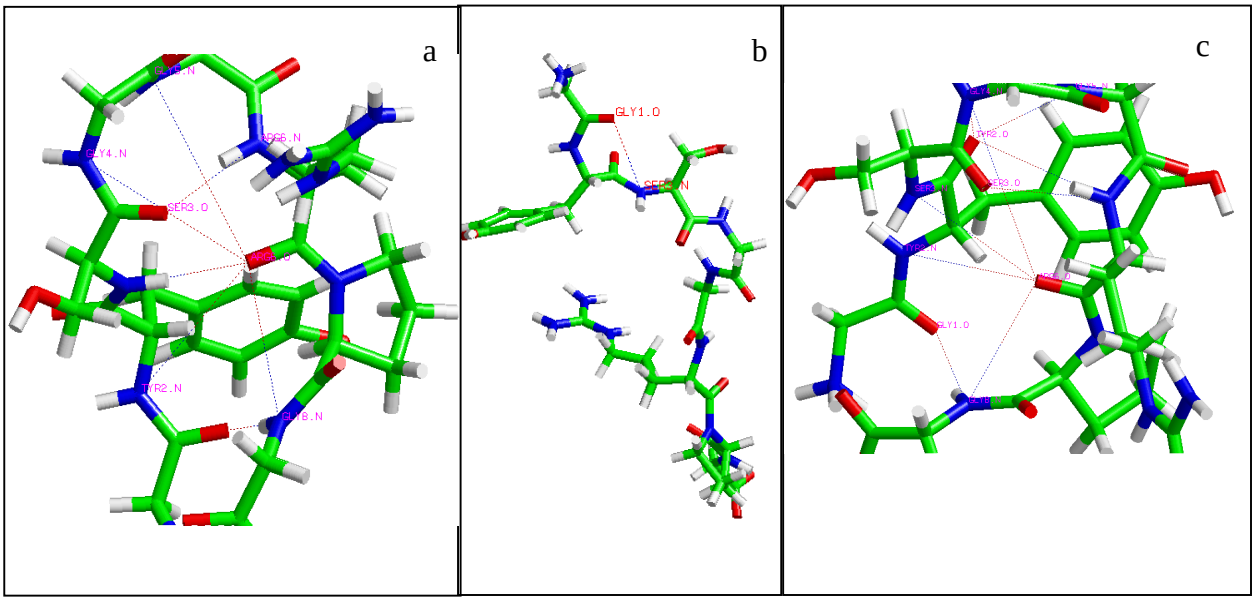

Fig. 5-2. Hydrogen bonds of GYSGGRPG (a) after clustering (b) after SMD pulling, and (c) after collapse. During the SMD pulling, hydrogen bonds were broken. These same hydrogen bonds reformed during the collapse simulation.

In Fig. 5-2b, it was observed most of the hydrogen bonds were broken during SMD. Hydrogen bonds did not break until the elongation reached to about 0.7 nm and continued to break upon further elongation (Fig. 5-3a). On the other hand, during the collapse simulations the hydrogen bonds reformed within few picoseconds as the bent structure formed, with the bent structure being maintained throughout the remainder of the simulations (Fig. 5-3b).

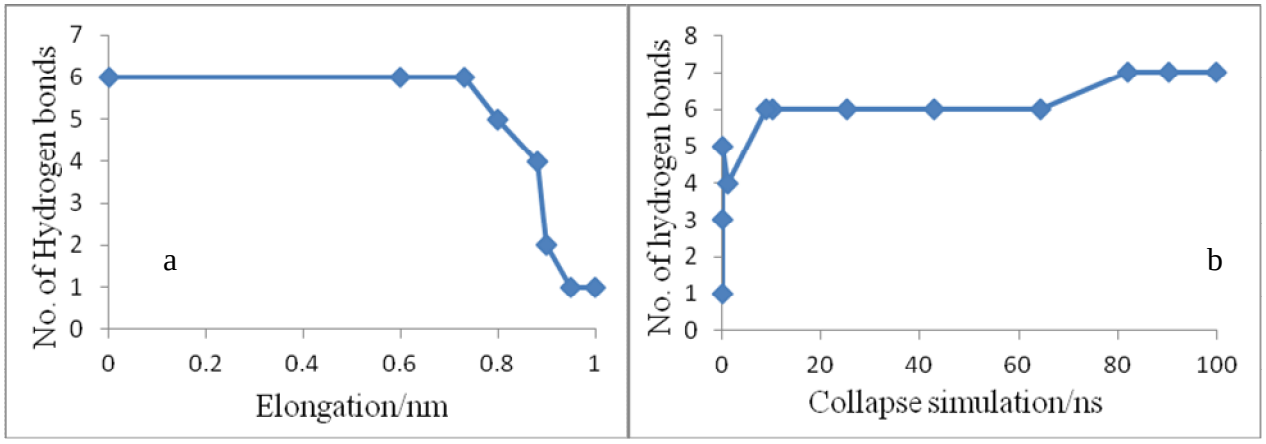

Fig. 5-3. (a) Change in number of hydrogen bonds of GYSGGRPG during the SMD (b) Hydrogen bonds formation in GYSGGRPG during the collapse simulations. Most of the hydrogen bonds formed within few picoseconds.

Considering the bent conformations of the motifs due to intramolecular hydrogen bond and low steric hindrance due to the presence of glycine, and also the repetitive nature in the insect's resilin gene, the motifs have potential similarity with the foldamers[34], though details were not explored.

During our characterization of recombinant resilin[8-9], we observed a transition at the doubly-shifted master curve while developing complex moduli master curves for recombinant resilin using time-temperature concentration superposition principle. The storage modulus at the plateau was too low (1 to 26 MPa) to be accepted as the glassy state. A similar transition was noticed by King[10] and Choudhury[11] while developing master curves on the natural resilin of dragonfly and cockroach. Muller et al.[35] working on polybutadiene, found a transition within the rubbery plateau of the master curves due to hydrogen bonding. Moreover, Adhikary et al.[6] and Takano et al.[7] discovered intramolecular hydrogen bonds within the protein chains which stabilize the conformation of the protein. Thus, the transition had the potential to be due to

intramolecular hydrogen bonds, evidence now favors interpreting the transition as a glass transition, with the low moduli resulting from the high water content within the hydrated hydrogels[8-9].

5.4.2 Elastin

Elastin can be found in the extracellular matrix of mammalian proteins, including a wide range of tissues within the human body[36]. It can extend and recoil reversibly for tissues which require the ability to deform repetitively, as is needed for function in heart, skin and the lungs[37]. Spectroscopic studies of elastin indicate that it has tetrapeptide (VPGG), pentapeptide (VPGVG), and hexapeptide (APGVGV) consensus repeat motifs, though only the polypentapeptide repeat shows elastomeric behavior observed in nature[3]. Spectroscopic studies by Urry et al.[38] indicate that β-turns are the dominant structural features of α-elastin.

The peptide VPGVG is hydrophobic in nature. MD simulations were conducted on the VPGVG repeat motif to investigate whether it forms a bent conformation. From the results, we found a similar bent structure after the clustering, with the bend occurring again at the central glycine residue (G), the location of least steric hindrance. After SMD pulling and collapse, a comparable bent structure was formed again (Fig. 5-4a). Like resilin, the repeat motif VPGVG of elastin also forms a favorable bent structure through hydrogen bonding (Fig. 5-4b).

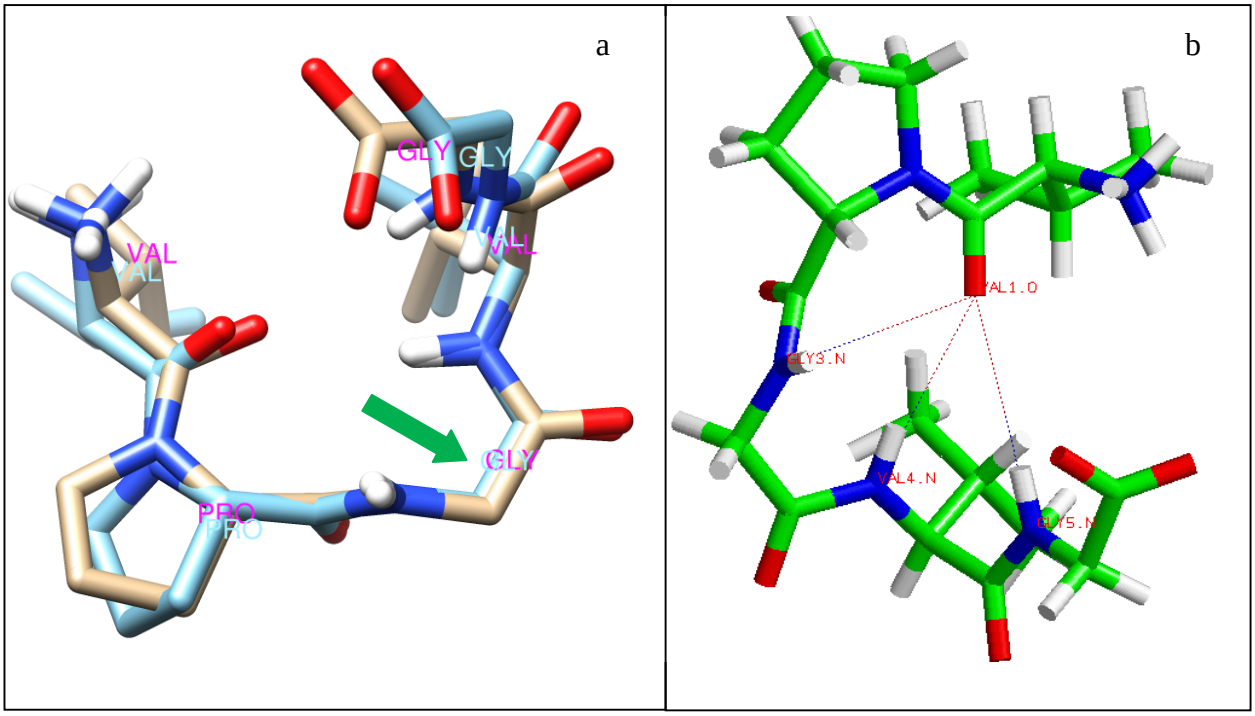

Fig. 5-4. (a) Alignment between the conformation after the clustering (gold) and after the collapse (blue) for elastic repeat motif VPGVG of elastin (b) Hydrogen bonding at the bent conformation of the motif.

On the other hand, the other repeat motif of elastin, hexapeptide (APGVGV), is not elastomeric in nature according to Tatham et al.[3], and the MD simulation results showed that it did not form a bent structure. The end-to-end distance of the most favorable conformation of APGVGV was 10.6 Å, which is double that of the repeat motif VPGVG (5.3 Å) that is elastomeric in nature. The reason for the greater end-to-end distance of APGVGV compared to VPGVG is that the oxygen of valine-1 (V) in VPGVG can form three hydrogen bonds, while APGVGV with alanine (A) in the first position forms fewer hydrogen bonds (Fig. 5-5). As a result, APGVGV cannot bend to the same extent as the elastomeric repeat motif VPGVG. However, rearranging the amino acid order of the non-elastomeric repeat motif APGVGV by

moving valine from the C terminus to the second position, forming AVPGVG, yields a bent conformation similar to VPGVG. Moreover, the end-to-end distance becomes 3.9 Å, which was almost one-third that of the APGVGV length due to formation of more hydrogen bonds (Fig 5.6). AVPGVG was formed reorganizing the non-elastic motif APGVGV based on elastic motif VPGVG to understand the amino acid sequence order effect. Most probably, the modified repeat motif would be elastic in nature, which agrees with our previous work that showed that the order of the amino acids in the repeat motifs is also a key factor for conveying elastomeric properties[20].

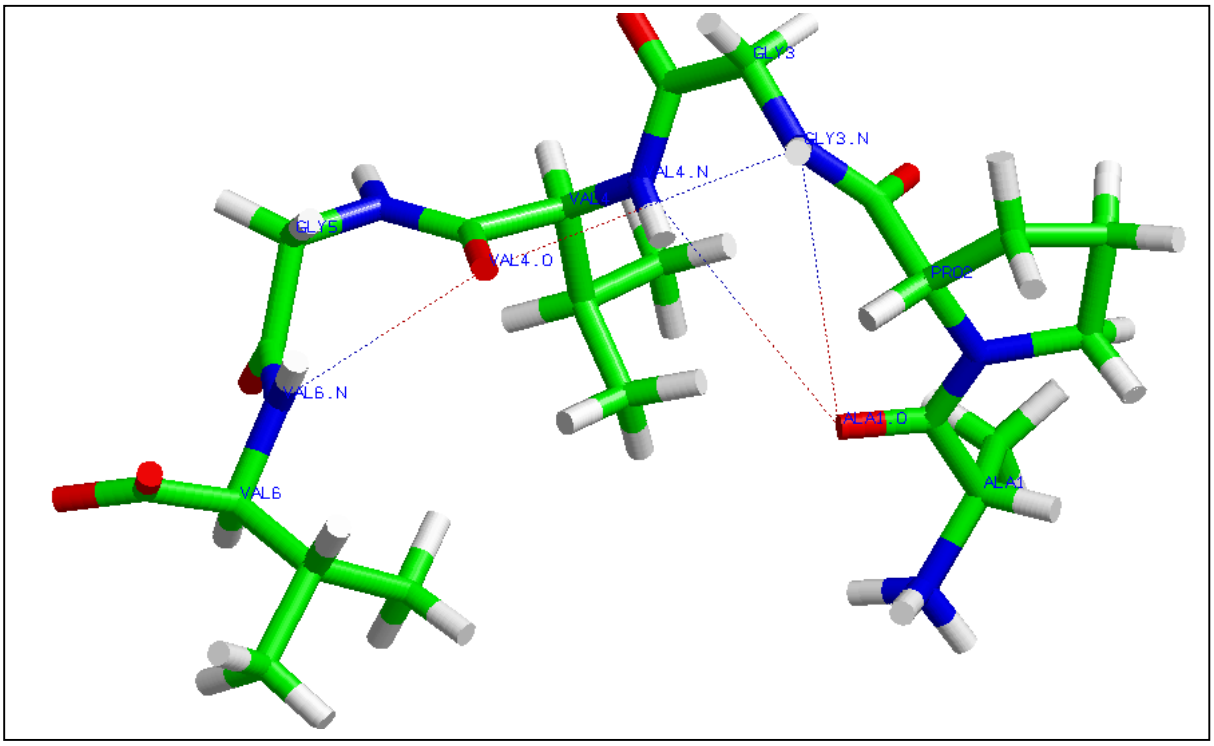

Fig. 5-5. Conformation of APGVGV with the hydrogen bonds. It has fewer hydrogen bonds and consequently did not bend to the same extent as VPGVG and has longer end-to-end distance.

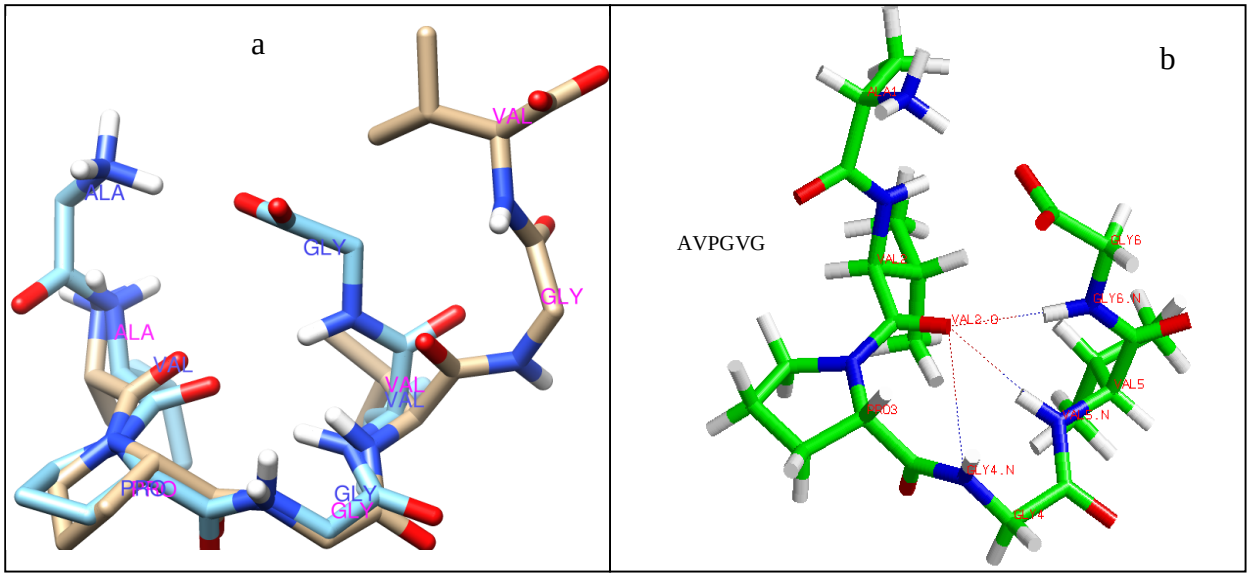

Fig. 5-6. (a) Alignment between APGVGV (gold) and AVPGVG (blue) after the clustering. End-to-end distance for AVPGVG is much shorter than the APGVGV (b) Hydrogen bonds of AVPGVG that facilitate forming favorable bend conformation. Compared to VPGPG (Fig. 5-4), A AVPGVG has more hydrogen bonds around the bend.

5.4.3 Spider Silk

There are two main types of spider silks: dragline silks and flagelliform silks. Dragline silks form the dropping line while flagelliform silks form the spiral of the web. Usually, flagelliform silks are more elastic than the dragline silks[12]. Higher flexibility of flagelliform silks might be due to their longer repetitive domain based on pentapeptide repeats GPGGX (where X can be any amino acid) than the repetitive domain in dragline silks[5]. Also, dragline silks have polyalanine domains that separate the glycine rich elastomeric repeat domains. These polyalanine domains can form non-covalent bonds to generate secondary structure, while glycine rich domains are mostly unstructured[39-40]. The elastomeric repetitive motifs in the dragline silks are GPGGY,

GPGQQ and GGYGPGS. These sequence motifs form β-turn structures, where the PG residues act as the central residues[3, 5].

For MD simulation, we chose repeat motif GPGGY for flagelliform silks and GGYGPGS for dragline silks. Both motifs form favorable bent structures after clustering analysis. After the SMD when the both N and C terminals were released, they returned to the bent structure as shown in Fig. 5-7. Hydrogen bonding during the formation of favorable bent structures is shown in Fig. 8. It is known that the material properties of flagelliform silk are more elastomeric in nature than dragline silks, and hydrogen bonding might be a contributing factor because GPGGY has a higher number of hydrogen bonds compared to GGYGPGS (Fig. 5-8). However, we do not know the strength of these hydrogen bonds, which is dependent on the length of the bonds that is affected by the molecular constraint. Also, it's less likely that other chains will overcome the steric hindrance and form intermolecular hydrogen bonds with the atoms which usually participate in forming intramolecular hydrogen bonds in the folded state within the short period of stretching.

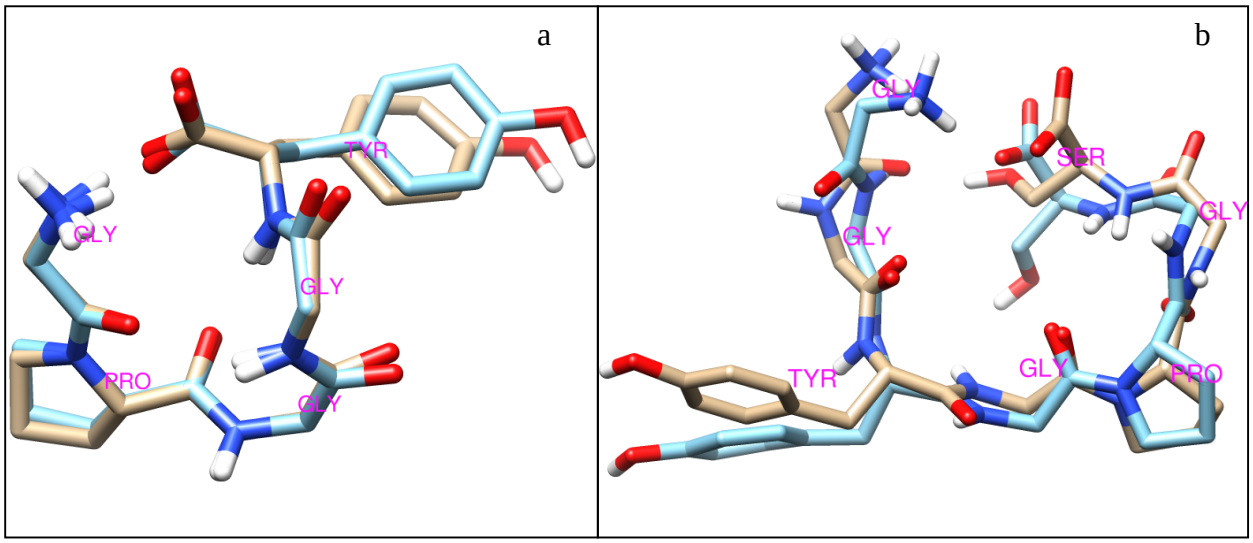

Fig. 5-7. Alignment between the conformations after the clustering (gold) and when termini were released after SMD (blue) (a) GPGGY (b) GGYGPGS conformation.

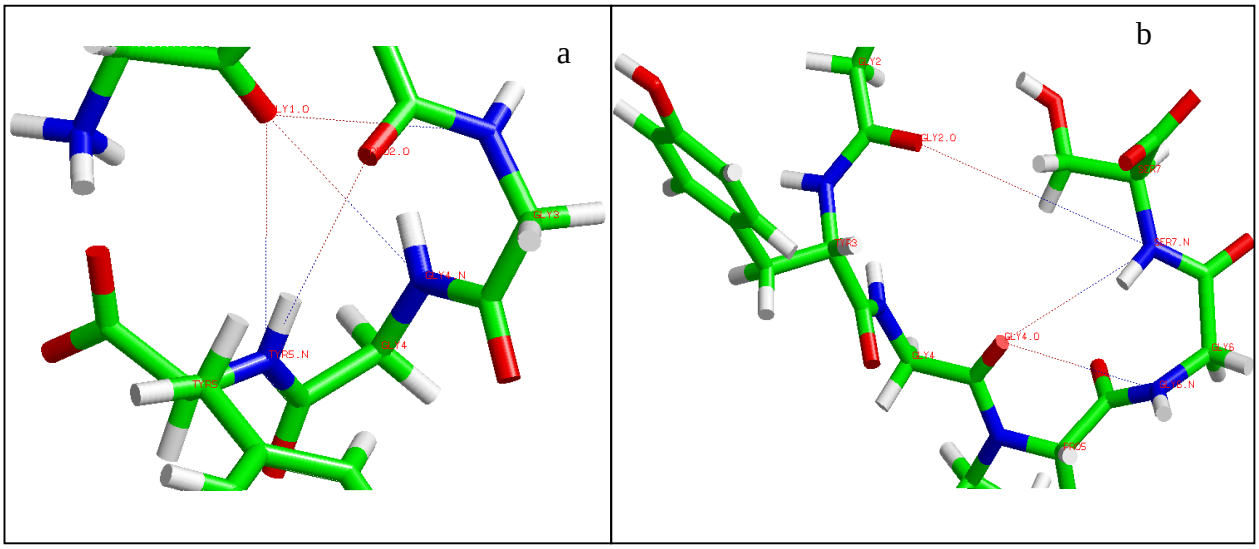

Fig. 5-8. Hydrogen bonds at the favorable bent conformations of (a) GPGGY and (b) GGYGPGS. GPGGY has more hydrogen bonds than the GGYGPGS, which might increase the elasticity of the proteins with the GPGGY elastic motifs.

5.4.4 Mussel Byssus

Mussel byssuses can be found in bivalve mollusks and their function is to attach the mollusks to a solid surface. Even though byssuses have considerable stiffness and strength, they are also very stretchy, a property necessary to prevent detachment under the force of crashing waves[3]. Along their length, byssal threads display gradient mechanical properties, from stiff to elastic; as a result mussels can attach to hard surfaces[5]. Elastic domains of byssal thread proteins contain a highly conserved pentapeptide motif, GPGGG[3]. Secondary structures of byssal threads are not known. However, based on findings for other elastomeric proteins, the elastic domains of byssal threads might be mostly unstructured due to the glycine-rich elastic repetitive motif GPGGG, although β-turns may be present as well.

We performed MD simulations, similar to those involving the other repeats reported here, on the mussel byssus elastomeric repetitive motif, GPGGG, to investigate favorable conformations and probability of associated hydrogen bonding. Results were in agreement with the previous findings. The GPGGG motif formed a bent structure during the MD simulation according to the clustering analysis, and returned to the bent structure when termini were released and allowed to move freely after the SMD (Fig 5.9a). Hydrogen bonding present in the bent conformation is shown in Fig. 5-9b, some of which breaks during SMD and reforms during the collapse simulation as reported here for other repeats (Fig. 5-2).

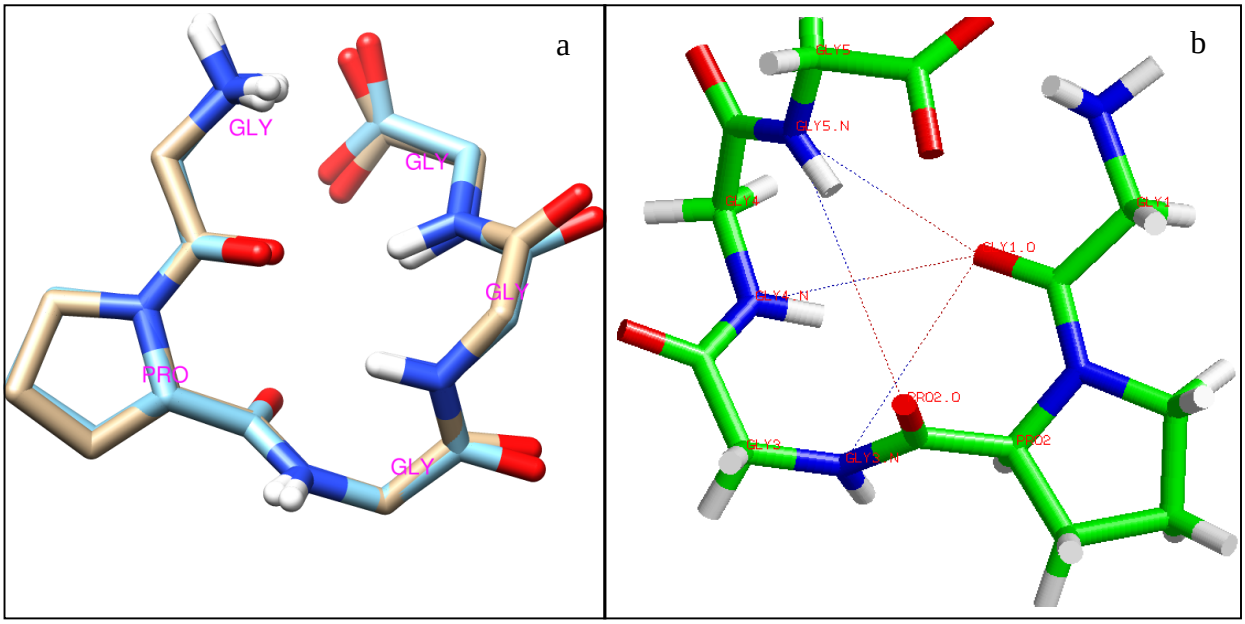

Fig. 5-9. (a) Alignment between the conformation after the clustering (gold) and after the collapse (blue) for the byssus elastic repeat motif GPGGG (b) Hydrogen bonds of GPGGG that facilitate favorable bend conformation.

Together our results show that the most frequent repetitive motifs in naturally occurring elastomeric proteins adopt bent conformations that may enable or confer elastomeric behavior at the macroscopic level. Moreover, when we hold one end and pull the other end of these elastomeric proteins, the peptide unfolds, breaking the hydrogen bonds. When the constraints were removed, allowing the motif to move freely, the repeat motifs returned to the similar bent conformation again and reformed the hydrogen bonds, as was demonstrated by the collapse simulations. From these results, we hypothesize that this propensity to form a reversible bent conformation is one of the key factors contributing to the elastomeric properties of the proteins studied in this investigation and possibly extending to other naturally occurring elastomeric proteins.

5.5 Conclusion

The amino acid sequences and mechanisms of elastomeric proteins have evolved to fulfill precise biological roles. One of the common features of all elastomeric proteins, constructed of repeated motifs, is that they have disordered elastic domains that control the elastic properties of the proteins. Understanding the role of the repetitive motifs found in elastomeric proteins is an emerging focus that could enhance the innovations and applications of new biomaterials. In this context, molecular modeling provides a means to enhance our understanding of underlying mechanisms at the atomistic level that may contribute to the extraordinary properties of these elastomeric proteins.

All the proteins considered during this work were diverse in nature and material properties such as resilin in insect cuticles, elastin in extracellular matrix of mammals, spider silk in the spider web to catch the prey, and byssus in bivalve mollusks. Under the appropriate conditions, these proteins exhibit reversible elastomeric properties. If we take into account the

functional roles of these proteins in the lives of animals, mechanical properties are crucial to their functions. The objective of this work was to investigate the conformation of the elastomeric proteins, which may control their macroscopic properties. The results after the clustering analysis suggest that the repetitive motifs formed favorable bent structures through a combined effect of hydrogen bonding and lack of steric hindrance. These hydrogen bonds break upon SMD pulling, but when the motifs are allowed to move freely, they return to the bent conformation, and hydrogen bonds are reformed. Due to the computational time and length scale limitations, only single repetitive motifs from each elastomeric protein were investigated. Nonetheless, these favored, reversible bent conformations might enable macroscopic elastomeric properties. Adhikary et al.[6] and Takano et al.[7] also observed intramolecular hydrogen bonds that stabilize the conformations of the proteins. Moreover, experimental work on the recombinant and natural resilin explored a transition at the rubbery plateau of the complex moduli master curves and that might be due to the intramolecular hydrogen bonds[8, 10-11]. Given this broad range of properties and functions, it is probable that the findings of this work will provide insights of conformations and mechanisms of elastomeric proteins which can lead to design and manufacture of high-performance, biocompatible rubbers with tailored mechanical properties.

References

1. S. Rauscher, S. Baud, M. Miao, F. W. Keeley and R. Pomes, Proline and Glycine Control Protein Self-Organization into Elastomeric or Amyloid Fibrils. *Structure*, 2006, **4**, 1667–1676.
2. P. Tompa, Intrinsically unstructured proteins. *Trends in Biochemical Sciences*, 2002, **269**, 2-12.
3. A. S. Tatham and P. R. Shewry, Elastomeric proteins: biological roles, structures and mechanisms. *Trends in Biochemical Sciences*, 2000, **25**, 567-571.
4. G. Qin, S. Lapidot, K. Numata, X. Hu, S. Meirovitch, M. Dekel, I. Podoler, O. Shoseyov and D. L. Kaplan, Expression, Cross-Linking, and Characterization of Recombinant Chitin Binding Resilin. *Biomacromolecules*, 2009, **10**, 3227–3234.
5. A. S. Tatham and P. R. Shewry, Comparative structures and properties of elastic proteins. *Philosophical Transactions of the Royal Society B*, 2002, **357**, 229–234.
6. R. Adhikary, J. Zimmermann, J. Liu, R. P. Forrest, T. D. Janicki, P. E. Dawson, S. A. Corcelli and F. E. Romesberg, Evidence of an Unusual N−H···N Hydrogen Bond in Proteins. *Journal of Americal Chemical Society*, 2014, **136**, 13474−13477.
7. K. Takano, Y. Yamagata, J. Funahashi, Y. Hioki, S. Kuramitsu and K. Yutani, Contribution of intra- and intermolecular hydrogen bonds to the conformational stability of human lysozyme. *BioChemicstry*, 1999, **38**, 12698-12708.
8. M. S. Khandaker, D. M. Dudek, E. P. Beers and D. A. Dillard, Expression, Crosslinking and Developing a Modulus Master Curve of Recombinant Resilin. in prep.

9. M. S. Khandaker, D. M. Dudek, E. P. Beers and D. A. Dillard, Investigation on the functions of exons and chitin binding domain (ChBD) on the mechanical properties of resilin., in prep.
10. R. King, Dynamic Mechanical Properties of Resilin. Master's, Virginia Polytechnic Institute and State University, 2010.
11. U. Choudhury, Dynamic Mechanical Properties of Cockroach (Periplaneta americana) Resilin. Master's Thesis, Virginia Polytechnic Institure and State University, 2012.
12. P. R. Shewry, A. S. Tatham and A. J. Bailey, ed.^eds., Cambridge University Press, 2003, p.^pp.
13. R. Petrenko, Computer simulations of resilin-like peptides. Doctoral Dissertation, University of Cincinnati, 2010.
14. J. Gasolin, Lillie, M., Carrington, E., Guerette, P., Ortlepp, C. and Savage, K., Elastic proteins: biological roles and mechanical properties. *The Royal Society*, 2002, **357**, 121-132.
15. H. Song and J. Parkinson, Modelling the Self-Assembly of Elastomeric Proteins Provides Insights into the Evolution of Their Domain Architectures. *PLoS Comput Biol*, 2012, **8**.
16. E. R. Wright, V. P. Conticello and R. P. Apkarian, Morphological characterization of elastin-mimetic block copolymers utilizing cryo- and cryoetch-HRSEM. *Microscopy and Microanalysis*, 2003, **9**, 171-182.
17. L. R. G. Treloar, The physics of rubber elasticity. Oxford University Press, 1975.
18. R. Kappiyoor, Mechanical Properties of Elastomeric Proteins. Virginia Polytechnic Institue and State University, 2013.

19. G. Qin, Hu, X., Cebe, P. and Kaplan, D. L., Mechanism of Resilin Elasticity. *Nature Communication*, 2012, **3**, 1-18.

20. M. S. Khandaker, D. M. Dudek, D. A. Dillard, E. P. Beers and D. R. Bevan, Molecular Modeling of the Elastomeric Properties of Repeating Units and Building Blocks of Resilin, a Disordered Elastic Protein. *Journal of the Mechanical Behavior of Biomedical Materials*, in review.

21. A. S. Inc, Discovery Studio Modeling Environment. (2011) Accelrys Software Inc., San Diago.

22. B. Hess, C. Kutzner, D. Van Der Spoel and E. Lindahl, GROMACS 4: Algorithms for Highly Efficient, Load-Balanced, and Scalable Molecular Simulation. *Journal of Chemical Theory and Computation*, 2008, **4**, 435-447.

23. A. D. Mackerell, D. Bashford, Bellott, R. L. Dunbrack, J. D. Evanseck, M. J. Field, S. Fischer, J. Gao, H. Guo, S. Ha, D. Joseph-Mccarthy, L. Kuchnir, K. Kuczera, F. T. K. Lau, C. Mattos, S. Michnick, T. Ngo, D. T. Nguyen, B. Prodhom, W. E. Reiher, B. Roux, M. Schlenkrich, J. C. Smith, R. Stote, J. Straub, M. Watanabe, J. Wiorkiewicz-Kuczera, D. Yin and M. Karplus, All-atom empirical potential for molecular modeling and dynamics studies of proteins. *The Journal of Physical Chemistry B*, 1998, **102**, 3586–3616.

24. W. L. Jorgensen, J. Chandrasekhar, J. D. Madura, R. W. Impey and M. L. Klein, Comparison of simple potential functions for simulating liquid water. *The Journal of Chemical Physics*, 1983, **79**, 926–935.

25. J. P. Ryckaert, G. Ciccotti and H. J. Berendsen, Numerical integration of the cartesian equations of motion of a system with constraints: molecular dynamics of n-alkanes. *Journal of Computational Physics*, 1977, **23**, 327–341.

26. T. Darden, D. York and L. Pedersen, Particle mesh Ewald: An N⍥ log(N) method for Ewald sums in large systems. *Journal of Chemical Physics*, 1993, **98**, 10089-10092.
27. A. Wolf and K. N. Kirschner, Principal component and clustering analysis on molecular dynamics data of the ribosomal L11·23S subdomain. *Jounal of molecular modeling*, 2013, **19**, 539-549.
28. E. F. Pettersen, T. D. Goddard, C. C. Huang, G. S. Couch, D. M. Greenblatt, E. C. Meng and T. E. Ferrin, UCSF Chimera--a visualization system for exploratory research and analysis. *Journal of Computational Chemistry*, 2004, **13**, 1605-1612.
29. P. Valadon, RasTop 2.2, Molecular Visualization Software. (2007) Glaxo Wellcome Research & Development, Hertfordshire, UK.
30. T. Weis-Fogh, A rubber-like protein in insect cuticle. *Journal of Molecular Biology*, 1960, **37**, 889-907.
31. T. Weis-Fogh, Molecular interpretation of the elasticity of resilin, a rubber-like protein. *Journal of Molecular Biology*, 1961, **3**, 648-667.
32. C. M. Elvin, A. G. Carr, M. G. Huson, J. M. Maxwell, R. D. Pearson, T. Vuocolo, N. E. Liyou, D. C. C. Wong, D. J. Merritt and N. E. Dixon, Synthesis and properties of crosslinked recombinant pro-resilin. *Nature*, 2005, **437**, 999-1002.
33. S. Lv, Dudek, D., Cao, Y., Balamurali, M. M., Gosline, J. and Li, H., Designed biomaterials to mimic the mechanical properties of muscles. *Nature*, 2010, **465**, 69-73.
34. S. H. Gellman, Foldamers: A Manifesto. *Accounts of Chemical Research*, 1998, **31**, 173-180.

35. M. Muller, U. Seidel and R. Stadler, Influence of hydrogen bonding on the viscoelastic properties of thermoreversible networks: analysis of the local complex dynamics. *Polymer*, 1995, **36**, 3143-3150.

36. J. Rosenbloom, W. R. Abrams, Z. Indik, H. Yeh, N. Ornstein-Goldstein and M. M. Bashir, Structure of the elastin gene. *Ciba Found. Symp.*, 1995, **192**, 59–80.

37. B. Vrhovski and A. S. Weiss, Biochemistry of tropoelastin. *European Journal of Biochemistry*, 1998, **258**, 1-18.

38. D. W. Urry, Elastic biomolecular machines. *Scientific American*, 1995, **272**, 44-49.

39. P. A. Guerette, D. G. Ginzinger, B. H. Weber and J. M. Gosline, Silk properties determined by gland-specific expression of a spider fibroin gene family. *Science*, 1996, **272**, 112-115.

40. J. D. V. Beek, S. Hess, F. Vollrath and B. H. Meier, The molecular structure of spider dragline silk: Folding and orientation of the protein backbone. *PNAS*, 2002, **99**, 10266–10271.

Chapter 6: Conclusion

6.1 Summary

In this dissertation, we focused on improving the fundamental understanding of elastomeric properties of resilin through synthesizing recombinant resilin-like hydrogels from different exons of the fruit fly gene and through atomistic molecular modeling on the repetitive motifs of resilin and other elastomeric protein sequences.

The first study focused on only clone-1 which was synthesized from exon-1 and exon-2 of the fruit fly resilin gene. The synthesized recombinant resilin-like hydrogel had 80wt% water and did not show any sign of tack even though its low modulus satisfies the Dahlquist criterion. Doubly-shifted master curves were generated using TTCSP for E', E" and tan δ, and master curves displayed a prominent transition. The relatively low upper storage modulus plateau (on the order of 1.1 MPa) initially seemed inconsistent with expected glassy behavior, suggesting that the transition could be due to intramolecular hydrogen bonds in the rubbery plateau. Further evaluation, however, suggests that the relatively low plateau modulus is likely to be the glass transition, as the modulus transition spans three orders of magnitude. If this were a hydrogen bonding transition, a subsequent rubbery to glassy transition would increase the modulus to a value which would be too high to accept as a glassy modulus. The moduli are significantly reduced by the low molecular chain density resulting from the highly swollen state due to high water content in the hydrogels. Another possibility might be increasing order or crystallization effects resulted from the change in secondary structure of the exons due to the presence of less cohesive ethanol. Master curves also indicated that the functional frequency of insects were multiple decades lower than the glass transition frequency.

During the second study, resilin-like hydrogels were synthesized from different exons: clone-3 (exon-3), clone-4 (exon-2 + exon-3) and full length, clone-5 (exon-1 + exon-2 + exon-3), and compared with the with clone-1 results from previous study and natural resilin from locusts. All the clones showed similar transitions in the doubly-shifted master curves as observed for the transition for clone-1. Thus, the transitions were likely to be due to intramolecular hydrogen bonds or glass transitions or crystalline effect for both clones, again multiple decades beyond the functional frequency of insects except clone-3. Results from the clones with and without chitin binding domains (ChBD) indicate that the transition for the clone without ChBD occurs at lower frequencies than for those with the ChBD, and that may be due to the disordered nature of the clone without ChBD.

The third and fourth study focused on atomistic molecular modeling on the elastomeric repetitive motifs of resilins and other elastomeric proteins from different species. Results showed that the repetitive motifs form favorable bent conformations through intramolecular hydrogen bonds. Upon SMD pulling, these hydrogen bonds broke but when the motifs were allowed to move freely again, they quickly returned to the bent conformations forming the hydrogen bonds.

The understanding from the doubly-shifted master curves of synthesized recombinant resilin and simulation results of the repetitive motifs of resilin provide better understanding of resilin's unique properties and may also be applicable to the biology and mechanics of other elastomeric biomaterials.

6.2 Future Work

While the results from these studies providing better understanding about mechanisms of the unique properties of resilins, there are still several unanswered questions. For instance, during the experimental works, is it possible to find a conclusive reason for the transition in the master

curves? How much water was drawn from the hydrogel at different ethanol concentrations? What are values of the dimensional change due to ethanol? Does the ethanol work as a plasticizer or anti-plasticizer or none in the hydrogel? What are the contributions of intramolecular hydrogen bonds and crosslinking on the elastomeric properties of resilin? Once we will get these answers, that will give us deeper understanding of the mechanism of elastomeric properties of these recombinant resilin.

During the molecular modeling works, though the repeating motifs formed favorable bent conformations, but we do not know whether all the similar repeating motifs in the resilin gene will form the same bent conformations, considering the different non-conserved amino acids within the repeat motifs. Moreover, investigations need to be done on the macroscopic level to conclude the functions of these repeat motifs on the elastomeric properties of resilin.

Appendix A Supplementary Documents for Chapter 2

A 1.1 Validation of the custom made DMA

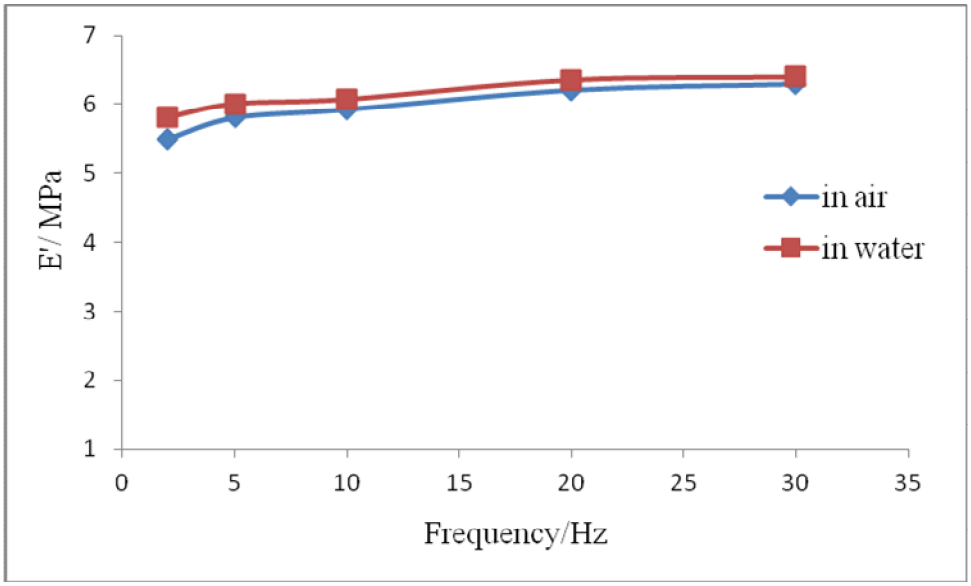

Fig. A.1 Storage modulus (E') of silicone rubber in air and in water for different frequencies at room temperature.

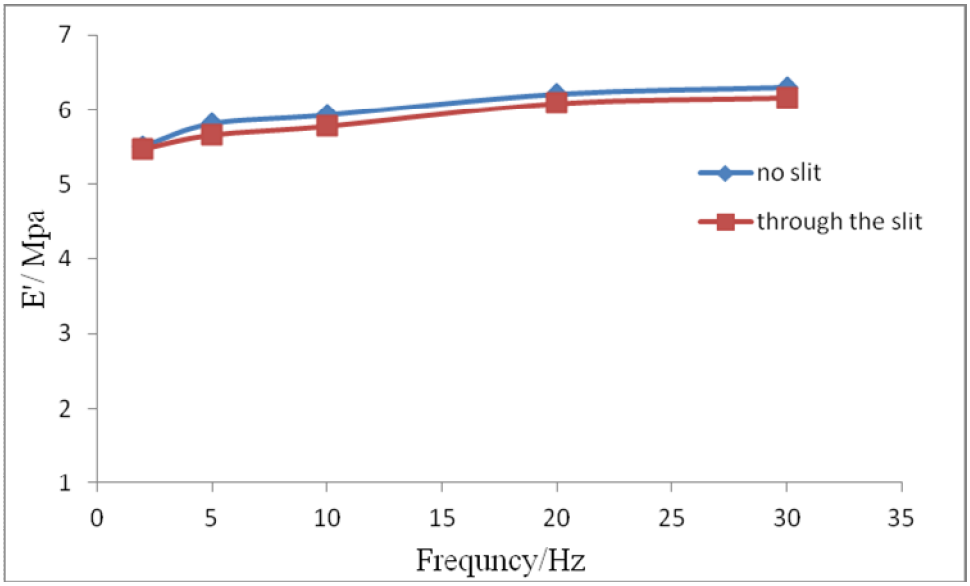

Fig. A.2 Storage modulus (E') of silicone rubber through slits and without chamber for different frequencies at room temperature.

A 1.2 Theoretical Glass Transition Temperature.

A 1.2.1 Methods

The glass transition temperature (T_g) represents a metric within the temperature range where a polymer transitions from a soft, rubbery state to a hard and glassy material. Information about the T_g of a material is very important to understand the characteristics like mechanical and dielectric properties, density and other properties as a function of temperature[1], and is often thought to be the single most important property for determining the applicability of a polymer to a given application. Though T_g can be determined experimentally though a number of mechanical, thermal, and electrical methods, one common method is dynamic mechanical analysis, which involves determining the complex modulus as a function of temperature, and in some cases, frequency as well. However, if we can predict the T_g theoretically[2], it will save time and effort, and also will help us design the experiments to determine the transition. Matveev et al.[1] developed a theoretical procedure to predict T_g for food proteins using the approach developed for polymer physics[3]. Here, a similar method is used to theoretically estimate T_g with slight modification to be suitable for our purpose. Equations used to calculate the T_g were:

$$T_{g,p}{}^{-1} = \sum_{i=1}^{20} \varphi_i T_{g,i}{}^{-1}$$

$$\varphi_i = \frac{n_i \Delta V_i}{\sum_{i=1}^{20} n_i \Delta V_i}$$

Here, ΔV_i = van der Waals volume of i-th amino acids, n_i = No. of amino acid residue of i-th type per mole of a protein, $T_{g,i}$ = Partial increment of T_g by the i-th residue and $T_{g,p}$ = T_g for protein.

Matveev et al.[1] calculated ΔV_i and $T_{g,i}$ for all 20 amino acids, which in principle, can then be used to predict the T_g of any protein. The T_g estimated by this approach can be considered an upper bound, because T_g depends on the average degree of polymerization of polypeptides in a protein, rather than the whole protein molecule being considered here. This T_g value can be called a polymer glass transition temperature of protein[1]. Also, we could not apply chemical crosslinking like di-tyrosine or tri-tyrosine during the calculation as these might change the T_g value.

The $T_{g,p}$ obtained from the previous equations was for pure proteins only. But, the resilin-like hydrogel had 20 wt% protein and 80 wt% water. We used the Fox equation[4] to calculate the T_g of the resilin, though we don't know whether Fox equation can be applied for high water hydrogel or not.

$$\frac{1}{T_g} = \frac{w_p}{T_{g,p}} + \frac{w_w}{T_{g,w}} \qquad \text{(Fox equation)}$$

where, w_p = weight fraction of protein, w_w = weight fraction of water, $T_{g,p}$ = glass transition temperature of protein only and $T_{g,w}$ = glass transition temperature of water (136 K for this case[5]). Interestingly, the experimental determination of a WLF C_2 constant on the order of 200 K for a reference temperature of 25^{o}C would suggest a glass transition temperature of approximately -123 ^{o}C or 150 K, which is in reasonable agreement with the Fox equation result.

However, uncertainties with the presence of free and loosely bound water for such high water contents made its application questionable. Similarly, uncertainties with accurately shifting the somewhat scattered moduli data could also lead to errors in the determination of C_2.

A 1.2.2 Group Contribution Theory Results

Theoretical glass transition temperatures for different clones based on group contribution theory are shown in Table A.1. $T_{g,p}$ was lowest for full length resilin (exon 1 + exon 2 + exon 3) due to the difference in number of amino acids. From the results of other clones, ChBD (exon 2) didn't have much effect on the $T_{g,p}$. But, these differences were negligible for T_g of solid resilin-like hydrogel samples, because proteins were only 20 wt% of the hydrogel while 80 wt% were water. The T_g obtained from this method were the upper estimated value, as the whole protein molecule considered instead of average degree of polymerization of polypeptides in protein[1], and also the chemical crosslinking could not be incorporated in the predictions which might change the T_g value. Group contribution theory calculations are just approximations, and the extension to complex proteins is uncertain. The glass transition values suggested using this method were noticeably higher than obtained using the Fox equation or the WFL fit of the shift factors.

Table A.1 Estimated glass transition temperatures of solid resilin-like hydrogel from recombinant proteins were all similar, even though they were of different size.

Clones	Exons	Glass transition temperature of protein only, $T_{g,,p}$ ˚C	Glass transition temperature of resilin-like hydrogel, T_g ˚C
1	Exon1+Exon2	149.05	-115.67
2	Exon1	146.81	-115.74
3	Exon1+Exon2+Exon3	-46.48	-125.19
4	Exon2+Exon3	152.92	-115.57
5	Exon3	151.07	-115.62

References

1. Y. I. Matveev, V. Y. Grinberg, I. V. Sochava and V. B. Tolstoguzov, Glass transition temperature of proteins. Calculation based on the additive contribution method and experimental data. *Food Hydrocolloids*, 1997, **11**, 125-133.
2. D. W. V. Krevelen and K. T. Nijenhuis, Properties of Polymers: Their Correlation with Chemical Structure; their Numerical Estimation and Predication from Additive Group Contributions. Fourth edn., Elsevier, 2009.
3. A. A. Askadskii and Y. I. Matveev, Chemical Structure and Physical Properties of Polymers. Moscow, 1983.
4. H. Paul and T. Lodge, Polymer Chemistry. CRC Press, Boca Raton, Florida, 2007.
5. K. Amann-Winkela, C. Gainarub, P. H. Handlea, M. Seidla, H. Nelsonb, R. Böhmerb and T. Loerting, Water's second glass transition. *PNAS*, 2013, **110**, 17720–17725.

A 1.3 Master Curve at 0% Ethanol for Clone-1 considering both vertical and horizontal shift.

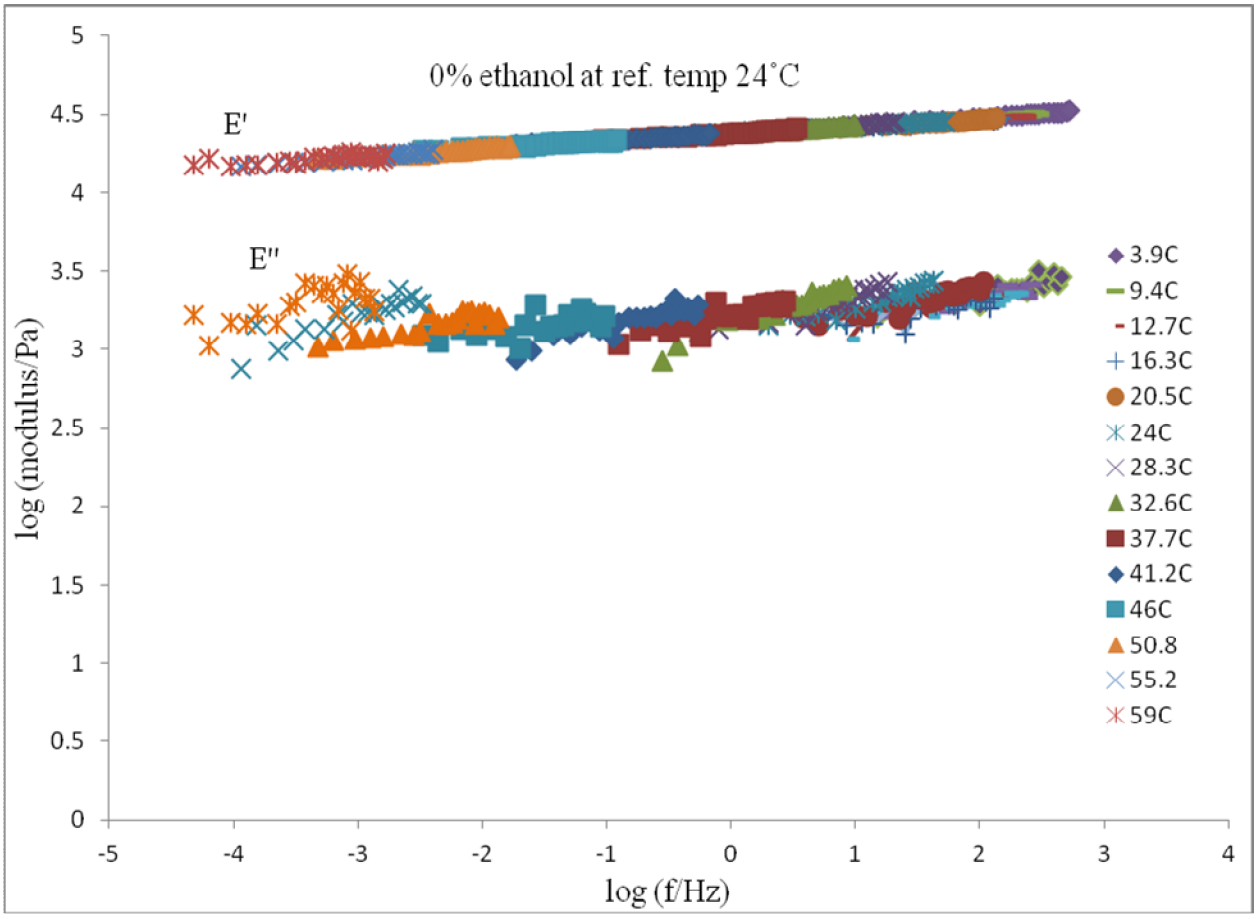

Fig. A.3 Master curves of storage modulus, loss modulus for 0% ethanol concentration using TTSP with the reference temperature 24˚C for clone-1 applying both horizontal and vertical shift.

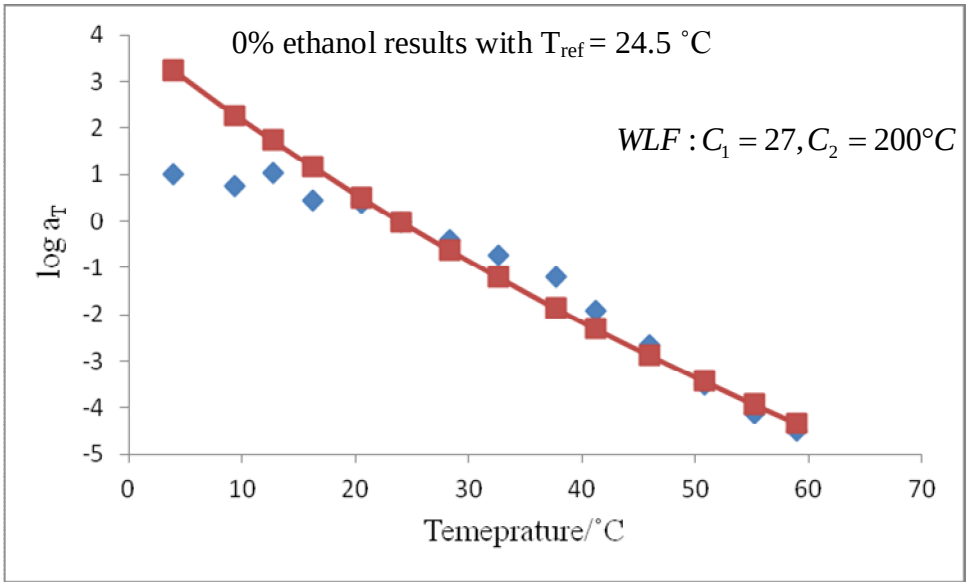

Fig. A.4 Thermal shift factor, plotted against temperature for 0% ethanol, and WLF fit with the values C1 = 27 and C2 = 200˚C at reference temperature 24.5˚C.

A 1.4 Master Curve at 73% Ethanol for Clone-1

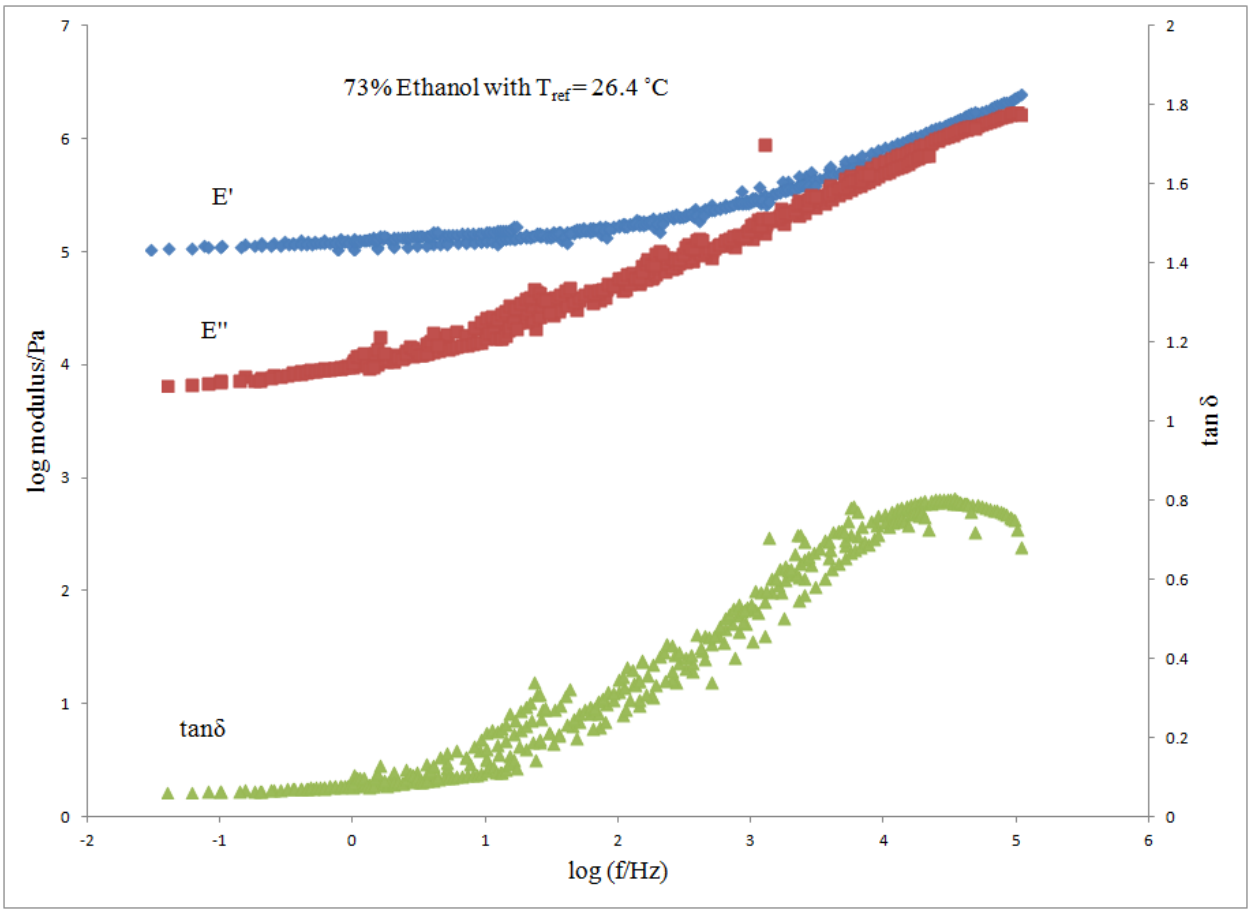

Fig. A.5 Master curves of storage modulus, loss modulus and tan δ for 73% ethanol concentration using TTSP with the reference temperature 26.4˚C for clone-1.

A 1.5 Differences in Mechanical Properties of Resilin in Nature

A 1.5.1 Methods

Resilins have diverse functions in different insects, and they work in broad frequency range too. However, we don't know the protein sequence of most of them to compare and understand the variations, and develop novel biomaterial for specific applications.

One of the sections of my work is to determine the protein sequence of two insects (i) Cockroach (*Periplaneta Americana)* (ii) Locust (*Schistocerca gregaria).* Synthetic biomaterials will be synthesized using the sequence (following the same method as of fruit fly) so that we can compare the properties with natural resilin and the recombinant resilin from fruit fly. This will give us the insight of the diversity of the functions of resilin. For both the insects, I have successfully sequenced the 3' end of the gene and trying to obtain the 5' end for full length.

Designing the Degenerate Primer for Cockroach Resilin. Resilin gene of cockroach is unknown to us. So, I have downloaded 27 sequences for insect gene for gene bank which are related to resilin or pro-resilin from different insects and then aligned them using the software "DNASTAR Lasergene 8". Using polygenetic tree option, I obtained three separate subgroup of the gene shown in Fig. A.5 Among the groups, Group 1 was from the same species (Drosophila). Group 2 and 3 were from different species. But, Group 3 didn't show any conserved region. For Group 2, there were some places which were conserved and I have designed the degenerate primer based on the conserved region.

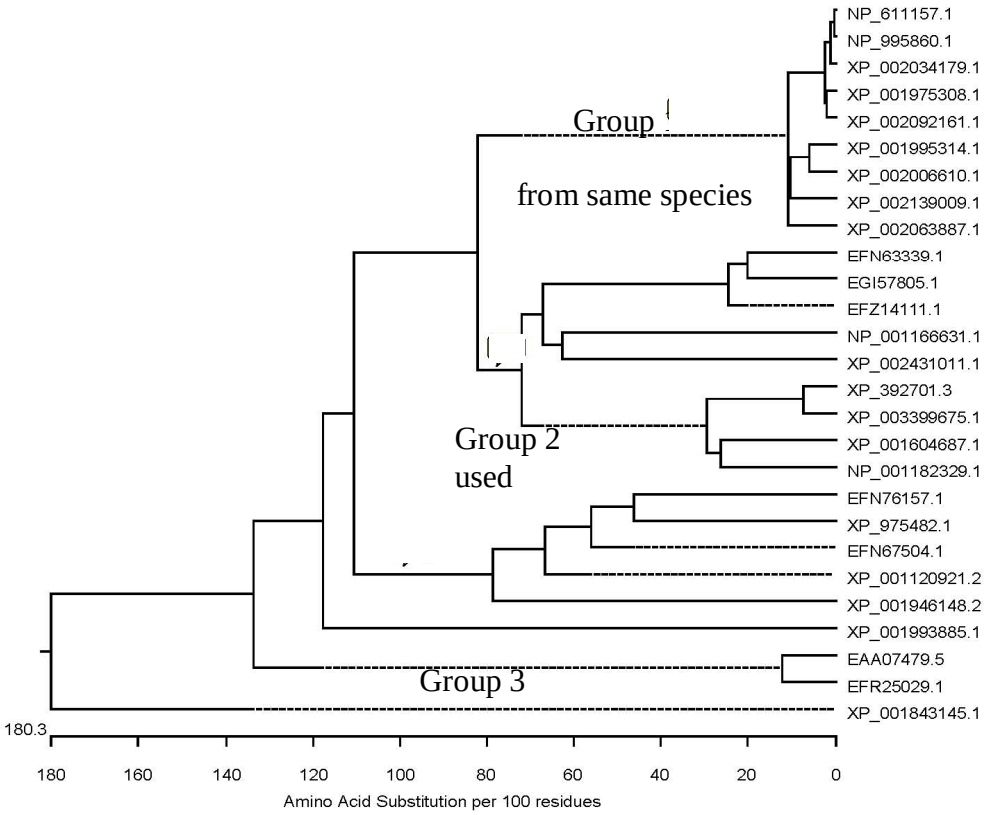

Fig. A.6 Phylogenetic tree from 27 gene sequences of insects where group 2 has the gene sequences of different insects.

The sequences of the insects in group 2 were aligned and degenerate primers were designed to obtain the resilin sequence of cockroach. The segments considered to design the primers are shown in Fig. A.6. Then, all sequence files were examined to find the codon for these amino acids and finally design the degenerate primer.

Degenerate primer 1: PVNSYLPP

Forward: 5’ CCN GTN AAY TCN TAY YTR CCN CC 3’

Degenerate primer 2 of EPAKYEF

Forward: 5’ GAR CCN GCN AAR TAY GAR TT 3’

Degenerate primer 3: EPAKYEF

Reverse: 5’ RAA YTC RTA YTT NGC NGG YTC 3’

Degenerate Primer 3: VEYEADQ

Reverse: 5’ YTG RTC NGC YTC RTA YTC NAC 3’

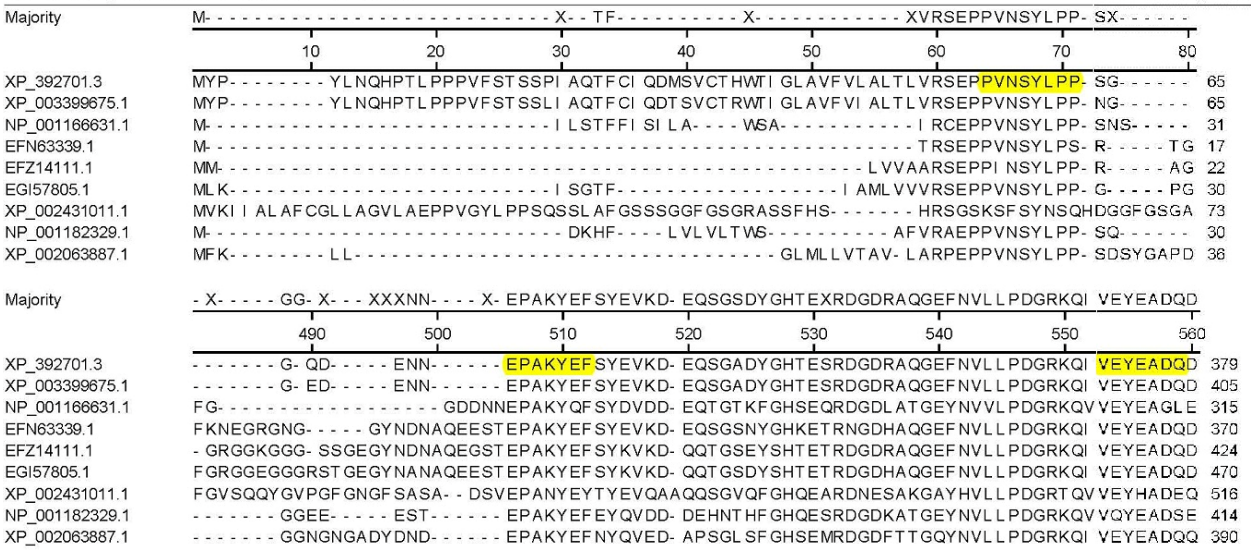

Fig. A.7 Alignment of the genes from group 2 which was used to design degenerate primers.

Designing the Degenerate Primer for Locust Resilin. Similar apploach has beed used to design degenrate primer of locust resilin.

Primer 1: GGNGGR

Forward: 5’ *GGATAACAATTTCACACAGG*GGIGGIAAYGGIGGIMG 3’

Primer 2: GNGNG

Forward: 5’ *GGATAACAATTTCACACAGG*GGIAAYGGIAAYGG 3’

Primer 3: YGAP

Forward: 5’ GGATAACAATTTCACACAGGTAYGGIGCICC 3’

Primer 4: GNGNG

Reverse: 5’ *CACGACGTTGTAAAACGAC*CCRTTICCRTTICC 3’

Primer 5: YGAP

Reverse: 5’ *CACGACGTTGTAAAACGA*CGGIGCICCRTA 3’

Primer 6: GYSSG

Reverse: 5’ *GGATAACAATTTCACACAGG*CCISWISWRTAICC 3’

Primer 7: SYGAP

Forward: 5’ *GGATAACAATTTCACACAGG*WSITAYGGIGCICC 3’

Amplification and Cloning of Full-length Resilin Genes. Using the degenerate primers, small fragments were sequenced for both the insects. Identification of flanking sequences of 5’ and 3’ ends was carried out using gene specific primers for both cockroach and locust by RACE (Rapid Amplification of cDNA Ends). Using the FirstChoice® RLM-RACE Kit (Invitrogen™, Part # AM1700), first strand cDNA synthesis and RACE reactions were performed on cockroach and locust RNA, according to manufacturer’s instructions.

A 1.5.2 Results

Sequence of 3’ RACE of cockroach resilin

GCGAAGTACGAATTCTCCTATGAGGTTAACGATCCTCCATCAGGCAGCGAATTTGGA
CATGAAGAGAGTCGTCAGGATGAGGAAGCTAGAGGATCCTACCACGTACTTCTCCC
AGACGGCCGCAGACAGATCGTGGAGTACGAAGCTAACCTCGAGGGCTACAAGCCAC
AGATCCGCTATGAGGAGACC

Protein Sequence of 3’ end of cockroach resilin

AKYEFSYEVNDPPSGSEFGHEESRQDEEARGSYHVLLPDGRRQIVEYEANLEGYKPQIR
YEET

Sequence of 3’ RACE of locust resilin

TGTAGGAGGTCTAAATGGGCTTGCCACGCAGTACGGAGCCCCTAATGGAGGTCTTTT

GGGAGCAAATGGTGGCCTTTCGGCTCAGTACGGTGCGCCAAATGGTGGAGGCAATG

GAATAGCAGCCAATGGGCTCTCCAGCGTCTACGGAGTACCTGGAGCTGCTGGCTAC

GGCAATGGAGGAGCGTCCCAAGATGATCTTGCAGAACCAGCTAACTACCAGTTCAG

CTACACAGTGGAGGACGCTGAAAGCGGTGTTGAATTTGGCCATGAGGAGTCTCGAG

AGGGAGACAGTGCTCAAGGTCAATACCACGTGTTGCTGCCTGATGGTCGCAGGCAG

GTGGTAGACTATGAAGCCGATCAGGGCGGCTACAGGCCGACCGTCAACTACGAGGA

GACTGGCCTAGGTAATGGAGGCTACGGCAATGGGGGCTATGCCAATGATGGGAACG

GCGGATATCCCAGCAGCAATGGAGGTTATCCTAGAGGAAACGGTGCTTACTCCAAT

GGTAATGGTGGCTACTCCAACGGCAATGGCGGCTACTCCAACGGCAATGGTGGCTA

CACCACAGGCCTGTGTGAAATTGTTATCCA

Protein Sequence of 3’ end of locust resilin

VGGLNGLATQYGAPNGGLLGANGGLSAQYGAPNGGGNGIAANGLSSVYGVPGAAGYG

NGGASQDDLAEPANYQFSYTVEDAESGVEFGHEESREGDSAQGQYHVLLPDGRRQVV

DYEADQGGYRPTVNYEETGLGNGGYGNGGYANDGNGGYPSSNGGYPRGNGAYSNGN

GGYSNGNGGYSNGNGGYTTGLCEIVI

Appendix B Supplementary Documents for Chapter 3

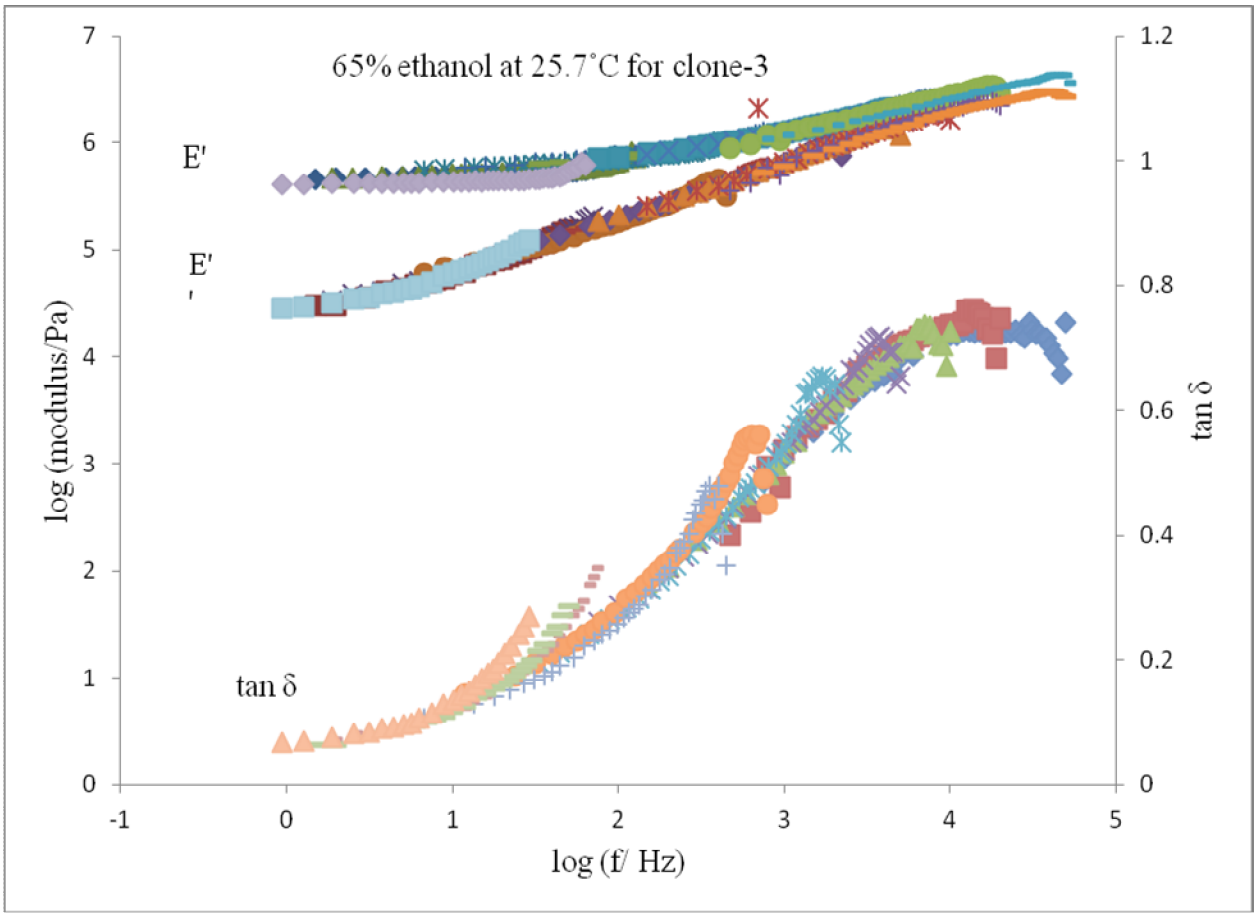

Fig. B.1 Master curves of storage modulus, loss modulus and tan δ for 65% ethanol concentration using TTSP with the reference temperature of 25.7˚C for clone-3.

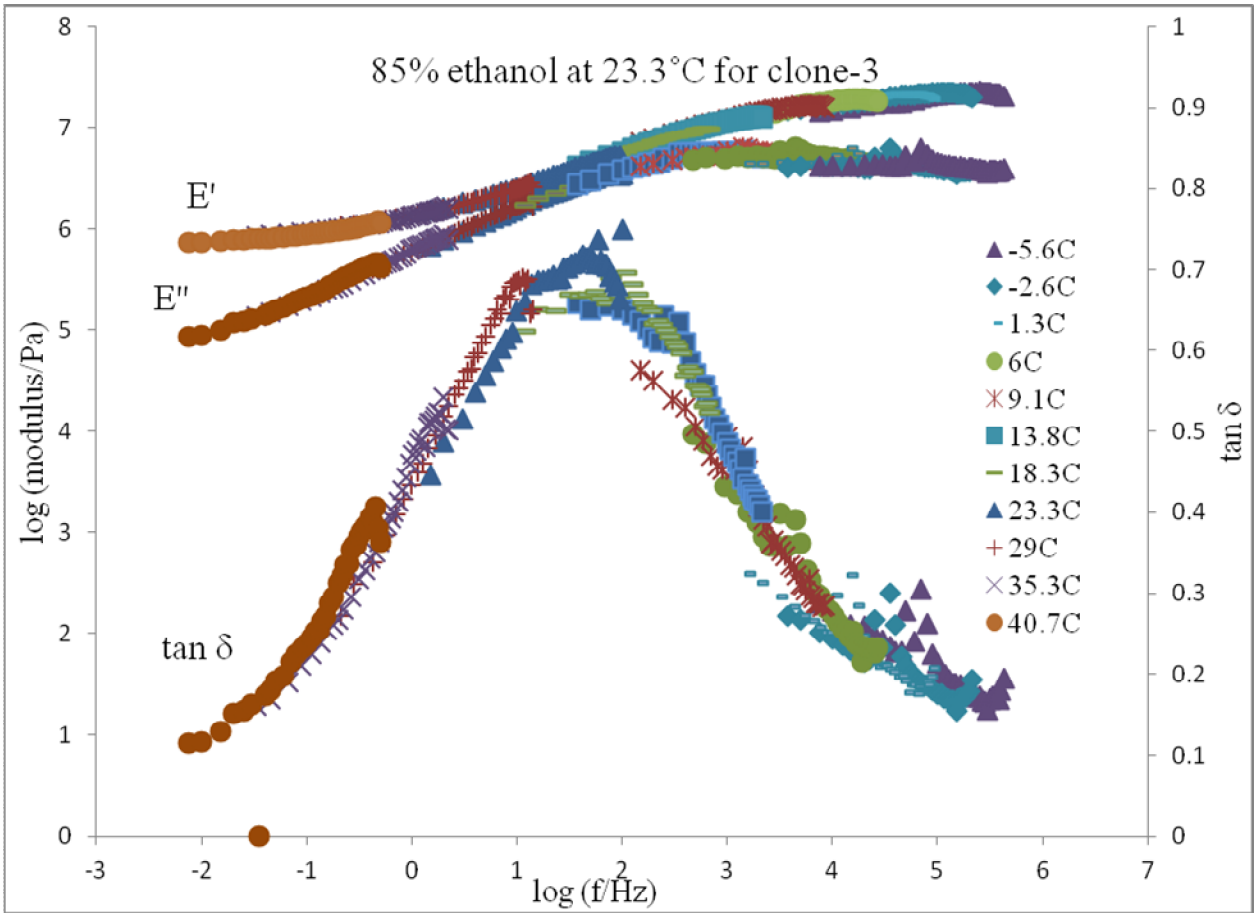

Fig. B.2 Master curves of storage modulus, loss modulus and tan δ for 85% ethanol concentration using TTSP with the reference temperature of 23.3˚C for clone-3.

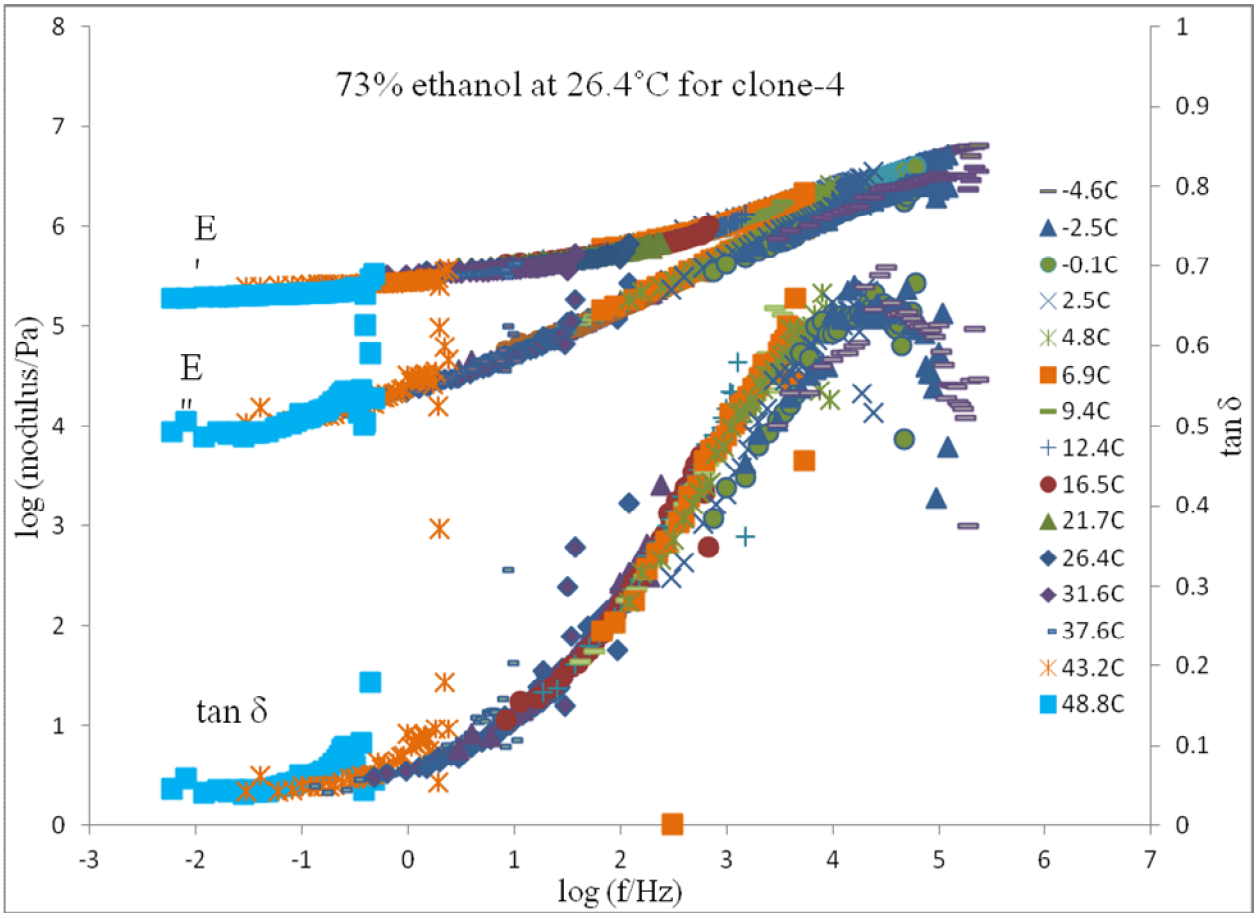

Fig. B.3 Master curves of storage modulus, loss modulus and tan δ for 73% ethanol concentration using TTSP with the reference temperature of 26.4˚C for clone-4.

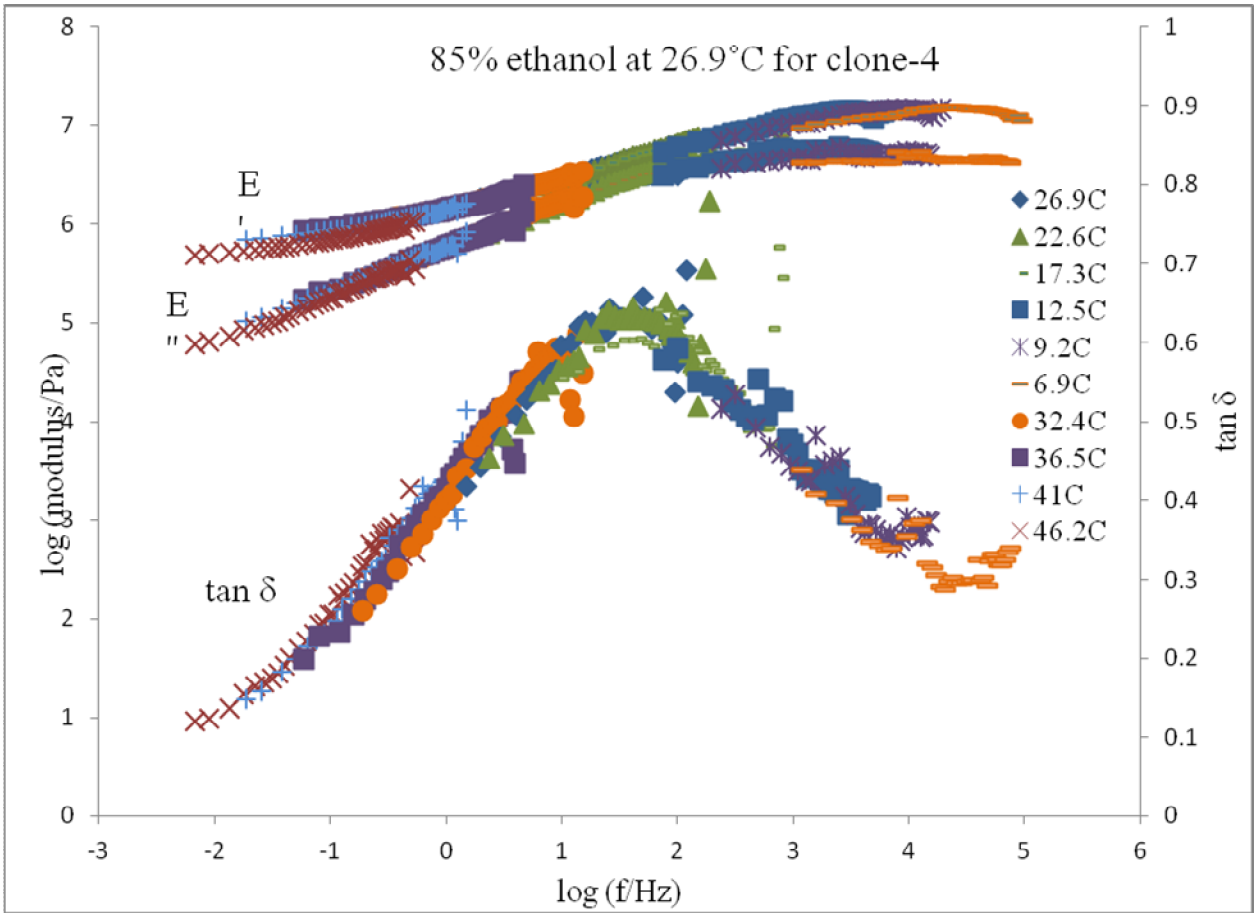

Fig. B.4 Master curves of storage modulus, loss modulus and tan δ for 85% ethanol concentration using TTSP with the reference temperature of 26.9˚C for clone-4.

Appendix C Supplementary Documents for Chapter 4

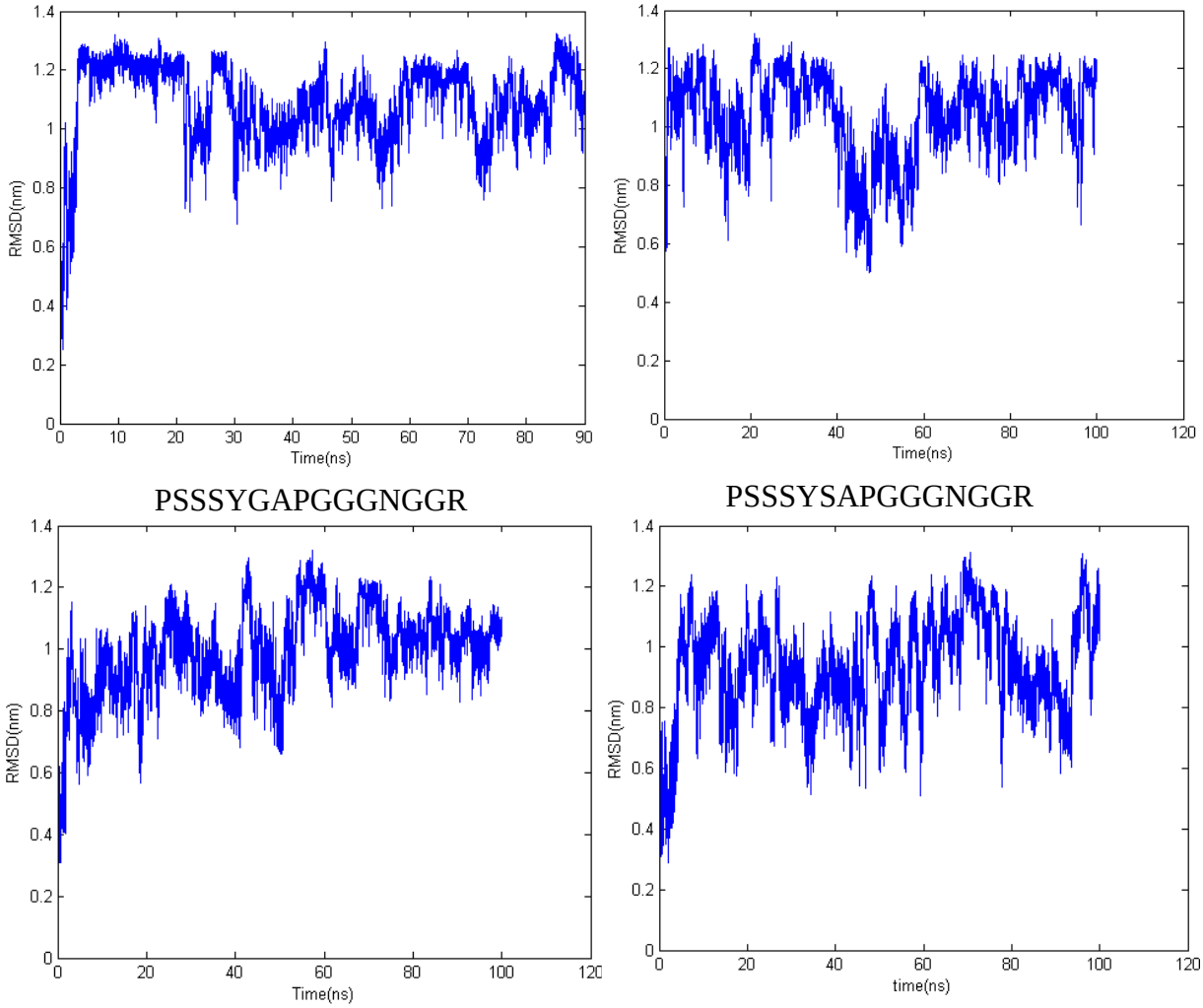

Fig. C.1 Root-mean-square deviation (RMSD) plot for (a) PSSSYGAPGGGNGGGR (b) PSSSYSAPGGGNGGR (c) PSSTYGAPGGGNGGR (d) PSSTYSAPGGGNGGR during the equilibrium.

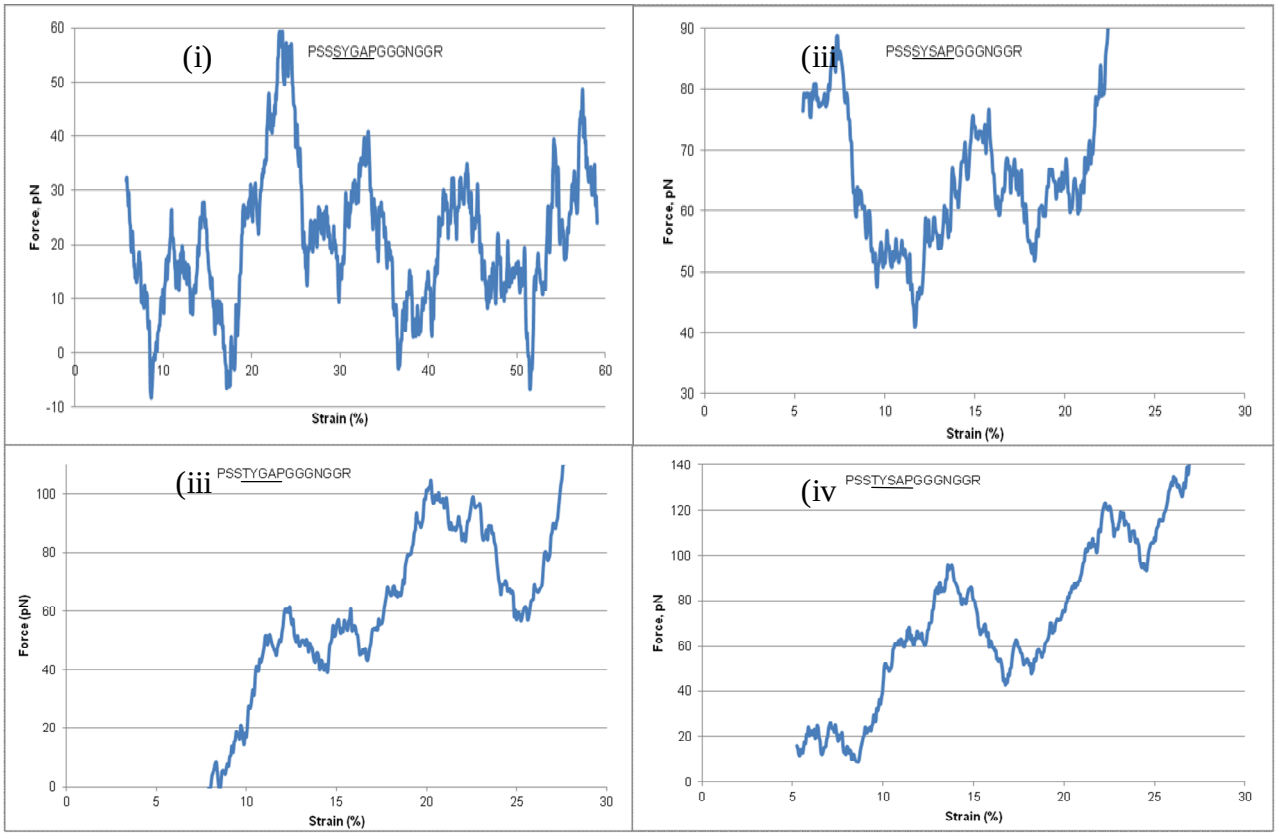

Fig. C.2 Force-displacement plot for (i) PSSSYGAPGGGNGGR (ii) PSSTYGAPGGGNGGR (iii) PSSSYSAPGGGNGGR (iv) PSSTYSAPGGGNGGR. All the motifs have similar fluctuations at comparable scale.

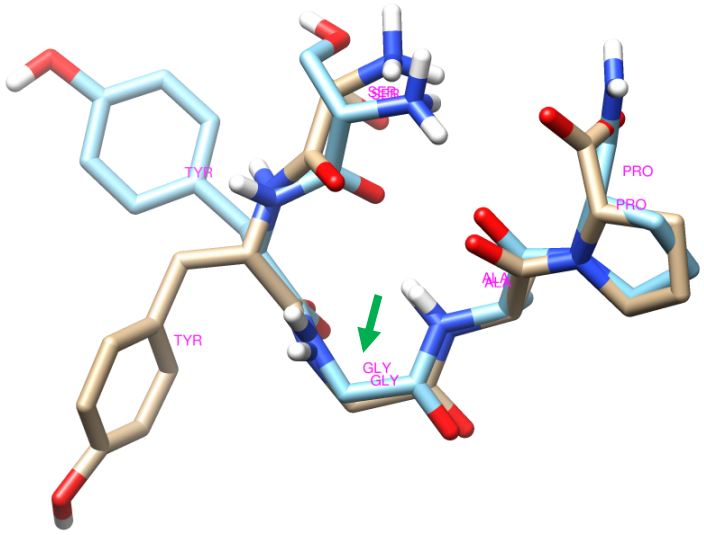

Fig. C.3 Alignment of SYGAP structure obtained before adding the cap (tan) and after adding the cap (blue). Both of them have a similar bend at the same location i.e. at glycine (see arrow).